Title
A Finely Tuned Molecular Motor: Mechanochemistry and Power Efficiency in the AAA+ Protease Machine ClpXP

Author
Rodriguez Aliaga, Piere

Publication Date
2016

Peer reviewed|Thesis/dissertation

“A Finely Tuned Molecular Motor:

Mechanochemistry and Power Efficiency in the AAA+ Protease Machine ClpXP”

By

Piere Angelo Rodriguez

A dissertation submitted in partial satisfaction of the

requirements for the degree of

Doctor of Philosophy

in

Biophysics

in the

Graduate Division

of the

University of California, Berkeley

Committee in charge:

Professor Carlos J. Bustamante, Chair
Professor Andreas Martin
Professor Michael P. Rape
Professor David E. Wemmer

Fall 2016

ABSTRACT

"A Finely Tuned Molecular Motor:
Mechanochemistry and Power Efficiency in the AAA+ Protease Machine ClpXP"

By

Piere Angelo Rodriguez

Doctor of Philosophy in Biophysics

University of California, Berkeley

Professor Carlos Bustamante, Chair

Molecular motors transduce chemical energy –usually from ATP hydrolysis– into directed motion and mechanical work, which is used to perform key functions in almost every cellular process. Molecular motors are particularly important in the maintenance of cellular proteostasis, i.e. the equilibrium between protein synthesis and degradation. ATP-dependent proteases of the AAA+ family, such as ClpXP from *Escherichia coli* and the eukaryotic 26S proteasome, play a central role in protein degradation. Given its extensive biochemical and structural characterization, ClpXP is a paradigm for the study of the operating principles of eukaryotic and prokaryotic protease machines of the AAA+ family. However, the molecular mechanism by which ClpXP couples the energy from ATP hydrolysis into mechanical work is still poorly understood. Here we used biochemical and single-molecule assays with optical tweezers to directly probe the operation of ClpXP as it unfolds and translocates its protein substrate.

Chapter one provides an introduction into the structure and function of ClpXP, which is considered an archetype for the study of AAA+ proteases. This chapter also introduces key concepts about single molecule studies assays with optical tweezers.

Chapter two focuses on the study of the mechanisms of force generation and intersubunit coordination of ClpXP. We establish that ClpXP translocates its substrate by using cycles of alternating dwell/burst phases. Phosphate release is the force generating step in the ATP cycle, and ClpXP translocates its substrate in bursts resulting from highly coordinated conformational changes in two to four ATPase subunits. Based on our results, we propose a model where ClpXP must use its maximum firing capacity of four subunits to unfold stable substrates like GFP. Interestingly, the average dwell duration between individual bursts of translocation is constant, regardless of the number of translocating subunits, implying a constant translocation cycle governed by an unidentified "internal clock". Together, our results indicate that ClpXP operates with constant "rpm" but uses different "gears".

Chapter three describes the complete mechanochemical cycle of ClpXP, as well as the coupling and power efficiency of the motor. We show that ADP release and ATP binding happen non-sequentially during the dwell, while ATP hydrolysis and phosphate release occur during the

burst. ADP release is the rate-limiting transition of the ATP cycle. Interestingly, the size of the highly-conserved translocating loops within the ClpX pore has been evolutionarily optimized to maximize motor power generation, as well as the coupling between chemical and mechanical cycles of the motor. Finally, we presente evidence showing that the conformational resetting of these loops between consecutive bursts seems to determine ADP release from individual ATPase subunits and the overall duration of the motor's cycle, which explains the observed "internal-clock mechanism" of ClpXP.

"Cuando creíamos que teníamos todas las respuestas,

de pronto,

cambiaron todas las preguntas."

—Mario Benedetti

To my parents—all that I am, or hope to be, I owe to you.

To Claudia—because of you, because of us.

...and to you, the reader—I hope you enjoy reading this work as much as I enjoyed writing it.

ACKNOWLEDGEMENTS

I would like to acknowledge all of the people who inspired me and supported me during this unforgettable journey to become a PhD. I would like to thank my advisor Carlos Bustamante for all the guide and support he has given me all these years. In addition to all the encyclopedic knowledge I acquired during our discussions, I learned that the most important question in any scientific enterprise is "What is the question?" I also learned that in any scientific problem the correct answer may not be immediately evident, and that most of the times "what is essential is invisible to the eye", as Antoine de Saint-Exupéry said in his book The Little Prince.

I would like to thank Andreas Martin, my unofficial co-advisor, with whom we have collaborated very closely all these years to study this amazing motor called ClpXP. I am grateful to him for the invaluable and constant advice he provided at every step of my PhD studies, starting in my qualifying exam until the elaboration of my manuscripts. Many of the approaches I took in my projects would not have been possible without him sharing his expertise and friendly guidance.

Rodrigo Maillard—previously a postdoc in the lab—was my mentor during the first three years of my PhD, and I could not have asked for a better one. I am grateful to him for teaching me a wide variety of lab techniques, for his advice on presentations, writing, and life. His quantitative approach to understand molecular mechanisms, together with his rigorous and hard work, triggered my transition into a biophysicist. His approach to science, and his rigorous protocol to make pisco sours, have left a lasting impression that will remain with me throughout my career.

I would also like to thank my fellow ClpXP teammates: Maya Sen, Kris Nyquist, and especially to Luis Ramirez and Frank Kim who often did more than requested. I am grateful to my colleagues in the Bustamante lab for fostering an intellectually challenging and supportive environment. I would like to especially thank Claudio Rivetti, Marta Kopaczynska, Shixin Liu, Maurizio Righini, Christian Kaiser, Jae Yen Shin, Lacramioara Bintu, Toyotaka Ishibashi, Dan Goldman, Gheorghe Chistol, Yves Coello, Troy Lionberger, Bibiana Onoa, Christian Wilson, Cesar Diaz, Errol Watson, Cristhian Cañari, Shannon Yan, Ronen Gabizon and Liang Meng Wee, for stimulating conversations and for sharing their expertise with me. Natalie Thung, Melina Winterton, and Kate Chase helped me to navigate through the university bureaucracy.

I want to express my gratitude to Dave Wemmer and Michael Rape for their comments and suggestions for this work. Thanks to John Kuriyan and Dave Savage for the opportunity to assist them in teaching their biophysical chemistry course; I really enjoyed it. Thanks to Ignacio Tinoco, from whom I learned that perseverance—and not intelligence—makes a good researcher.

My career as a scientist began at Cayetano Heredia University in Peru, thanks to the support of Oswaldo Ramirez, Margarita Arana, Mirko Zimic, and Daniel Guerra. They welcomed me into their research groups and allowed me to make my first steps in the scientific world. Thanks also to Jorge Arevalo, Abraham Vaisberg, Daniel Clark, and Alberto Cazorla for their advice and for sharing their gift of teaching with me. Science in Peru is promising because of all of them.

I thank all of my friends for their support during my PhD. Michael Souza was a partner in many adventures, from jumping from an airplane to the close encounter with a tornado. With my classmates Tim Wendorff and Vlad Belyy we shared the ups and downs of our graduate work

while listening to R Kelly and trying to form the first biophysics rock band. I also want to thank my oldest friends, Lian, Renato, Ali, Ernesto, Carrique, Americo, Simon, and Sergio, for the good times we always spend together in Lima, for all the stories we wrote together, and for their unconditional friendship and moral support, despite the distance.

Thanks to all my family, grandparents, uncles, and aunts, both in Peru and Spain, for the moral support, and for their unflagging belief that—despite their incomprehension about what I do—I must be *curing cancer*.

Special thanks to my parents, Gustavo and Maria, and my brother Luiggi for their incessant support. My gratitude to them is beyond words. Through all of their sacrifices they gave me wings to fly, to reach for the stars and chase my dream of being a scientist. Thanks for watching with me all those documentaries about nature and space when I was little, for the scientific books, for the philosophical and thought-provoking discussions during lunch and dinner, for my first electric guitar, and for showing me Pink Floyd, Led Zeppelin, and Queen. You are my heroes.

Most importantly, I am endlessly thankful to Claudia for her love and support, for her omnipresent smile, and for staying with me despite being in different hemispheres for three years. Thanks for being my source of inspiration and motivation to complete this dissertation.

TABLE OF CONTENTS

LIST OF FIGURES

— Chapter 1 —

Introduction

1.1. CLPXP AS A MODEL SYSTEM FOR THE STUDY OF ATP-DEPENDENDENT PROTEIN TRANSLOCATION AND UNFOLDING

Protein homeostasis is a key process that ensures proper cellular functions by maintaining appropriate levels of well-folded and functional proteins. To this end misfolded, damaged, or no longer needed proteins are recognized and degraded by the cellular proteolytic machinery to avoid aggregation and cell death. Protein quality control is driven mainly by ATP-dependent proteases of the AAA+ family (*A*TPases *a*ssociated with various cellular *a*ctivities), which use the energy of ATP binding/hydrolysis to unfold and translocate protein substrates. These protease machines share a common architecture consisting of a ring-shaped protein ATPase associated to a barrel-shaped peptidase.

Members of this family, such as the prokaryotic ClpXP and the eukaryotic 26S proteasome, encounter unique chemical and mechanical challenges during their task of protein unfolding and polypeptide translocation: i) these protease machines must translocate along a heterogeneous and flexible polypeptide track composed of amino acids with highly diverse chemical and physical properties, and ii) these motors must unravel a diverse array of folded protein domains with a range of stabilities that represent mechanical obstacles along the track. Thus, in a mechanistic sense, it is likely that protein translocating machines have unique operating principles compared to their DNA/RNA translocating machines counterparts.

Despite the significant amount of information available in the literature regarding the roles and functions of AAA+ protease machines in the cell, the molecular mechanisms by which they operate are still poorly understood. Here, we study the protein unfolding and translocation trajectories of ClpXP at the single molecule level in order elucidate with great detail the molecular mechanisms behind its operation. This protease machine has been extensively characterized biochemically and structurally, and because its architecture is shared by most AAA+ proteases, ClpXP is considered an archetype for the study of AAA+ proteases and translocases—such as ClpAP, ClpCP, HSlUV, FtsH, PAN/20S, CbbX—and other protein translocating machines such as the SecA ATPase (Baker and Sauer, 2012; Bauer et al., 2014; Mueller-Cajar et al., 2011).

1.2. CLPX STRUCTURE AND FUNCTION

Like most AAA+ proteases, the bacterial ClpXP consists of two major components (Fig. 1.1):

i) The AAA+ ATPase ClpX, formed by six identical subunits that together form an homo-hexameric ring with an axial processing pore. Each ClpX subunit, containing a AAA+ ATPase motif, is composed of a large and small domain connected by a hinge. ATP binds to a cleft formed by these two domains.

ii) The barrel-shaped ClpP peptidase, which contains proteolytic active sites sequestered in an internal chamber. Proteolytic sites are located within the barrel of ClpP, which are accessible only through a narrow axial pore that limits passage of folded proteins.

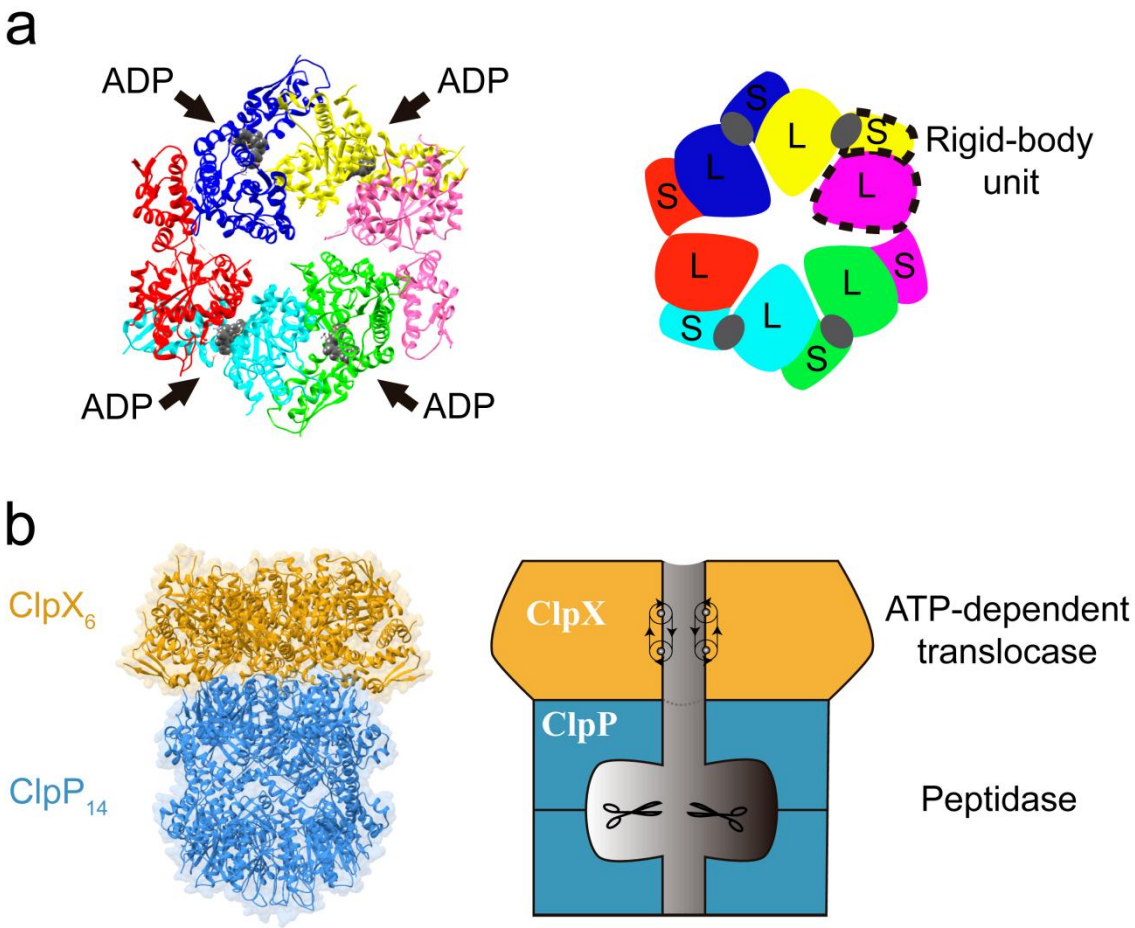

Figure 1.1. ClpXP structure. **(a)** Left, top view of the ClpX hexamer structure with four nucleotides bound (PDB 3HWS). Each subunit is depicted in different color. ADP-bound molecules are indicated in gray. Right, scheme of the ClpX structure showing the large (L) and small (S) domains for each subunit, and the nucleotide binding sites in gray. The rigid-body unit formed by two subunits is indicated with discontinuous lines. **(b)** Left, side view of the structure of the ClpXP complex (ClpP PDB 3MT6). Right, scheme of the ClpXP complex showing the function and structure of each component.

One of the signals that target protein substrates for degradation by *E. coli* ClpXP is the ssrA-tag, a 11-amino acid sequence that is appended to the C-terminus of incompletely translated proteins at the ribosome (Moore and Sauer, 2005). SsrA-mediated degradation comprises three ATP-dependent steps (Baker and Sauer, 2012; Gottesman et al., 1998; Kim et al., 2000): i) recognition and engagement of the protein through ssrA-tag binding to the ClpX pore, ii) force-induced unfolding, which results from the mechanical pulling and translocation of the ssrA-tagged protein into the narrow central pore, and iii) translocation of the unfolded polypeptide into the associated ClpP peptidase for degradation (Fig. 1.2).

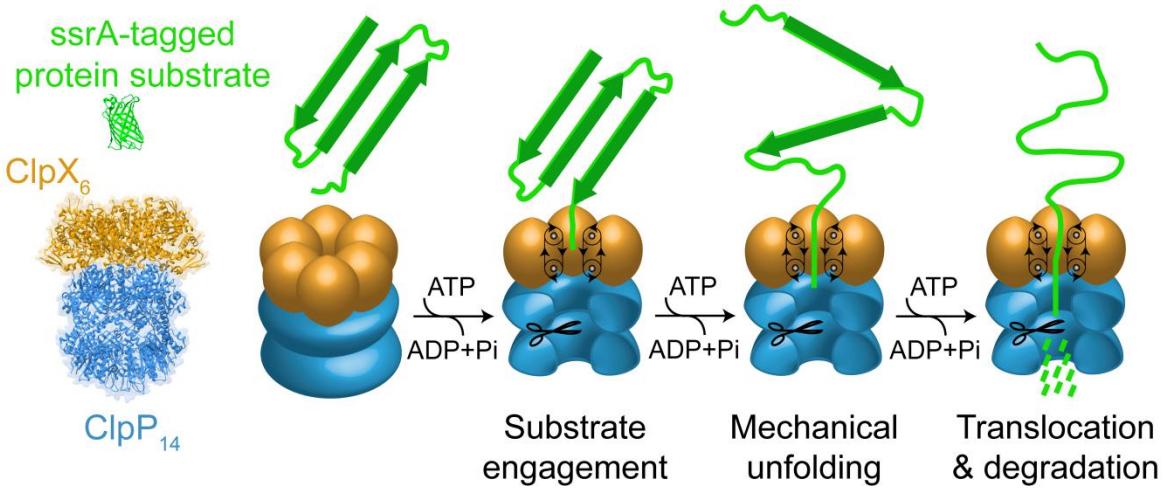

Figure 1.2. Cartoon of the general mechanism of protein degradation by ClpXP (ClpX PDB ID: 3HWS; ClpP PDB ID: 3MT6).

Polypeptide translocation is therefore the fundamental mechanical activity of ClpXP. A translocating loop with a highly-conserved glycine-tyrosine-valine-glycine (GYVG) motif protrudes from every ClpX subunit into the central pore (Fig. 1.3). These GYVG loops (also referred to as pore-1 loops) make direct contact with the substrate and transduce the ATP-hydrolysis-driven motions of the motor subunits to propel the substrate by individual power strokes (Martin et al., 2008a, 2008b; Siddiqui et al., 2004). Translocation by ClpXP is a remarkably promiscuous process, demonstrated by the successful degradation of homopolymeric segments of glycine, proline, lysine and even D-aminoacids (Barkow et al., 2009). However, bulk studies of ClpXP (Barkow et al., 2009) have shown that the identity of the substrate side chain significantly affects translocation parameters (Vmax, Km, ATP consumption) and unfolding rate. Together, these observations indicate that ClpXP translocation may be driven mainly by contacts of the GYVG loops with the substrate peptide backbone, but that the identity of the protein substrate side chain affects efficiency of translocation by a mechanism that remains to be elucidated.

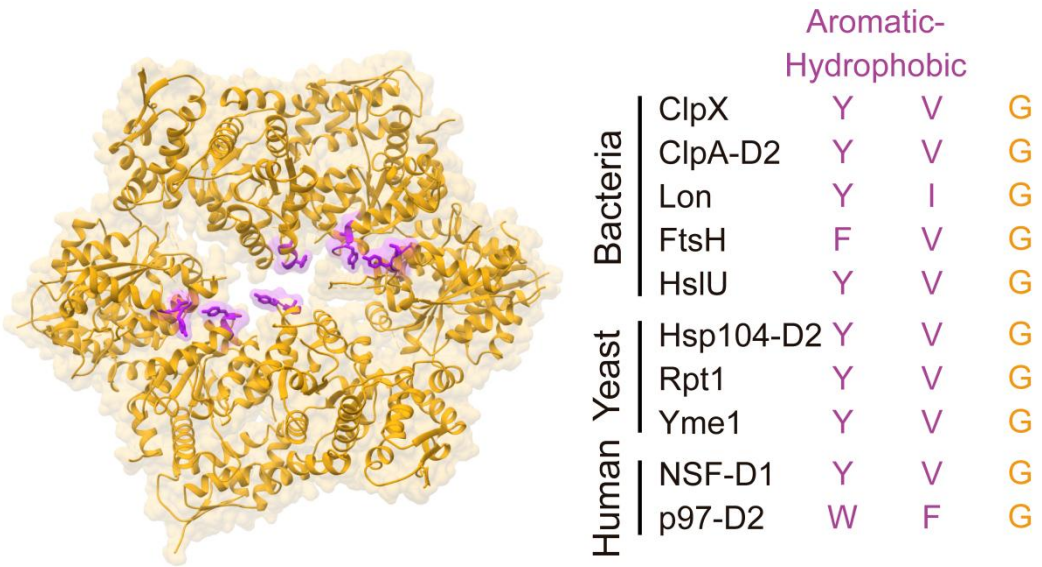

Figure 1.3. Left, top view of the ClpX hexameric ring showing the translocating GYVG loops (pore-1 loops) in purple (PDB ID: 3HWS). Right, aromatic-hydrophobic motif in the translocating pore-1 loops of prokaryotic and eukaryotic AAA+ protein translocases.

Biochemical and structural studies have shown that—despite being a hexamer—ClpX can bind a maximum of four nucleotides (Glynn et al., 2009; Hersch et al., 2005). Specifically, crystal structures of ClpX from *E. coli* have revealed structural asymmetry in the ring-shaped ClpX hexamer, despite being formed by six identical ClpX subunits (Glynn et al., 2009; Stinson et al., 2013). This asymmetry arises from the observation of two major classes of subunits within the hexamer (Fig. 1.1a): i) "Loadable subunits" (L), which contain an intact nucleotide-binding pocket due to the relative orientation of the large and small, and ii) "Unloadable subunits" (U), which contain a 80° rotation between the large and small domains which disassembles the nucleotide binding pocket. The observation of four L subunits within the hexamer thus indicates the motor can bind a maximum of four nucleotides.

Importantly, the orientation of the large domain of a subunit with respect to the small domain from the counterclockwise subunits remained remarkably unchanged among all six subunits, both in the nucleotide-bound and nucleotide-free free ClpX hexamer (Glynn et al., 2009) (Fig. 1.1a). Given that this interface is structurally conserved, this suggests that neighboring domains comprise a rigid-body unit, which moves around restricted swivel points defined by the conformations of the linkers in each subunit (Fig. 1.1a). Because the rotation between the large and small domains within a ClpX subunit change depending on the nucleotide state of the subunit (Glynn et al., 2009), it has been proposed that these nucleotide-dependent changes will cause movement of the rigid-body units through the ClpX hexamer, which could power protein unfolding and translocation by coupling these movements to the GYVG loops (Glynn et al., 2009).

1.3. INTERSUBUNIT COORDINATION IN CLPX

The crystal structure of ClpX suggests that nucleotide-dependent conformational changes initiated in one subunit can be transmitted to the rest of the hexameric ClpX ring through the rigid-body units (Fig. 1.1a). This structure-based observation suggests some kind of coordination within the ClpX hexamer. However, it has been reported that single-chain ClpX hexamers with different arrangements of inactive and active subunits (Martin et al., 2005) still support protein unfolding and polypeptide translocation, although at a reduced rate. This observation rules out scenarios where chemical transitions among all subunits occur in a strictly successive manner (with temporal and spatial order) or concerted manner (all subunits firing at once) (Fig. 1.4). Instead, these results favor, in principle, a scenario where intersubunit coordination within the ring occurs stochastically, i.e. every ClpX subunit operates independently of others (Fig. 1.4).

However, certain arrangements of active and inactive subunits within the ClpX ring affect the operation of the motor (Martin et al., 2005), which suggests that the motor is not completely stochastic and uncoordinated. Together these results indicate that ClpXP has certain degree of intersubunit coordination, favoring instead a probabilistic coordination model, or a scenario in which coordination among subunits can be maintained by skipping inactive subunits. The exact mechanism of coordination in ClpX is still unclear.

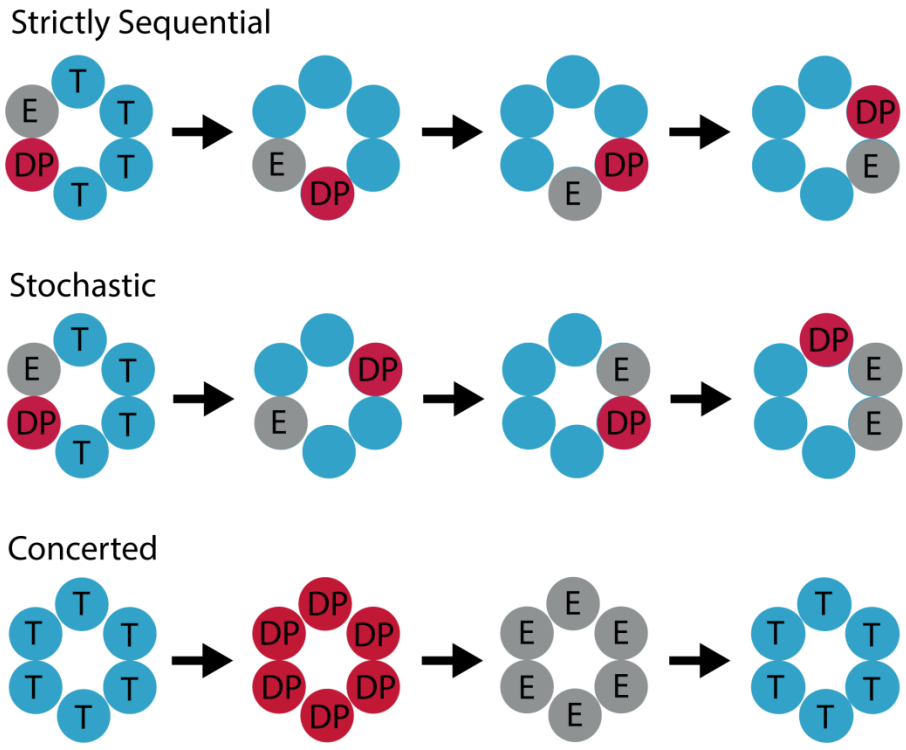

Figure 1.4. Intersubunit coordination models for ring-shaped molecular motors. Each subunit is represented by a colored circle, where the ATP state (T) is blue, ADP state (DP) is red, and the empty state (E) is gray.

1.4. STUDYING CLPXP AT THE SINGLE MOLECULE LEVEL WITH OPTICAL TWEEZERS

As shown in the previous sections of this dissertation, a lot of progress has been made to understand how ClpX and other AAA+ protease machines unfold and translocate proteins. However, central questions about the operation of ClpX—such as the mechanisms of intersubunit coordination and mechanochemical coupling—still remain unsolved. To address these mechanistic questions it is necessary to study the individual translocating steps of the motor. This is not possible by using bulk methods because: i) they study the behavior of the average of the population and therefore a lot information can be hidden or lost, and ii) it is not possible to synchronize all ClpX motors due to the random nature of kinetics. Similar limitations are also present in a structure-based approach because—despite its high spatial resolution—it lacks of dynamic information and, more importantly, a ClpX structure in the presence of a translocating substrate is missing. In this context, all these technical limitations can be overcome by using single-molecule techniques which make it possible to study the protein unfolding and translocation trajectories of a single ClpX motor with high spatial/temporal resolution. In particular, the optical tweezers have been used to understand with unprecedented detail mechanical properties of biopolymers and molecular machines at the single-molecule level (Bustamante, 2008).

The optical-tweezers technology is based on the following physical observation: micron-sized particles can be trapped in stable optical potential wells using only the force of radiation pressure from a highly focused laser beam, a principle which was first demonstrated by the pioneering work of Arthur Ashkin (Ashkin, 1970). The optical tweezers are very sensitive instruments that are capable of the manipulation micron-size particles and detection of sub-nanometer displacements, pico Newton force measurements, and millisecond events. As a result, the optical tweezers allow precise measurements of aspects of ClpXP operation that otherwise were not accessible through other tools, such as translocation velocities, pauses during translocation, force and power produced by the motor. More importantly, they allow the direct observation and analysis of discrete translocation steps during the mechanical cycle, which are crucial to understand the mechanism of ClpXP coordination and mechanochemical coupling.

Single molecule optical-tweezers assays of the substrate translocation and unfolding by ClpXP have been developed in our laboratory (Maillard et al., 2011). Specifically, our optical-tweezers assays are performed in an instrument with dual-trap geometry (Fig. 1.5), where a single laser beam is split in two different optical paths to produce two optical traps, which allow to establish correlations in the motions of particles immobilized in both traps and therefore reduce the Brownian noise (Moffitt et al., 2008). Here, we use a dual-trap setup, similar to the one previously described (Maillard et al., 2011), to track in real-time a single ClpXP molecule as it mechanically unfolds and translocates an ssrA-tagged protein in the presence of ATP (Fig. 1.5). Our model substrate contains a ybbR tag—used for attachment with the DNA handle—a green fluorescent protein (GFP) moiety and four C-terminally fused titin I_{27} domains that are permanently unfolded by carboxymethylation (Ti^{CM}), followed by an ssrA tag. Together they form the ybbR-GFP-$(Ti^{CM})_4$-ssrA protein substrate. ClpXP and its protein substrate were individually immobilized on the surface of two micron-sized polystyrene beads that were held in separate optical traps. After engaging the substrate, ClpXP immediately proceeds to translocate the Ti^{CM} moieties, decreasing the distance between the beads held in the fixed traps (passive

mode; Fig. 1.5). GFP unfolding events appear as sudden extension gains, which are followed by a steady decrease in extension due to the processive translocation of the unfolded substrate into ClpXP. Periods with no extension change for longer than ~1s indicate motor pauses off the main translocation pathway.

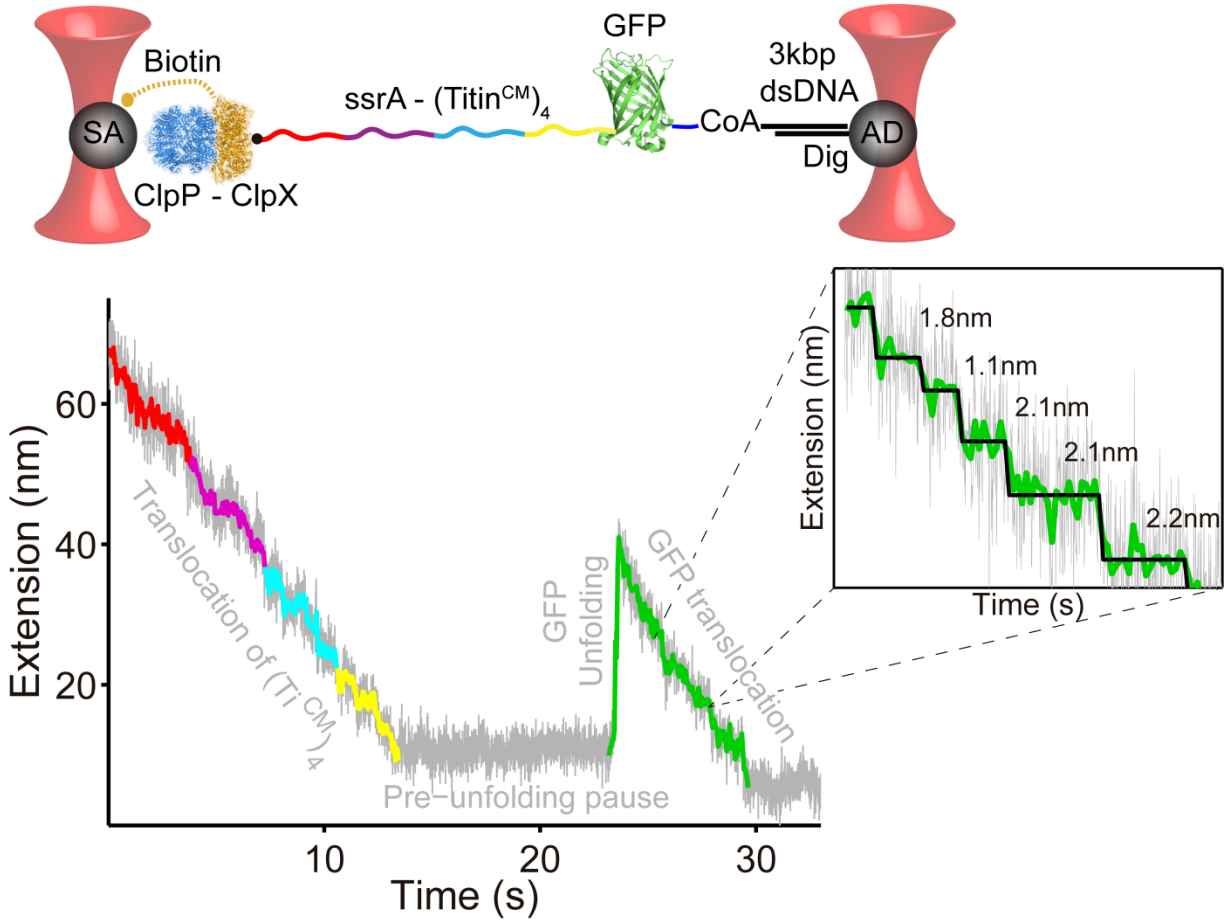

Figure 1.5. Top, experimental geometry of the dual-trap optical tweezers assays. ClpXP is immobilized on a micron-sized bead coated with streptavidin (SA), and the substrate is bound to an anti-digoxigenin-coated bead (AD) via a DNA handle. The ssrA-tagged substrate has four permanently unfolded (carboxymethylated, CM) titin I_{27} domains (Ti^{CM}) C-terminally fused to a green fluorescent protein (GFP). Bottom, single-molecule trajectory in passive mode of substrate translocation and unfolding by ClpXP. Raw data (2.5 kHz in gray) were filtered and decimated to 100 Hz (in red, purple, cyan, yellow, and green to indicate individual domains of the substrate). Inset, segment of a ClpXP translocation region displaying individual translocating bursts. Raw data were filtered and decimated to 800 Hz (in gray) or 70 Hz (in green). *t* test fits to the data are shown in black.

By using high-resolution optical tweezers, important findings about ClpXP and related protease machines have been made in recent years. It has been established that ClpX transforms the energy of ATP hydrolysis into mechanical force to drive unfolding and translocation, and that polypeptide translocation occurs in cycles composed of a dwell phase, during which the substrate does not move, and a burst phase, during which ClpXP near-instantaneously translocates its

substrate (Aubin-Tam et al., 2011; Maillard et al., 2011; Sen et al., 2013). Some aspects of the intersubunit coordination and the mechanochemistry of ClpX have also been elucidated (Cordova et al., 2014; Sen et al., 2013). A similar characterization has been performed in the double ring AAA+ machine ClpA (Olivares et al., 2014). More recently, a coordinated-gripping mechanism involving the six translocating loops of ClpXP has been proposed (Iosefson et al., 2015a, 2015b).

Despite the significant advances described in this chapter to understand how ClpX operates, many central aspects of its mechanism remain poorly understood or incomplete. This dissertation presents novel and detailed mechanistic insights showing how ClpXP converts chemical energy from ATP hydrolysis to mechanical work, how individual ClpX subunits are coordinated, and the underlying molecular processes that govern the translocation and unfolding efficiency of this motor. We present important new insights into how evolution has optimized AAA+ proteases and other protein translocating machines for efficient protein unfolding and translocation.

— Chapter 2 —

Mechanism of Force Generation and Intersubunit Coordination

The results & models described in this chapter have been adapted and modified from the following publication:

Sen, M., Maillard, R.A., Nyquist, K., Rodriguez-Aliaga, P., Pressé, S., Martin, A., and Bustamante, C.
"The ClpXP protease unfolds substrates using a constant rate of pulling but different gears".
Cell, 155:636-646, 2013.

2.1. SUMMARY

ATP-dependent proteases are vital to maintain cellular protein homeostasis. Here, we study the mechanisms of force generation and intersubunit coordination in the ClpXP protease from *E. coli* to understand how these machines couple ATP hydrolysis to mechanical protein unfolding. Single-molecule analyses reveal that phosphate release is the force generating step in the ATP-hydrolysis cycle and that ClpXP translocates substrate polypeptides in bursts resulting from highly coordinated conformational changes in two to four ATPase subunits. ClpXP must use its maximum successive firing capacity of four subunits to unfold stable substrates like GFP. The average dwell duration between individual bursts of translocation is constant, regardless of the number of translocating subunits, implying that ClpXP operates with constant "rpm" but uses different "gears".

2.2. BACKGROUND AND QUESTIONS TO ADDRESS

Escherichia coli ClpXP has been extensively characterized both biochemically and structurally, which is why it is considered a model system to investigate the operating principles of ATP-dependent proteases of the AAA+ family (Baker and Sauer, 2012). Single-molecule manipulation techniques have shed light on aspects of the ClpXP that otherwise were not accessible through traditional biochemical and structural studies. By using optical tweezers—which allow to probe the motor's mechanochemical coupling by applying external forces while simultaneously perturbing the chemical cycle of the motor—it has been shown that ClpX uses the energy of ATP hydrolysis to generate mechanical force, which drives protein unfolding and translocation (Aubin-Tam et al., 2011; Maillard et al., 2011). Because of the high spatio-temporal resolution of the optical tweezers it was possible to show that polypeptide translocation occurs in cycles

composed by two phases (Fig. 1.5 and 2.1): a dwell phase, during which the substrate does not move, and a burst phase, during which ClpXP near-instantaneously translocates the polypeptide by a certain length (Aubin-Tam et al., 2011; Maillard et al., 2011).

These results show evidence of the coupling between the mechanical and the chemical cycles of the motor. However, the processes that lead to this mechanical-chemical coupling are largely unknown not only for the ClpXP machine, but also for members of the AAA+ family in general. In this context, this chapter will focus on addressing the following questions:

- In a mechanistic sense, how is the chemical energy from ATP hydrolysis coupled to the mechanical cycle?
- Within the ATP cycle—which involves ATP binding, ATP hydrolysis, phosphate & ADP release—what is (are) the force generating transition(s)?
- Do all ClpX subunits participate during protein translocation?
- What is the mechanism of intersubunit coordination within the hexameric ring?
- How does ClpXP unfold metastable proteins like GFP?

To address these questions, we perturbed the chemical cycle of the motor by using ATP analogs and analyzed their effects on the operation and intersubunit coordination of ClpXP by using single-molecule assays with optical tweezers. This chapter describes the results from these experiments, and presents ClpXP as a motor that employs a novel mechanism of translocation that significantly deviates from canonical motor mechanisms.

2.3. RESULTS & DISCUSSION

2.3.1. Single-Molecule Assays

We used dual-trap optical tweezers in passive mode (constant trap position, variable force) to monitor a single ClpXP complex as it unfolds and translocates protein substrates in an ATP hydrolysis- dependent manner (Fig. 1.5). ClpXP was immobilized on one polystyrene bead and the ssrA-tagged protein substrate was attached to another. Each bead was held in an optical trap, and a tether formed between the beads once ClpXP engaged its substrate (Maillard et al., 2011). We used two fusion substrates of the green fluorescent protein (GFP) and a permanently unfolded variant of the I_{27} domain of titin (titin^{CM}): i) GFP-(titin^{CM})$_2$-GFP-titin^{CM}ssrA, and ii) GFP-(titin^{CM})$_4$-ssrA. Substrate unfolding was measured as a sudden gain in extension of the tether (rip), whereas polypeptide translocation was monitored as the gradual decrease of extension with time. Because ClpXP cannot efficiently unfold GFP at ATP concentrations below 200 mM, the second substrate allowed the measurement of extended translocation of titin domains without the requirement for GFP unfolding.

2.3.2. Phosphate Release is the Force-Generating Step in the ClpXP ATPase Cycle.

The ATP cycle within a single ClpX subunit can be described as a sequence of chemical steps involving ATP binding, hydrolysis, and ADP/Pi release (Fig. 2.1). Progress along this chemical-

reaction coordinate is coupled to the mechanical movement that drives substrate translocation, which can occur at any step of the chemical cycle. In order to probe the relationship between the generation of mechanical work and the ATPase cycle, we studied the operation of ClpXP in the presence of various concentrations of ATP, ADP, and inorganic phosphate (Pi).We focused our analysis to the titin^{CM} regions of the fusion substrate in order to minimize potential effects of amino acid sequence differences between titin^{CM} and GFP. Noteworthy, translocation was punctuated by rare pauses that are typically longer than 1 to 2 s, and that are in kinetic competition with translocation and therefore off the main translocation pathway (Maillard et al., 2011).

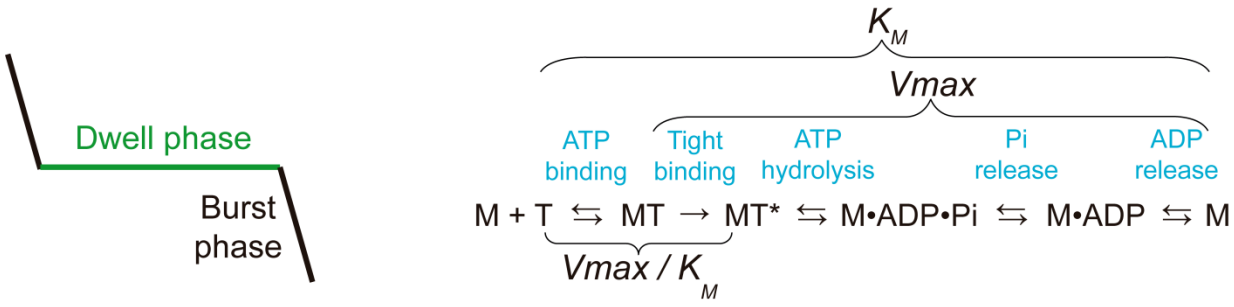

Figure 2.1. Left, ClpXP translocation is composed of two phases: i) dwell, during which the substrate does not move, and ii) burst, during which ClpXP near-instantaneously translocates the polypeptide by a certain length. Right, general scheme of the ATPase cycle in a single ClpX subunit "motor" (M). The subunit binds ATP (T), undergoes a tight-binding transition, hydrolyzes ATP, and finally releases Pi and ADP. The Michaelis constant (K_M), the effective catalytic rate constant (*Vmax*), and the effective binding rate constant ($Vmax/K_M$) depend on specific rate constants of the ATPase cycle, as indicated by the brackets (Keller and Bustamante, 2000).

First, we studied the operation of ClpXP as function of ATP concentration ([ATP]) (Fig. 2.2a). Pause-free translocation as a function of the ATP concentration followed a general Michaelis-Menten behavior (Fig. 2.2b). To determine whether ATP binding is the force-generating step, we examined how the translocation velocity depends on the opposing force at high and low ATP concentrations. If ATP binding is coupled to force generation, then conditions in which ATP binding becomes rate limiting should make the conformational changes that drive translocation also rate limiting. In this case, the motor velocity would be highly sensitive to the applied external force. However, we found that the translocation velocity of ClpX is largely insensitive to opposing forces at low [ATP] (Fig. 2.2c). In contrast, at saturating [ATP] (above 500 mM) and opposing forces between 12 and 20 pN, the force-generating step has become rate limiting and ClpX translocation is force sensitive (Fig. 2.2c). These results clearly indicate that ATP binding does not power substrate translocation.

Next, we analyzed the force dependence of the Michaelis- Menten parameters Vmax and K_M to determine where the force generating step may be located in the ATP cycle. K_M and Vmax are kinetic parameters that depend on particular rate constants within the chemical cycle (Fig. 2.1). Since the step in the chemical cycle that is coupled to mechanical work will be force dependant, the values of K_M, Vmax or both also will change with opposing force. Importantly, it has been established how the force dependence of K_M, Vmax, and K_M /Vmax change when the force generating transition is located at a particular transition within the ATP cycle (Fig. 2.1) (Keller and Bustamante, 2000).

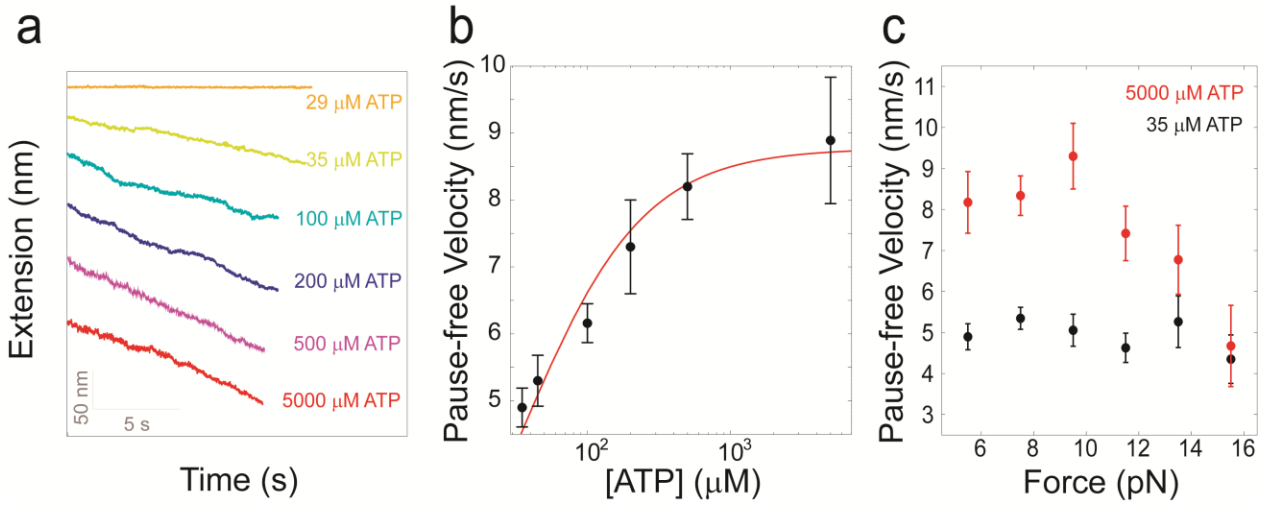

Figure 2.2. (a) Representative trajectories for translocation of the titin^{CM} moiety of the substrates, measured between 6 and 12 pN at different ATP concentrations. **(b)** Pause-free velocity is shown as a function of [ATP] at 7.5 pN opposing force. Data followed Michaelis-Menten equation with K_M = 31 ± 6 μM (SEM) and Vmax = 8.7 ± 0.4 nm/s (SEM). **(c)** Force dependence of the pause-free translocation velocity at saturating and near K_M ATP concentrations.

The Michaelis-Menten fits to our data revealed that both Vmax and K_M decrease as the opposing force increases (Fig. 2.3a), but the K_M/Vmax ratio remains force insensitive within error (Fig. 2.3b). As shown in Figure 2.1, a force-independent K_M/Vmax is consistent with a scenario where ATP binding does not power translocation. Instead, this indicates that the force-generating step must occur after the first irreversible transition connected to ATP binding (Chemla et al., 2005; Keller and Bustamante, 2000; Visscher et al., 1999).

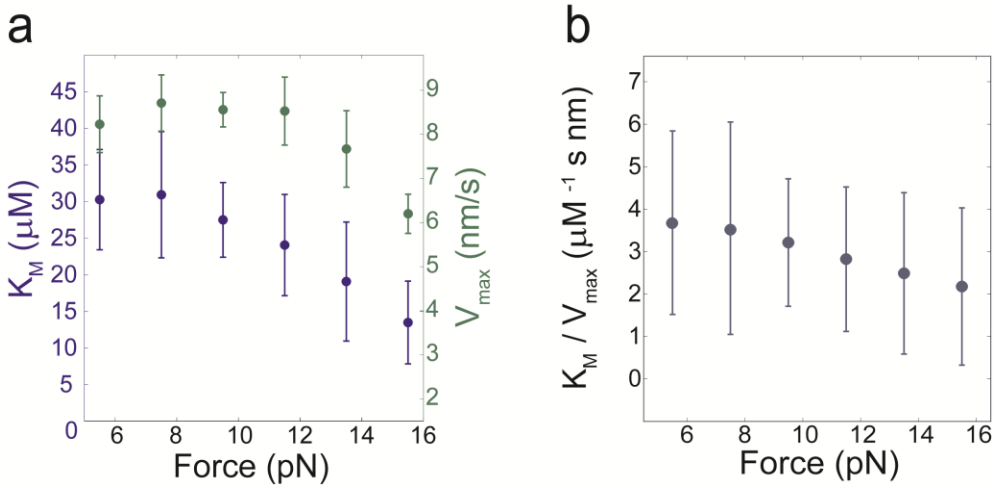

Figure 2.3. (a) K_M (blue) and Vmax (green) are plotted against force**. (b)** K_M/Vmax ratio plotted for forces between 5 to 15 pN. Error bars are from the fits (SEM).

This first irreversible transition is most likely the tight binding of ATP, as previously seen in other ring ATPases such as the F1-ATPase and the ϕ29 DNA packaging motor (Adachi et al., 2007; Chemla et al., 2005; Oster and Wang, 2000). In order to confirm whether this is also true for ClpXP, we calculated the rate constant of tight ATP binding (k_{TB}) as follows: because tight ATP binding is apparently not rate limiting during translocation, k_{TB} can be estimated by using a

lower bound that corresponds to the translocation rate of the motor, k_{cat} = ~9 s^{-1} (Fig. 2.2b), while the reverse transition from tight to loose binding, k_{-TB}, is given as the inverse of the mean ATPγS-pause duration, ~0.6 s^{-1} (Fig. 2.6b). Thus, we obtain a k_{TB} / k_{-TB} = 15 and a corresponding free energy change associated with tight binding $\Delta G_{TB} > 2.7\ k_BT$. The tight binding of ATP can therefore be considered the first irreversible transition following ATP binding.

The results above leave only ATP hydrolysis, ADP release, or Pi release as possible transitions that may be coupled to the force generating step (Fig. 2.1). ATP hydrolysis is unlikely to power translocation, because the small rotation of the terminal phosphate upon hydrolysis does not provide the free energy change required for the power stroke (Oster and Wang, 2000). Thus, either Pi or ADP release correspond to the force generating step. To investigate the role of product release in the mechanochemical cycle, we varied the concentrations of ADP and Pi. Consistent previous biochemical studies (Burton et al., 2003; Hersch et al., 2005), we observed that ADP behaved as a competitive inhibitor (Fig. 2.4a). The apparent K_M for ATP increased linearly with [ADP] according to $K_M = K_M^{\,o}\,(1 + [ADP] / K_i)$, whereas Vmax remained constant (Fig. 2.4a). In contrast, increasing [Pi] from 5 μM to 10 mM did not affect the translocation velocity (Fig. 2.4b), indicating that Pi release is a largely irreversible transition.

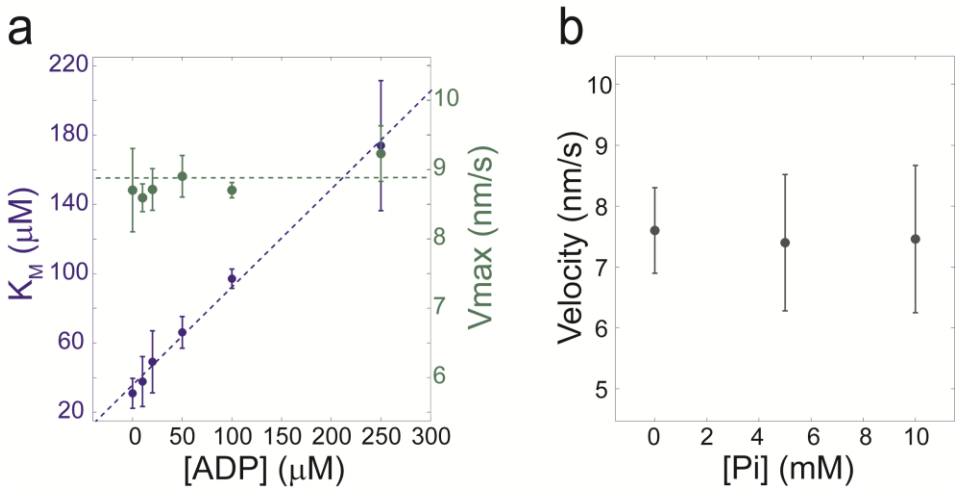

Figure 2.4. (a) K_M (blue) and Vmax (green) plotted against [ADP] at 7.5 pN**.** Error bars indicate SEM. **(b)** Pause-free velocity (mean ± SEM) plotted against phosphate concentration [Pi] 7.5 pN at fixed [ATP] = 500 μM.

To discriminate between the possible roles of ADP and Pi release in the mechanism of force generation, we estimated the free energy changes of these events based on their respective dissociation constants and compared them to the observed maximum work performed by ClpXP. Using 1 nm as the fundamental step size of ClpXP (Aubin-Tam et al., 2011; Glynn et al., 2009; Maillard et al., 2011) and a stall force of at least 20 pN (Maillard et al., 2011), we estimate that ClpX subunits perform a near-maximum work of 20 pN * 1 nm or ΔG = 4.8 k_BT when taking 1 nm steps near stall. Using K_i = 33 μM as a dissociation constant for ADP (Fig. 2.4a), the change in free energy from ADP release is ΔG_D ~ 1.8 k_BT (at [ADP] = 5 μM). This value is almost 3 fold smaller than the near-maximum work that ClpXP can produce, and thus is insufficient to account for the work performed by ClpXP. In contrast, phosphate release is considered irreversible because the velocity is unaffected even at high [Pi] (10 mM). Therefore, the dissociation constant

for phosphate release must be K_D >> 10 mM, with a corresponding change in free energy of ΔG_P >> 7.6 k_BT (for [Pi] = 5 μM). Phosphate release would thus provide sufficient energy to power the work produced by ClpXP in every translocation step and is the most likely candidate for the force-generating step of the motor.

The results in this section present evidence that exclude the possibility of ATP binding, hydrolysis, or ADP release being coupled to the force-generating step, and reveal instead that force generation likely occurs upon Pi release. We summarize these results into a mechanochemical model for ClpXP that identifies the force-generating step in the chemical cycle of ATP hydrolysis (Fig. 2.8). Interestingly, in this aspect ClpX resembles other members of the ASCE family, such as the ϕ29 DNA-packaging motor and F1-ATPase, harnessing Pi release as a force-generating step despite the distinct architectures and functions within this large family of motors (Chemla et al., 2005).

2.3.3. Intersubunit Coordination within the ClpX Hexamer

After the identification of the force-generating step within the mechanochemical cycle of a single ClpX subunit, we asked: what is the mechanism by which individual subunits within the ClpX hexamer coordinate their mechanical and chemical cycles as they unfold and translocate its substrate. To address this question, we focused on studying how individual subunits coordinate their ATP hydrolysis activities as they translocate a protein substrate. We slowed down the ATP-hydrolysis rate in a given subunit by using ATPγS—an ATP analog which ClpX hydrolyzes ~90 times slower than ATP (Fig. 2.5 and Supplementary Figure 1)—and determined how binding of this analog affected the polypeptide translocation by the remaining ATP-bound subunits in the ring. We held [ATP] fixed at 500 μM and increased [ATPγS] from 0 to 250 μM. In the presence of ATPγS, we observed pauses longer than 1 s (Fig. 2.5a)—which were extremely rare in the presence of ATP alone—and whose frequency and length changed with [ATPγS]. Thus, we attributed these long pauses to ATPγS-bound ClpX subunits.

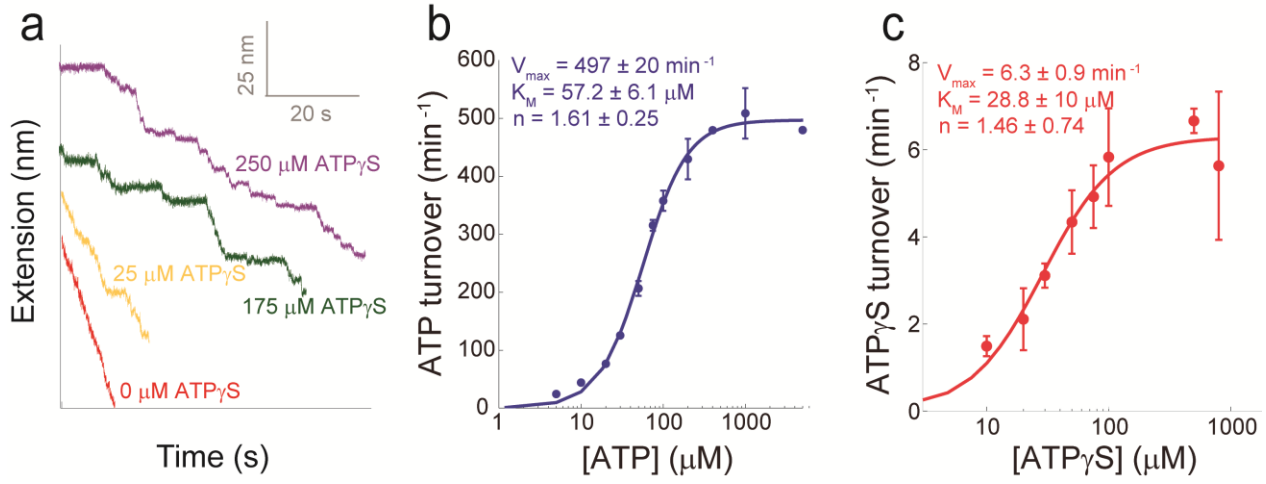

Figure 2.5. (a) Representative translocation trajectories with increasing [ATPγS] and fixed [ATP] = 500 μM. **(b)** ATPase rate (mean ± SEM) in the presence of Ti^{CM}. **(c)** ATPγS hydrolysis rate (mean ± SEM) in the presence of Ti^{CM} obtained by thin layer chromatography (See Methods). Data fit well to the Michaelis-Menten equation.

We observed that the pause density (PD)—the number of pauses per nm of translocated polypeptide—increased with [ATPγS], indicating that the entry into a pause was caused by the binding of ATPγS to the ring (Fig. 2.6a). The maximum PD, PD_{max}, reflects the ATPγS concentration at which the motor has nearly 100% probability of binding the minimum number of ATPγS molecules required to stall translocation. Accurate pause detection became difficult at high concentrations of ATPγS (greater than 200–250 μM). By plotting the inverse of [ATPγS] against the inverse of PD we estimated PD_{max} ~ 0.5 nm^{-1} (Fig. 2.6a). Because the motor has a PD ~ 0.25 nm^{-1} at [ATPγS] = 200 μM (Fig. 2.6a), we conclude that ClpXP has a 50% probability of entering into an ATPγS-induced pause at this [ATPγS].

We then asked what dictates the duration of the ATPγS-induced pause. One of two different processes is likely to dictate the kinetics of exit from a pause: i) the dissociation, or ii) the hydrolysis of ATPγS. To distinguish between these two scenarios, we compared the ATPγS hydrolysis rate with the average duration of the ATPγS-induced pauses. By using thin-layer chromatography (TLC) we measured that the hydrolysis of a single ATPγS molecule takes ~10 s in the presence of $titin^{CM}$-ssrA (k_{cat} ~6 min^{-1} $hexamer^{-1}$), which is ~90 times slower than the rate of ATP hydrolysis under identical conditions (Fig. 2.5b-c; See Methods). Because the observed mean pause durations are significantly shorter than the time for ATPγS hydrolysis, the duration of ATPγS-induced pauses reflect the off-rate of ATPγS from the motor. Interestingly, the mean duration of the ATPγS-induced pauses increased from 1.5 to 2.5 s as [ATPγS] increased from 50 to 250 μM (Fig. 2.6b). Thus, the exit from a pause takes longer as the motor loads with an increasing number of ATPγS molecules, likely reflecting the extra time required to eject multiple ATPγS molecules until a very low number of ATPγS molecules remain bound to the ring.

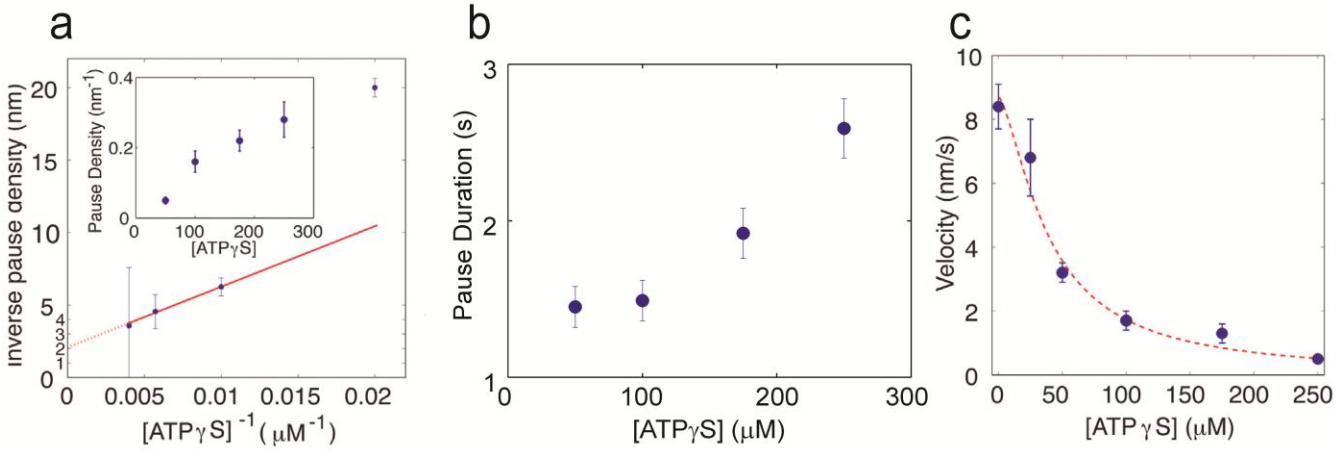

Figure 2.6. (a) Inverse density of ATPγS-induced pauses (mean ± SEM) plotted against the inverse of [ATPγS], with the linear fit shown in red. Inset: pause density (mean ± SEM) plotted as a function of [ATPγS]. **(b)** Pause duration (mean ± SEM) as a function of [ATPγS]. **(c)** Average translocation rate (mean ± SEM) plotted against [ATPγS], with the fit shown in red.

We then analyzed the effect of [ATPγS] on the translocation velocity of the motor. We observed that the average translocation velocity—which is computed including translocation pauses—decreased in a nonlinear fashion as a function of [ATPγS] (Fig. 2.6c). The trend could be fitted

well to a modified Hill equation with a Hill coefficient $n_{ATP\gamma S} = 1.5 \pm 0.3$ (SEM) (Fig. 2.6c; See Methods for calculation details), indicating that more than one ATPγS binding to the ring is necessary to induce a long pause during translocation. Consequently, intersubunit coordination around the ring does not require the involvement of all ATP binding-competent subunits. The analysis of the minimum number of ATPγS molecules required to induce a pause during translocation is explained in Chapter 3.

The fact that more than one ATPγS molecule is required to stall ClpXP translocation rules out models of strict intersubunit coordination described previously for other molecular motors (Fig. 1.4) (Lyubimov et al., 2011). This observation also excludes models of concerted hydrolysis, where the subunit power strokes occur simultaneously after all subunits have been loaded with nucleotide (Fig. 1.4). It also contradicts strictly sequential hydrolysis models, in which the power stroke of one subunit occurs only after the power stroke of its neighbor. If one of these models of intersubunit coordination were to apply to ClpX, a single ATPγS binding event would be sufficient to stall the motor. Furthermore, our data are also inconsistent with stochastic or probabilistic hydrolysis models, where all subunits act independently from each other. In a stochastic scenario, all the active subunits would have to bind ATPγS in order to stall translocation, which is not the case for ClpXP—as it will be seen in Chapter 3. Thus, we find that the ATPase cycles of individual ClpX subunits are neither strictly coordinated nor completely independent from each other. Instead, for a particular cycle, coordination in ClpXP seems to involve a subset of its subunits as it operates.

2.3.4. ClpXP subunits are highly coordinated during translocation bursts.

Our observation that more than one ATPγS molecule is required to stall the motor led us to investigate in greater detail the mechanism by which subunits communicate with each other around the ring. Previous single-molecule studies showed that ClpXP translocates polypeptide in bursts of 1, 2, and 3 nm (Maillard et al., 2011). Because the ClpX crystal structure shows ~1 nm displacement in the positions of the translocating loops in an ATP-bound state compared to empty states (Glynn et al., 2009), a 1 nm step was thought to reflect the size of the fundamental power stroke of a single ClpX subunit (Aubin-Tam et al., 2011; Maillard et al., 2011). Accordingly, the 2, 3, and 4 nm bursts are then interpreted as the near-simultaneous firing of two, three, and four ClpX subunits, respectively (Maillard et al., 2011). Furthermore, dividing the maximum translocation velocity, $V_{max} = 8.5$ nm/s (Fig. 2.2b), by the rate of ATP hydrolysis $k_{cat} = 8.3$ ATP s^{-1} (Fig. 2.5b), yields 1.02 ± 0.03 nm per hydrolyzed ATP. Therefore, together the structural, biochemical, and single molecule evidence suggest that if one ATP is hydrolyzed per ClpX subunit, the fundamental translocation step size must be ~1 nm.

The analysis of burst sizes thus provides direct evidence for how many subunits participate in translocation during a single burst phase. In this context, we analyzed how different ATP concentrations affected the translocation velocity of the motor as well as the distributions of burst sizes and dwell times. As shown in Figure 2.2, translocation velocity of the motor decreases as the [ATP] decreases. Thus, the observed reduction in velocity at limiting [ATP] should be the result from a longer dwell duration, a smaller burst size, or a combination of both. We observed the presence of burst sizes of 2–4 nm when [ATP] >> K_M (Fig. 2.7b). The distribution of burst

sizes has a maximum at ~3 nm, with a correspondingly lower number of ~2 and ~4 nm bursts, and very few 1 nm bursts. In contrast, when [ATP] is near its K_M, i.e. [ATP] = 35 μM, ClpXP translocates mostly in 2 or 3 nm bursts, and bursts of 4 nm are notably absent (Fig. 2.7b). Thus, these results suggest that the number of subunits participating in a single translocation cycle depends on the availability of ATP.

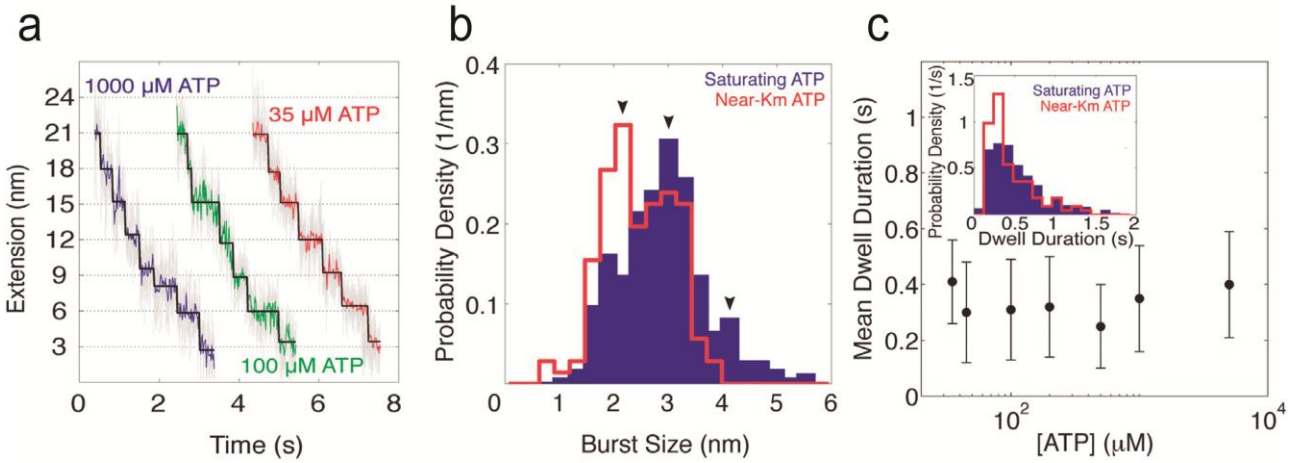

Figure 2.7. (a) Representative trajectories of ClpXP translocating substrate in 3 nm steps at 10–14 pN and different ATP concentrations. Raw data were filtered and decimated to 1250 (in gray) or 50 Hz (in red, blue, green). t test fits to the data are shown in black. **(b)** Burst size distributions for ATP concentrations near K_M (red) and saturating ATP (blue). **(c)** Mean dwell duration (± SEM) plotted against [ATP]. Inset: dwell-time distribution for near-K_M conditions (red) and saturating ATP (blue).

The maximum burst-size of 4 nm suggests that up to four subunits in the hexamer bind and hydrolyze ATP during a single translocation cycle. This is consistent with previous bulk biochemical assays and crystal structures of ClpX (Glynn et al., 2009; Hersch et al., 2005; Stinson et al., 2013) that reveal that—despite being a hexamer—ClpX can bind a maximum of four nucleotides (Fig. 1.1a), explaining the absence of 5 or 6 nm bursts. These findings most likely reflect the state of the ring preceding a 4 nm burst, a state that is only one of a larger ensemble of nucleotide-bound configurations.

These observations establish an upper limit for the number of ClpX subunits that can be coordinated. We then asked if there is a lower limit for the intersubunit coordination of ClpXP. Here we show that the smallest observed burst size is ~ 2 nm (even at limiting [ATP] = 35 μM) which indicates that the most relevant translocation cycle of the ClpX motor involves the coordinated hydrolysis and conformational change of at least two subunits. This result can be best rationalized in the light of two previous observations: i) two different classes of ATP binding sites with different binding affinities have been previously identified in ClpX (Hersch et al., 2005), and ii) recent mutational studies of ClpX have shown strong evidence for a dynamic mechanism of subunit switching, whereby nucleotide binding can affect the affinities of the remaining subunits within the ring (Stinson et al., 2013). Therefore, we propose a model where the affinity of these two subunits that bind ATP first must be significantly higher than the apparent K_M of 35 μM here reported for the entire ClpX hexamer. The notably absence of 4 nm bursts at ATP concentrations near 35 μM indicates that the remaining subunits have a higher K_M

value than the first two high-affinity sites, and therefore contribute to translocation only at saturating [ATP]. In this scenario, we envision that future ClpX crystal structures in the presence of a translocating substrate will likely show two or three subunits bound with a nucleotide, as evidenced from the prevalence of 2 and 3 nm bursts compared to 4 nm bursts.

Together, these observations shed light onto how the coexistence of subunits with high and low ATP affinity affects the dynamics of the translocation cycle, and allow us to propose a model where the burst phase to be initiated with either two ATPs (both binding to high-affinity subunits), three ATPs (two high- and one low-affinity subunits), or four ATPs (two high- and two low-affinity subunits) bound to the motor (Fig. 2.8). These results thus provide direct evidence for the operational flexibility of ClpX during polypeptide translocation.

2.3.5. Number of Rate-limiting Transitions within the Dwell

Next, we analyzed the duration of the cycle time (the sum of the dwell and burst phase duration) at various ATP concentrations to better understand the translocation mechanism of this motor. Surprisingly, we observed that the mean cycle time has no apparent dependence on [ATP]. We found that the mean duration of the dwell phase $< \tau >$ is 350 ± 20 ms in the range between 35 μM and 5 mM (Fig. 2.7c). In addition, the duration of the burst phase contributes to less than ~3% of the cycle time and has a mean duration of less than ~10 ms. Over this range of nucleotide concentrations, the motor translocation rate approximately doubles from 5 to 9 nm/s. Consequently, the observed change in translocation velocity is not due to changes in the mean dwell time, but rather to a systematic increase in motor burst size with increasing [ATP].

To obtain insight into the molecular processes that occur during the dwell time, we calculated the kinetic parameter n_{min}, which is defined as the ratio of the squared mean of dwell times over the variance of the dwell times, $n_{min} = < \tau >^2 / (< \tau^2 > - < \tau >^2)$ (Moffitt et al., 2006; Schnitzer and Block, 1995). It has been shown that this parameter provides a strict lower bound to the number of rate-limiting events during the dwell phase (Moffitt et al., 2006). We sought to understand how the number of rate-limiting events (n_{min}) changes with the [ATP].

At saturating and near-K_M concentrations of ATP, we measured n_{min} = 2.1 ± 0.4 and 2.0 ± 0.6 (SEM), respectively, suggesting that for both conditions there are at least two rate-limiting transitions in the dwell leading up to the burst phase. Similar values of n_{min} = 1.9 ± 0.6 were obtained at the intermediate ATP concentrations of 100 and 200 mM. Therefore, at least two processes—not associated with ATP binding—control the duration of the dwell in the [ATP] range between 35 μM (near K_M) and 5 mM (saturating). It remains to be elucidated if these nonbinding events in the dwell correspond to conformational changes within the ClpX ring that either (1) result from or (2) are completely independent of ATP binding.

2.3.6. An "Internal Clock" Triggers Polypeptide Translocation

Our results provide a model to rationalize the observed invariant dwell-time distribution and the variable burst-size distribution of ClpX as a function ATP concentration. The dwell duration is

largely determined by two slow, non-ATP-binding events. By the time these slow transitions occur, the two high-affinity subunits are ATP bound and, depending on the ATP concentration, one or two of the low-affinity subunits are occupied with ATP as well. Due to the constrained ring geometry, only four of the six subunits can be ATP bound (Glynn et al., 2009), which provides an explanation for why we do not observe bursts of more than 4 nm even at saturating [ATP]. After the motor hydrolyzes all of the bound ATP molecules, Pi release and concomitant subunit power strokes occur near simultaneously around the ring, resulting in a burst size that is proportional to the number of hydrolyzed ATP molecules (Fig. 2.8).

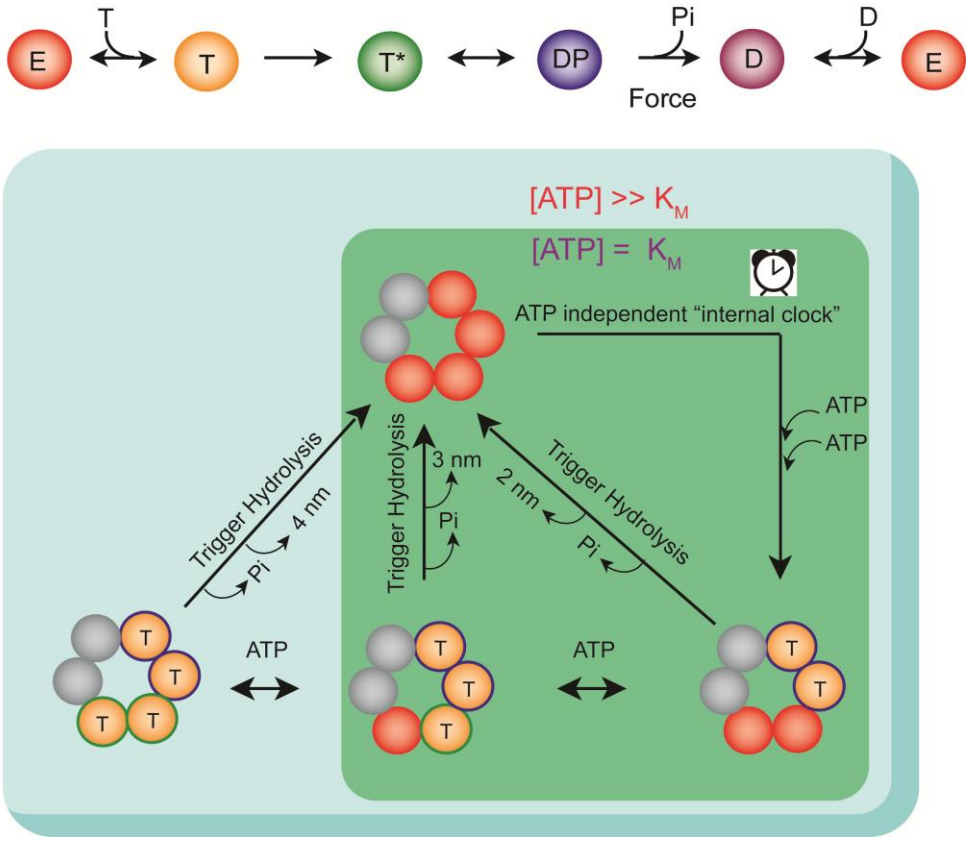

Figure 2.8. Top, the pathway of ATP hydrolysis for a single subunit of ClpX. An empty subunit (E, red) binds ATP (T, orange) and undergoes a tight binding of ATP (T*, green). Then, the subunit hydrolyzes ATP to ADP and Pi (DP, blue), the force-generation step occurs upon phosphate release (D, purple), and ADP dissociates, leaving an empty subunit (E, red).Bottom, schematic depiction of intersubunit coordination at saturating (light green box) and limiting ATP concentrations (dark green box) for one possible scenario depicting sequential ATP binding. The subunits in gray correspond to those that do not bind ATP. During the dwell phase—whose duration is timed by and ATP independent "internal clock"—at least two ATPs are bound to the high affinity subunits (T, blue outline), and additional ATPs can bind to the low affinity ClpX subunits (T, green outline), depending on [ATP]. During the burst phase, the motor hydrolyzes all bound ATPs, releases phosphate, and translocates the substrate by 2, 3, or 4 nm into the central pore.

The essence of this model is that the mean duration of the dwell phase is constant and set by an "internal signal" or "clock", which may or may not follow ATP binding and could, for instance, correspond to the reaching of a strain threshold in the ring or the hydrolysis of the first-bound

ATP. In contrast to this constant average dwell phase, the burst size is variable and proportional to the number of subunits bound to ATP before the clock triggers the initiation of a translocation cycle around the ring. As a result, the ClpXP motor operates at a constant frequency (fixed "rpm") and a variable burst size (different "gears"). Although our current model, depicted in Figure 2.8, suggests a spatial and temporal order of ATP-docking events, future single-molecule studies of ClpX mutants will be required to definitively establish the order of ATP-binding and hydrolysis events around the hexameric ring.

Altogether, these results present a mechanism of translocation that is strikingly different from those of other motors. The well-characterized DNA packaging motor of bacteriophage ϕ29 exhibits a variable [ATP]-dependent dwell time, followed by a constant [ATP]-independent burst size of 10 bp, which reflects a high degree of coordination among the ring subunits that must all load ATP before the motor can initiate translocation (Chistol et al., 2012; Moffitt et al., 2009). In sharp contrast, ClpXP exhibits an ATP-independent cycle time, during which a variable number of ATP molecules bind to the motor, resulting in a distribution of burst sizes.

2.3.7. GFP presents two intermediates as it is unfolded by ClpXP

In order to elucidate the coordination mechanism by which ClpXP successfully unfolds GFP, we characterized the intermediates observed as ClpXP mechanically unfolds GFP (Fig. 2.9a). Unraveling of GFP from the C terminus proceeded via two transient intermediates, with mean lifetimes of 45 ± 10 and 130 ± 15 ms, respectively (Supplementary Figure 2).

By using the wormlike chain (WLC) model of polymer elasticity (Bustamante et al., 1994), we estimated that the transition from the folded state "F" to the first intermediate "I" (F→I) has a contour length increase $\Delta Lc^{F\rightarrow I}$ of 8.3 ± 0.4 nm (SEM) corresponding to the extraction of β strand 11 (β11) from the GFP barrel (Fig. 2.9b-c; See Methods for calculation details). The second transition from "I" to the second intermediate "II" (I→II) has a $\Delta Lc^{I\rightarrow II}$ of 31.2 ± 0.8 nm, and most likely corresponds to the unfolding of β strands 10 through 7 (Fig. 2.9b-c). The last transition from "II" to the unfolded state "U" (II→U) has a $\Delta Lc^{II\rightarrow U}$ of 42.2 ± 0.8 nm and reflects the unraveling of the remaining six β strands, as described previously (Maillard et al., 2011) (Fig. 2.9b-c). The total contour length increase, i.e. from the F state to the U state, is $\Delta Lc^{F\rightarrow U} = (\Delta Lc^{F\rightarrow I} + \Delta Lc^{I\rightarrow II} + \Delta Lc^{II\rightarrow U}) = 82.8 \pm 3.2$ nm, which is in good agreement with the expected value for the complete unfolding of GFP (Fig. 2.9b-c; See Methods).

2.3.8. ClpXP Requires Four Highly Coordinated Power Strokes to Successfully Unfold GFP

Having established the GFP unfolding pathway as well as the effect of [ATP] on the burst size, we asked two important questions about the mechanism by which the motor successfully unfolds protein substrates: i) how are the power strokes of individual subunits coordinated during protein unfolding?, and ii) what is the kinetic competition between the motor translocation bursts and the substrate's resistance to unravel and its tendency to refold? To answer these questions, we first quantified how variations in [ATP] affect the ability of the motor to unfold GFP. We found that reducing [ATP] decreased the probability of GFP unfolding by ClpXP nonlinearly, from a

maximum of 0.6 when [ATP] ≥500 μM to less than 0.1 when [ATP] ≤50 μM (Fig. 2.10a). The nonlinear relationship between GFP unfolding probability and [ATP] suggests that GFP unfolding requires the coordinated and near-simultaneous ATP hydrolysis of multiple ClpX subunits in the ring.

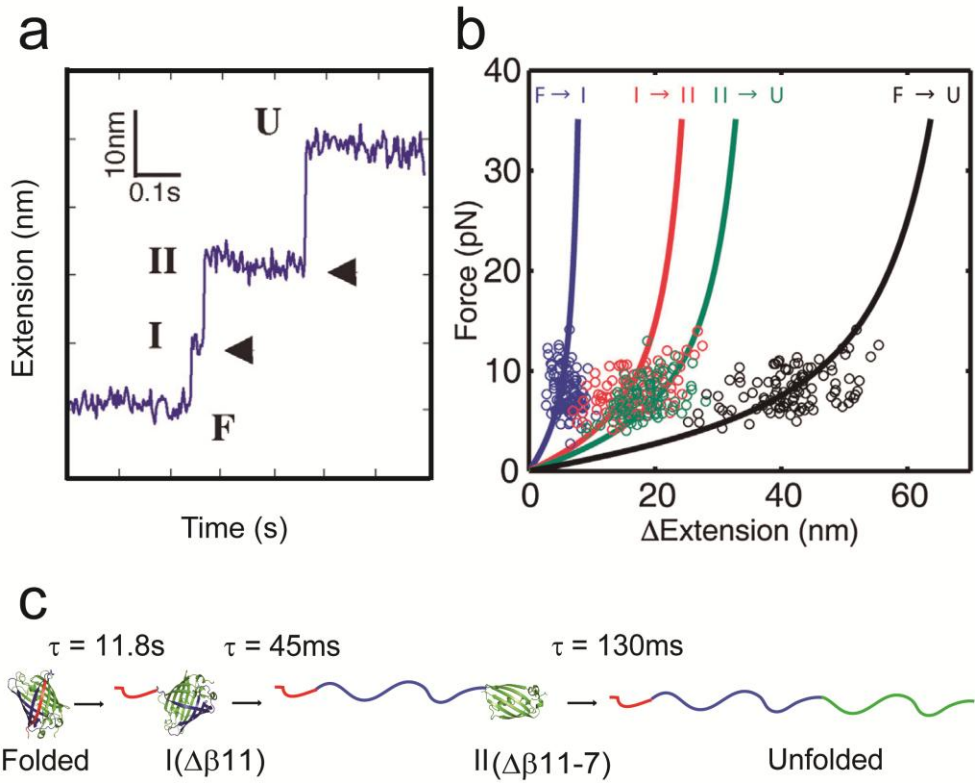

Figure 2.9. (a) GFP unfolding events display two intermediates (arrows) at 300Hz. **(b)** Plot of force versus change in extension for the transition to the first intermediate F/I (blue), the second intermediate I/II (red), the unfolded state II/U (green), and the sum of all transitions F/U (black). See Methods for details on the derivation of these values. **(c)** Mechanism of GFP unfolding by ClpXP at saturating [ATP].

Interestingly, at [ATP] ≤200 μM, we detected small unfolding and refolding events before ClpXP completely unraveled GFP (Fig. 2.10b). The change in contour length of these unfolding/refolding transitions is similar to $\Delta Lc^{F\rightarrow I}$, suggesting that these events most likely correspond to the extraction and quick refolding of β11. Analysis of these reversible transitions revealed that β11 snaps back into the GFP barrel with a mean refolding time constant ~230 ms at forces between 7 and 9 pN (Fig. 2.10c). These results provide direct experimental evidence of the molecular tug-of-war between the motor, attempting to unravel folded structures, and a substrate with a strong tendency to refold. Hence, protein-unfolding machines have to perform not only the thermodynamic function of mechanically destabilizing the native state, but also the kinetic task of quickly capturing the unstructured polypeptide before it can refold.

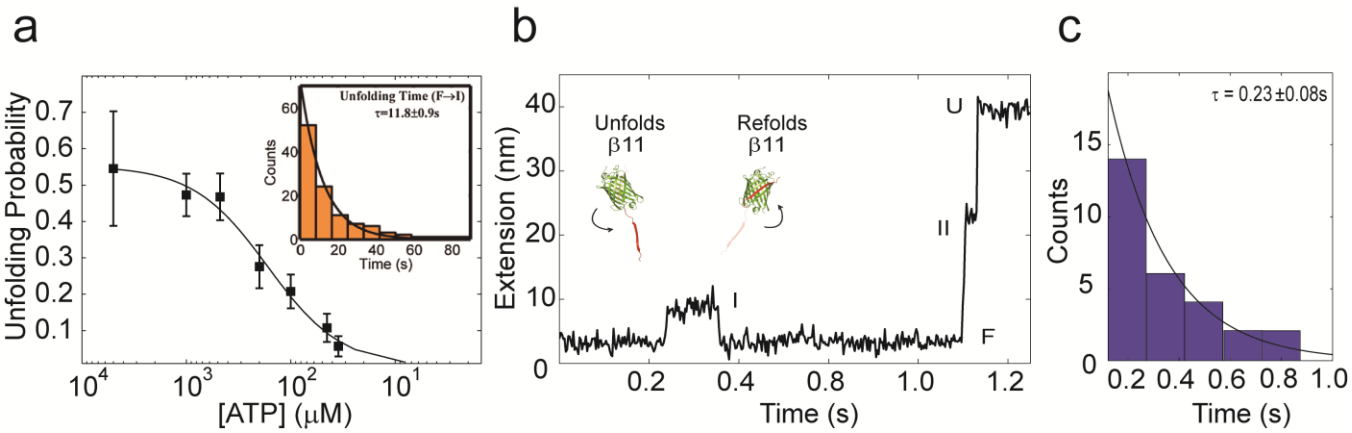

Figure 2.10. (a) Probability of GFP unfolding (mean ± counting error) as a function of [ATP]. Inset, distribution of lifetimes of the folded state, which corresponds to the GFP unfolding time. **(b)** Trajectory at [ATP] = 200 μM illustrating the ClpXP-induced unfolding and refolding of β11. **(c)** β11 refolding time fits well to a single-exponential with a $\tau = 0.23 \pm 0.08$ (mean ± SEM).

When [ATP] >> K_M, ClpXP is able to move in bursts of 4 nm during a single translocation cycle. Such coordinated translocation is sufficient to trap most of the dislodged β11 and prevent its refolding. These observations indicate that the efficient unfolding of GFP by ClpXP requires not only a 4 nm burst, but also this burst to occur faster than the refolding time of β11 (<240 ms). Using the distribution of burst size and dwell duration determined here, we estimated the probability of ClpXP taking a 4-nm burst in less than 240 ms to be on average 0.031. This result indicates that ClpXP must pass through ~33 translocation cycles before it can unfold GFP and trap the first intermediate for subsequent unfolding. Multiplying 33 translocation cycles by the mean duration of the dwell (~0.35 s) predicts a mean GFP unfolding time of ~11.5 s, which agrees well with the observed mean unfolding time obtained from the distribution of GFP unfolding times, $< \tau > = 11.8 \pm 0.9$ s (Fig. 2.10a), as well as from previous single-turnover GFP degradation measurements (Martin et al., 2008c).

At [ATP] ≈ Km, ClpXP moves in bursts of at most 3 nm, which may be sufficient to promote the extraction of β11 from the GFP barrel (ClpX succeeds in carrying out the thermodynamic task) but are too small to prevent the refolding of β11 (ClpX fails to accomplish the kinetic task). Thus, under limiting [ATP] the kinetic competition between ClpXP attempts to translocate the unfolded region and the tendency of that region to refold greatly reduces the unfolding efficiency of the motor.

The unfolding mechanism proposed here provides a framework to understand how ClpXP successfully unfolds stable protein substrates. The ability of the motor to bind four ATP molecules allows it to translocate in large bursts and thus destabilize and rapidly trap partially unfolded intermediates. For instance, to successfully unfold GFP, ClpX subunits must near-simultaneously take a 4 nm burst, which results in the extraction and translocation of β11 from GFP before this strand can refold onto the β barrel. At saturating [ATP], the time required for ClpX-induced unfolding of GFP is determined by the time that passes before the motor makes a 4 nm burst. In contrast, ClpX rarely unfolds GFP at ATP concentrations near K_M because hydrolysis under these conditions is always triggered before four ATP molecules can bind to the

motor. Our results reveal that the decreased probability of the motor taking a 4 nm burst is responsible for the observed nonlinear decrease of GFP unfolding probability with the ATPase rate.

The mechanisms described in this chapter thus provide important insights into the operating principles of ATP-dependent proteases and may have critical implications for the understanding of other ring-shaped ATPases of the AAA+ and RecA families in general.

2.4. METHODS

2.4.1. Sample Preparation

Biotinylated ClpX single-chain hexamers, GFP-titin^{CM} I_{27} fusion proteins, and 3 kbp dsDNA handle for protein attached via ybbR tag/Sfp system were prepared as described previously (Maillard et al., 2011; Martin et al., 2005) .Tethers were assembled in a buffer (25 mM HEPES-KCl [pH 7.4], 20 mM $MgCl_2$, 100 mM KCl, and 0.5 mM EDTA) supplemented with (1) [ATP] = 35 μM, 45 μM, 100 μM, 200 μM, 0.5 mM, 1 mM, and 5 mM with ATP regeneration system (Kenniston et al., 2003), (2) [ADP] = 10 μM, 20 μM, 50 μM, 100 μM, and 250 μM in the presence of [ATP] = 100 μM, 200 μM, 500 μM, 1,000 μM and [Pi] = 5 μM, (3) 5 μM, 5 mM, 10 mM NaPO4 (Sigma), (4) [ATPγS] = 25 μM, 50 μM, 100 μM, 175 μM, and 250 μM (Roche) in the presence of [ATP] = 500 μM. All single-molecule experiments required 500 nM of ClpP for the formation of the ClpXP complex (K_D = 90 nM) (Joshi et al., 2004).

2.4.2. Data Collection

Two different dual-trap optical trapping instruments with 1,064 nm laser were employed (Moffitt et al., 2006). The unfolded polypeptide contour length was calculated as previously described (Bustamante et al., 1994; Cecconi et al., 2005; Maillard et al., 2011) by using the worm like chain model for polymer elasticty. Using 0.9 mm polystyrene beads, an oxygen scavenging system was added to prevent the formation of the reactive species singlet oxygen (100 mg/ml glucose oxidase, 20 mg/ml catalase, 5 mg/ml dextrose; Sigma-Aldrich) (Moffitt et al., 2009).

2.4.3. Pause detection and translocation velocity calculation

Pauses were removed from velocity using a previously described modified Kalafut-Visscher (KV) algorithm with a pause threshold and penalty (Chistol et al., 2012; Kalafut and Visscher, 2008). A cutoff threshold was calculated by taking three standard deviations of a gamma-fitted distribution. Velocity was calculated as the end-to-end distance $\Delta x/\Delta t$. To calculate pause-free velocity, the selected pauses were removed in the Δt component. Furthermore, we analyzed the pause density and frequency of ATPγS using the modified KV algorithm. ATPγS-induced pauses were extracted by removing ATP-only dwells using a double exponential fit with one time constant fixed to the mean dwell duration measured at saturating [ATP]. The unfolding events and its related measurements were measured by a previously described method (Maillard et al., 2011).

2.4.4 Step fitting methodology

Steps and dwells were analyzed using pairwise distribution and t test (Moffitt et al., 2009). Data were filtered to 15–25 Hz and binned into 0.3 and 0.4 nm for the pairwise distributions. Regions of traces with high signal-to-noise ratio exhibited step-like patterns in translocation regions. Stepping correlations were confirmed by visualizing the pair-correlation function of data points within the selected region, which shows the distribution of pair distances between data points. Confirmed regions of stepping were fit using a sliding window t-test to detect the change points that occur during the burst phase of translocation.

2.4.5 Measurements of ATP-hydrolysis rate

The ATP hydrolysis rate of ClpXP was measured in bulk using an NADH-coupled ATP-regeneration system as previously described (Martin et al., 2008b; Maillard et al., 2011). Assembled hexamers of ClpX (0.3 μM) where mixed with ClpP (1.5 μM) in a ClpX-100 buffer (25 mM HEPES pH 7.6, 20 mM $MgCl_2$, 100 mM KCl, and 0.5 mM EDTA) containing an NADH-coupled regeneration system (3 U/mL pyruvate kinase, 3 U/mL lactate dehydrogenase, 1 mM NADH, and 7.5 mM phosphoenolpyruvate). The ATP-hydrolysis rate of ClpX was measured both in the presence and absence of 10 μM titinCM-ssrA by monitoring the absorbance of NADH (340 nm) at 30°C. The observed ATPase rates were consistent with previous studies (Martin et al., 2005; Aubin-Tam et al., 2011).

2.4.6 Measurements of ATPγS-Hydrolysis Rate

The ATPγS-hydrolysis rate of ClpXP was measured using thin-layer chromatography of ^{35}S-labeled ATPγS. Hydrolysis was measured at room temperature by mixing 0.3 μM single-chain ClpX hexamer and 1.5 μM ClpP with variable concentrations of ATPγS (5-800 μM) and trace amounts (70 nM) of ^{35}S-labeled ATPγS (Perkin-Elmer Inc.) in ClpX-100 Buffer (see above), with or without ssrA-titinCM (10 μM). One-microliter aliquots from each 20 ml reaction were removed at different times and immediately quenched with 2.5 ml of stop buffer (50 mM Tris-HCl pH 7.6, 100 mM EDTA, 20 mM ATPgS, and 20 Mm Na_3PO_3S). Each quenched sample was spotted onto a plastic-backed PEI-cellulose sheet (J.T. Baker Inc.) and chromatographed at room temperature in 1.5 M formic acid and 0.4 M LiCl. After the sheet was dried, radioactivity in each spot was quantified using a Molecular Dynamics Phosphorimager. In the control experiment with only ^{35}S-labeled ATPgS, we observed that the single radioactive spot, corresponding to the un-hydrolyzed ^{35}S-ATPgS, hardly migrated from its loading position (Supplemental Figure 1). In the presence of ClpXP, we observed a second, fast-migrating radioactive spot whose intensity increased in a time-dependent fashion (Supplemental Figure 1). This spot corresponds to ^{35}S-PO_3 that is released by ClpXP upon ^{35}S-ATPγS hydrolysis, and its absence in samples without ClpX indicates that spontaneous hydrolysis of ATPγS is negligible under our experimental conditions.

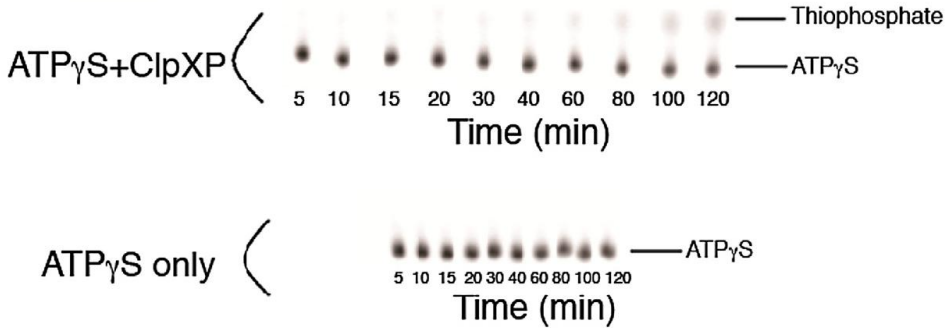

Supplemental Figure 1. Thin-layer chromatography assay of ^{35}S-labeled ATPγS hydrolysis by ClpXP. ^{35}S-ATPγS was incubated with 0.3 μMClpX and 1.5 μMClpP (top) or buffer only (bottom) for the time indicated, before being quenched with 2.5 volumes of stop buffer and spotted on TLC plates. The positions of ATPγS and PO_3S are indicated.

2.4.7 Motivation for Fitting ATPγS-Induced Pauses to the Hill Equation

The reaction pathway for an ATPγS-induced pause can be written as

$$Ma + n(ATP\gamma S) \leftrightarrow Mp, \quad (1)$$

where *Ma* is the actively translocating state of the motor, *Mp* is the ATPγS-induced paused state of the motor bound to the analog, and *n* is the number of ATPγS molecules required to induce a pause. The apparent dissociation constant Kd of n(ATPγS) molecules binding to the motor can be expressed as

$$Kd = \frac{P(Ma)[ATP\gamma S]^n}{P(Mp)}, \quad (2)$$

where *P(Ma)* is the probability of the motor being in an actively translocating state and *P(Mp)* is the probability of the motor being in an ATPγS-induced paused state. The pause density *PD([ATPγS])*, or number of pauses per unit length of translocated polypeptide, should be directly proportional to *P(Mp)*. Because intrinsic pauses in the absence of ATPγS are infrequent—on average one pause per 50 nm of translocated polypeptide (Maillard et al., 2011)—the approximation is appropriate.

$$P(Ma) + P(Mp) = 1, \quad (3)$$

Using Equation 3 in Equation 2 to eliminate *P(Ma)* results in

$$PD([ATP\gamma S]) \approx P(Mp) = \frac{[ATP\gamma S]^n}{Kd + [ATP\gamma S]^n}. \quad (4)$$

Hence, *PD([ATPγS])* takes the form of the Hill equation with n reflecting the number of ATPγS molecules that must bind to the motor in order to induce a pause.

2.4.8 Spatial/Temporal Resolution of the Optical Tweezers

The lifetime distributions of each intermediate in GFP unfolding (Supplemental Figure 2) follow a single exponential decay function. To calculate the probability of observing an intermediate with duration t we must first transform this function into its corresponding probability density function, which is expressed as

$$f(x) = ae^{-at}, \quad (5)$$

where $a \geq 0$, and corresponds to the inverse of the time constant in seconds, and $x = [0, \infty >$. The probability of observing a GFP unfolding intermediate whose lifetime is between 0 and τ can be calculated by obtaining the area under the curve given by the following expression:

$$P(0 \leq x \leq \tau) = \int_0^{\tau} ae^{-ax}\,(dx), \quad (6)$$

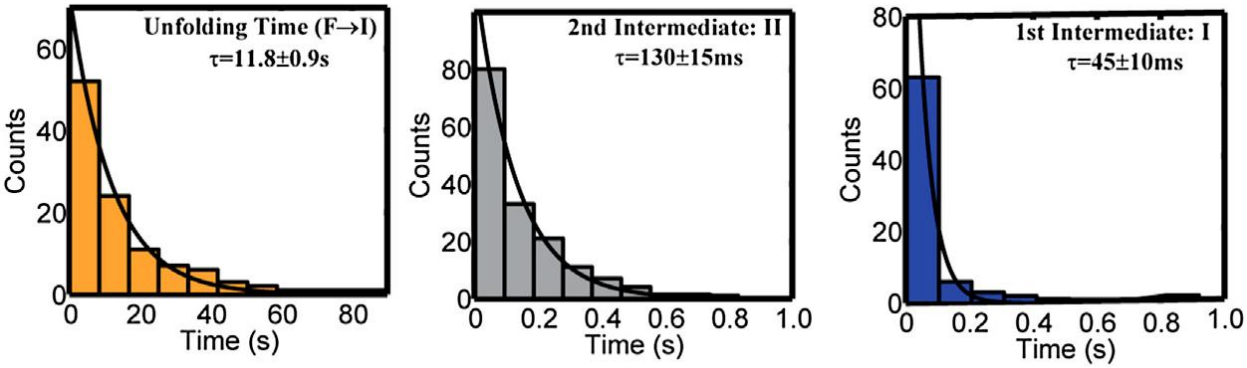

Supplemental Figure 2. Distribution of lifetimes for the folded state, first and second intermediates during GFP unfolding by ClpXP. The leftmost panel shows the distribution of lifetimes of the folded state, which corresponds to the GFP unfolding time. The distribution of lifetimes for the first and second intermediate (middle and right panel, respectively) was well fitted by a single-exponential function. The first intermediate has a lifetime of 45 ± 10 ms, whereas the second intermediate exhibits a lifetime of 130 ± 15 ms. All fitted values are mean ± SEM.

Using the time constants from the exponential fit of the distributions in Supplemental Figure 2, we can use the Equation 6 to test if the apparent absence of the first or the second intermediate in some traces is because i) they may be shorter in duration than the detection limit of the instrument, or ii) GFP unfolding may follow multiple pathways where the first or second intermediates may not be obligatory transitions in this process.

To address the first scenario, we established the spatial/temporal detection limits of our instrument. We calculated the fluctuations of the noise at different forces and different bandwidths through the analysis of the power spectrum of a trace where ClpXP translocation has been stalled with 100% ATPγS. Because we analyzed the GFP-unfolding intermediates at 300Hz (i.e., 300 data-points per second), we found that fluctuations of the noise at this bandwidth are approximately 3nm. With this value, we calculated the signal-to-noise ratio (SNR), which corresponds to the size of the signal divided by the size of fluctuations of the noise. We included this SNR in the following expression:

$$\Delta l \geq \frac{\sqrt{2KTN\gamma}}{\sqrt{<\tau>}\, ktether} SNR, \quad (7)$$

which predicts the minimal duration of a step that is required to be observed given its size. Here, Δl corresponds to the mean size of the step, K is the Boltzmann constant, T is the temperature, N is the number of uncorrelated measurements per average dwell, γ is the drag coefficient of the beads, $<\tau>$ is the mean duration of a dwell, *ktether* is the stiffness of the tether, and *SNR* is the signal-to-noise ratio that we have calculated (Moffitt et al., 2008). Using this expression for a burst size of 8.3nm (corresponding to the mean extension of the first rip), we found that its corresponding mean dwell duration (first intermediate duration) should be at least of 30 ms to be observed at 300Hz. With this threshold, we calculated the theoretical probability of not observing an intermediate due to limitations of the instrument by calculating the probability $P\ (0 \leq x \leq 30)$ using the expression in Equation 6. Finally, we compared this theoretical probability with the experimental probability of not observing the first or second intermediate in our traces. In other words, based on their lifetimes, we estimated the probability of missing the first and second intermediates in the unfolding trajectories to be 0.52 (0.44 0.65, Confidence Interval 95%) and 0.15 (0.13 0.19, Confidence Interval 95%), respectively. The predicted numbers were in good agreement with the fraction of single-molecule traces in which we did not observe either intermediate (0.65 ± 0.11 and 0.15 ± 0.03 for the first and second intermediate, respectively). Thus, the simplest conclusion is that the four different unfolding scenarios described in Supplemental Figure 3 result from a single ClpXP-mediated GFP unfolding pathway that has two obligatory intermediates rather than a branched unfolding pathway. In conclusion, a subset of GFP unfolding intermediates was not detected due to instrument limitations.

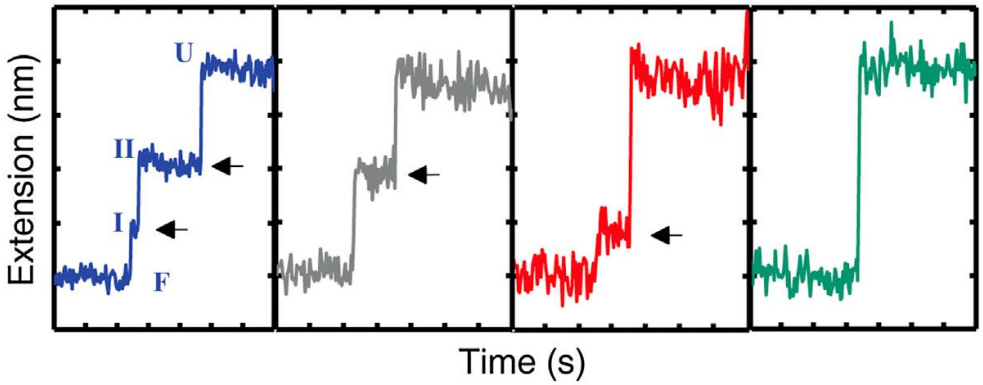

Supplemental Figure 3. The rips (sudden increases in bead extension) during GFP-unfolding revealed three well-defined transitions, indicating the presence of two unfolding intermediates at saturating [ATP]. The second intermediate was observed in 90% of all traces (gray), while both intermediates were present in only 40% of them (blue). We rarely observed traces displaying only the first intermediate (red) or no intermediates at all (green) (10%).

2.4.9 Identifying the Structures of ClpXP-Mediated GFP Unfolding Intermediates

The crystal structure of GFP (PDB ID: 1GFL) was used to map the observed rip size of each unfolding transition in our traces to the corresponding extraction of GFP structural elements using a previously established methodology (Dietz and Rief, 2004; Maillard et al., 2011). The observed change in contour length DLC could be written as

$$\Delta Lc = \underbrace{(m_i)(L_{aa})}_{Lc} - \left(X^F_{m_i+1:N} - X^F_{m_{i-1}+1:N}\right). \qquad (8)$$

The first term (*Lc*) describes the actual contour length of each unfolding transition, where m_i is the number of residues that unfold during the transition to the ith state, and *Laa* is the contour length of one amino acid (0.365 nm/aa). The second term comprises the shift in the distance between the last structured residue at the N terminus (residue position 1) and the last structured residue at the C terminus as the transition occurs. Both distances ($X^F_{m_i+1:N}$ and $X^F_{m_{i-1}+1:N}$) are determined from the reported crystal structure coordinates.

Equation 8 provides an iterative means to determine which structural elements of GFP were extracted during each intermediate transition (Fig. 2.9). The force at which each unfolding transition occurred was plotted as a function of its corresponding change in extension in nanometers. Using the worm-like-chain model of polymer elasticity (Bustamante et al., 1994), a force extension curve was generated to calculate the *Lc* of an unfolding transition occurring at each amino acid position from Equation 8 (by iterating the value of *m*). Selecting the contour length (*Lc*) that minimized the root-mean-square deviation (RMSD) from the WLC fit allowed us to establish optimal location of the unfolding segment for each intermediate (Supplemental Figure 4).

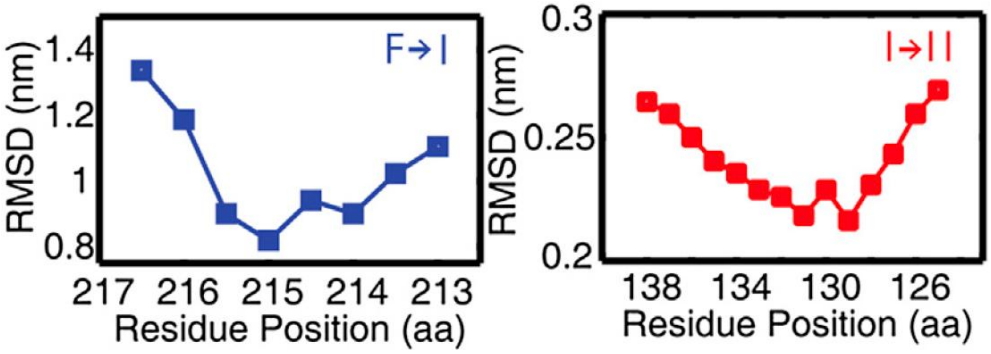

Supplemental Figure 4. Mapping the measured changes in contour length for each intermediate transition to the extracted structural elements of GFP. Root-mean-square-deviation (RMSD) of the measured extension changes from the predicted WLC extension change as a function of linker residue position for the transition to the first intermediate (left) and the second intermediate (right). The transition to the first intermediate is identified to be the extraction of β11, and the transition to the second intermediate corresponds to the extraction of β10-7.

This approach provided an unambiguous identification of the first intermediate, namely, a state with β-strand 11 (β11) extracted from the GFP barrel. For the second intermediate, however, the RMSD versus amino acid position yielded two minima with similar RMSD values (Supplemental

Figure 4): one solution corresponded to the extraction of β10-7 and a second solution to the extraction of β10-6. A simple line of reasoning allowed for distinguishing between these two possibilities. When GFP unfolding occurred in the absence of the first small intermediate (Supplemental Figure 3), the RMSD versus amino acid position had a single minimum corresponding to the extraction of β11-7. Importantly, the distribution of intermediate lifetimes was identical to the distribution of second-intermediate lifetimes when the first intermediate was observed (Supplemental Figure 5), suggesting also similar structural stability of the unfolded intermediate. Thus, the most parsimonious explanation is that the second unfolding transition both in presence and absence of the first one corresponds to the same structural intermediate, with b11-7 unraveled from the GFP barrel.

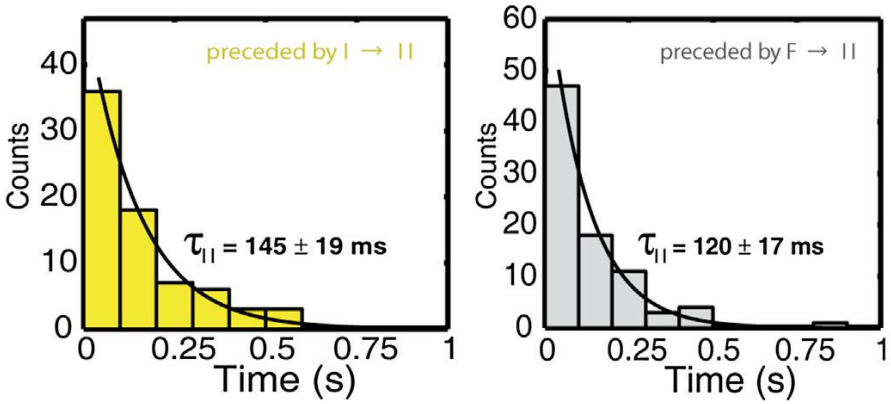

Supplemental Figure 5. Lifetime distribution of the second intermediate when the preceding transition was observed to be (H) I→II, or (I) F→II.

2.4.10 Prediction of GFP Unfolding Time Based on Burst Size Distribution and Dwell Durations

Using the distribution of burst size and dwell duration (Fig. 2.7b-c), we estimated the probability of ClpXP taking a 4 nm burst in less than 240 ms (mean refolding time of β11 from Fig. 2.10c) to be on average 0.031 (0.018 - 0.046, confidence interval [C.I.] to 95%). This result indicates that ClpXP must pass through on average ~33 translocation cycles before it can unfold GFP and trap the first intermediate for subsequent unfolding. Multiplying 33 translocation cycles by the mean duration of the dwell (~0.35 s) predicts a mean GFP unfolding time of 11.5 s (7 s - 21 s, C.I. 95%), which agrees very well with the mean time constant obtained from the distribution of GFP unfolding times, $< \tau >$ = 11.8 ± 0.9 s (Fig. 2.10a).

— Chapter 3 —

Mechanochemical Coupling and Power Efficiency

The results & models described in this chapter have been adapted and modified from the following publication:

Rodriguez-Aliaga, P., Ramirez, L., Kim, F., Bustamante, C., and Martin, A.
"Substrate-translocating loops regulate mechanochemical coupling and
power production in AAA+ protease ClpXP."
Nature Structural & Molecular Biology. 23: 974–981, 2016.

3.1. SUMMARY

ATP-dependent proteases of the AAA+ family, including *Escherichia coli* ClpXP and the eukaryotic proteasome, contribute to maintenance of cellular proteostasis. ClpXP unfolds and translocates substrates into an internal degradation chamber, using cycles of alternating dwell and burst phases. The ClpX motor performs chemical transformations during the dwell and translocates the substrate in increments of 1–4 nm during the burst, but the processes occurring during these phases remain unknown. Here we characterized the complete mechanochemical cycle of ClpXP, showing that ADP release and ATP binding occur non-sequentially during the dwell, whereas ATP hydrolysis and phosphate release occur during the burst. The highly conserved translocating loops within the ClpX pore are optimized to maximize motor power generation, the coupling between chemical and mechanical tasks, and the efficiency of protein processing. Conformational resetting of these loops between consecutive bursts appears to determine ADP release from individual ATPase subunits and the overall duration of the motor's cycle.

3.2. BACKGROUND AND QUESTIONS TO ADDRESS

In the previous chapter we described important and novel aspects of the operation of ClpXP, which were not accessible by traditional bulk or structural studies. By using single-molecule assays with optical tweezers, it was established that substrate translocation by ClpXP is composed of two phases: a "dwell" or stationary phase, where ClpXP does not move its substrate, and a "burst" phase, wherein ClpXP translocates the substrate in increments of 1, 2, 3 or 4 nm, resulting from the near-simultaneous ATP-driven conformational changes of 1, 2, 3, or 4 ClpX

subunits, respectively (Aubin-Tam et al., 2011; Maillard et al., 2011; Sen et al., 2013) (Fig. 2.7b). Furthermore, it was observed that translocation is occasionally interrupted by pauses longer than 1s, during which the motor temporally accesses a state off the main translocation pathway (Maillard et al., 2011), as shown by the inverse correlation between the translocation velocity and the pause density (Maillard et al., 2011).

Perhaps the most striking finding described in Chapter two refers to the unique translocation mechanism of ClpXP, which shows that while the ClpXP burst size is variable, the mean dwell duration between individual bursts is constant (Fig. 2.7c) (Sen et al., 2013). This mechanism deviates significantly from those of canonical ring-shaped molecular machines such as the ϕ29 DNA-packaging motor (Chistol et al., 2012; Moffitt et al., 2009) and the F1-ATPase rotary motor (Adachi et al., 2007), which display constant translocation bursts followed by dwells of variable length. Yet, the underlying molecular processes behind this distinct ClpXP operation remain unknown. In this context, this chapter aims to address the following points:

- It has been shown in that, within the ATP cycle, Pi relase is coupled to the force-generating step, and therefore occurs during the burst phase (Fig. 2.3 and 2.4) (Sen et al., 2013). However, to understand the operating principles of the motor it is central to dissect the complete mechanochemistry of the motor. Here we set out to establish the location and order of each transition of the ATP-hydrolysis cycle—i.e. ATP binding, ATP hydrolysis, and ADP release—within the dwell/burst cycle of the motor.

- In Chapter 2, it was shown that the dwell phase is timed by an "internal clock" that is insensitive to [ATP] (Fig 2.7c). Here we aim to establish the identity of this "internal clock", and dissect the molecular mechanism by which it determines the duration of the dwell. Similarly, here we seek to establish the molecular processes that govern the burst phase.

- It was shown that binding of more than one ATPγS molecule to the motor is required to stall the motor (Fig. 2.6b-c). In order to understand how many subunits are coordinated during ATP hydrolysis, here we aim to establish the exact number of ATPγS molecules that need to bind to the motor to induce a translocation pause.

- In Chapter two we showed evidence supporting the coupling between the mechanical and the chemical cycles of the motor; however, it remains unclear what determines the coupling efficiency. Here we aim to establish the molecular processes that determine the mechanochemical coupling, and the underlying molecular processes that regulate it.

- Translocation is the fundamental activity of the ClpX, which is driven by loops located along its axial pore. Interestingly, the amino acid sequence of this translocating loops is highly conserved among bacterial, yeast, and even human AAA+ proteases. The reason behind this interesting coincidence is unknown. Here we investigate what are the functional attributes and advantages conferred by the amino acid identity in these translocating loops, in order to understand why evolution may have selected such sequence.

- Our results in Chapter 2 indicate that Pi release is coupled to the power stroke of the motor. However, the motor must reset both its ATP cycle as well as the conformation of its translocating loops in order to proceed with a subsequent translocation cycle. Here we set out to dissect the resetting mechanism of the motor.

- Based on our results, we presented in Chapter 2 a burst-size dependent model for GFP unfolding by ClpXP. Here we explore whether the burst size is the only feature important to drive substrate unfolding, or if instead it requires synergy with other properties of the motor, such as grip of the substrate or pulling rate.

To address these questions, we analyzed the effect of ATP analogs and ClpX mutations on the operation and intersubunit coordination of ClpXP by using single-molecule assays with optical tweezers. This chapter describes the results from these experiments, and presents ClpXP as a motor that employs a novel mechanism of translocation that significantly deviates from canonical motor mechanisms.

3.3. RESULTS & DISCUSSION

3.3.1. ATP hydrolysis occurs in the burst phase

To characterize the mechanochemical cycle, we inhibited hydrolysis in different numbers of ClpX subunits by using various concentrations of ATPγS—an ATP analog hydrolyzed ~ 90 times slower than ATP (Fig. 2.5b-c) (Sen et al., 2013), and analyzed its effects on the dwell and burst phases. We reported previously that the addition of ATPγS in the presence of ATP induces translocation pauses, whose duration and frequency increase with the ATPγS concentration (Fig. 2.5a and 2.6) (Sen et al., 2013). It is noteworthy that those ATPγS-induced pauses occur with equal probability over the entire length of the substrate polypeptide and are not significantly affected by sequence features.

First, we determined how many subunits needed to bind ATPγS to induce a translocation pause. Because only four of the six ATPase sites in ClpX can bind nucleotide in every cycle (Glynn et al., 2009; Hersch et al., 2005), the probability of binding *i* or more ATPγS molecules to the motor is given by

$$\sum_{i}^{4} \frac{4!}{i!(4-i)!} p^{i} q^{4-i},$$

where *p* is the fraction of all nucleotide-bound subunits that is occupied with ATPγS at particular ATPγS and ATP concentrations, and $q = 1 - p$ (See Methods for calculation details). Because bound ATPγS cannot be readily exchanged for ATP—as shown by the low nucleotide off-rate after initial binding (Hersch et al., 2005; Martin et al., 2005) and by the observation that ATP tight-binding is the first irreversible step in the ATPase cycle of ClpX (Sen et al., 2013)—it is therefore possible to directly correlate ATPγS occupancy of the motor with the probability of entering a pause. As shown in Figure 2.6a, the probability that the motor enters into a pause is 50 % at [ATPγS] = 200μM and [ATP] = 500μM (Sen et al., 2013). Using this information here we calculated the exact number of ATPγS molecules bound to the motor required to induce such a pause. We found that under the same buffer conditions the probability of binding two or more

ATPγS molecules to ClpX is also ~ 50 % (Fig. 3.1). This coincidence between the pausing probability of the motor with its ATPγS occupancy leads us to conclude that binding of two or more subunits to ATPγS temporarily stalls the motor.

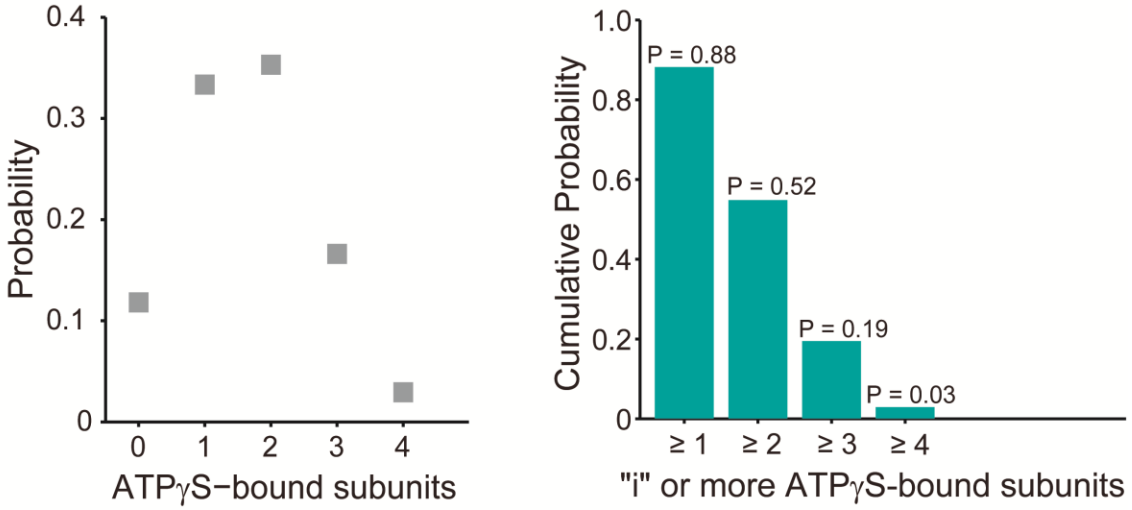

Figure 3.1. Left, individual probability for certain numbers of ATPγS molecules bound to the motor under the same buffer condition. See Methods for calculation details. Right, Cumulative probability of "*i*" or more ATPγS molecules bound to the motor at [ATP] = 500 μM and [ATPγS] = 200 μM.

Next, we analyzed the effect of ATPγS on the dwell duration and the burst size during pause-free translocation. While the mean dwell duration remained unchanged, the mean burst size decreased with increasing [ATPγS] (Fig. 3.2), as indicated by the absence of 4-nm bursts and the increase of 1-nm bursts.

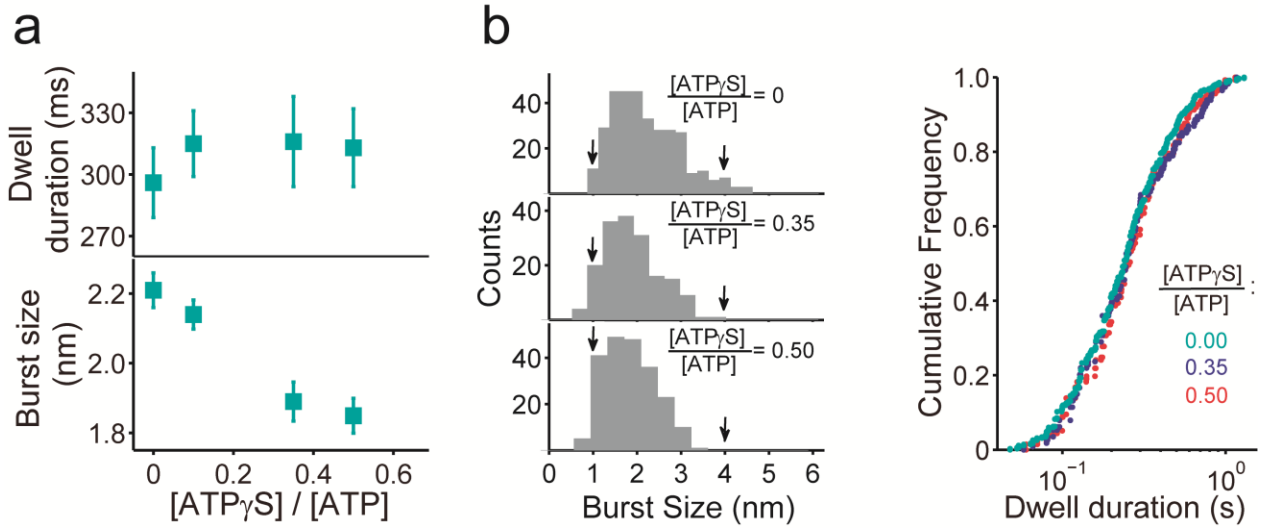

Figure 3.2. **(a)** Dependence of the dwell duration and burst size on [ATPγS] (mean ± SEM). **(b)** Distribution of bursts sizes (n = 1154 bursts) and dwell durations (*n* = 1060 dwells) at increasing ratios of [ATPγS] / [ATP]. The arrows indicate the bursts whose populations increase (1nm burst) or decrease (4nm bursts) with increasing [ATPγS].

We reasoned that ATPγS reduces the mean burst size likely because it decreases the number of subunits that can bind and hydrolyze ATP every cycle. Since under our experimental conditions the probability of one or more ATPγS molecules binding to ClpXP is ~ 90% (Fig. 3.1), the absence of 4-nm bursts is likely due to the presence of at least one ATPγS-bound subunit in the hexamer during every cycle. Thus, although binding of a single ATPγS cannot induce a pause, it hinders the binding of an ATP molecule to the motor and thereby reduces the burst size. Based on these observations we can conclude that the burst size reflects the number of ATP-loaded ClpX subunits during a particular cycle.

Having established that binding of two or more ATPγS molecules to the ClpX motor causes an ATPγS-induced pause, we sought to utilize these pauses for determining where in the dwell/burst cycle ATP hydrolysis occurs. We observed that ATPγS-induced pauses are both preceded and followed by bursts of only 1 or 2 nm, with 3 and 4-nm bursts being notably absent (Fig. 3.3a). This behavior is consistent with a model in which one or two subunits hydrolyze ATP and translocate the substrate, before the ATPγS-bound subunits attempt to hydrolyze and induce a pause that terminates the ongoing burst. The burst subsequent to the ATPγS-induced pause would also be truncated, because the ATPγS-bound subunits were not available for ATP binding in that following cycle. ATP hydrolysis thus appears to occur during the burst phase, which is further supported by our finding that the addition of ATPγS has no effect on the dwell duration (Fig. 3.2). Moreover, the existence of smaller bursts before an ATPγS-induced pause (Fig. 3.3a) suggests that hydrolysis events are interlaced with the power-stroke-generating release of phosphate (Fig. 3.7b), i.e. successful ATP hydrolysis in a ClpX subunit is immediately followed by phosphate release, conformational changes, and substrate translocation by a 1-nm increment, before hydrolysis in a neighboring subunit is initiated.

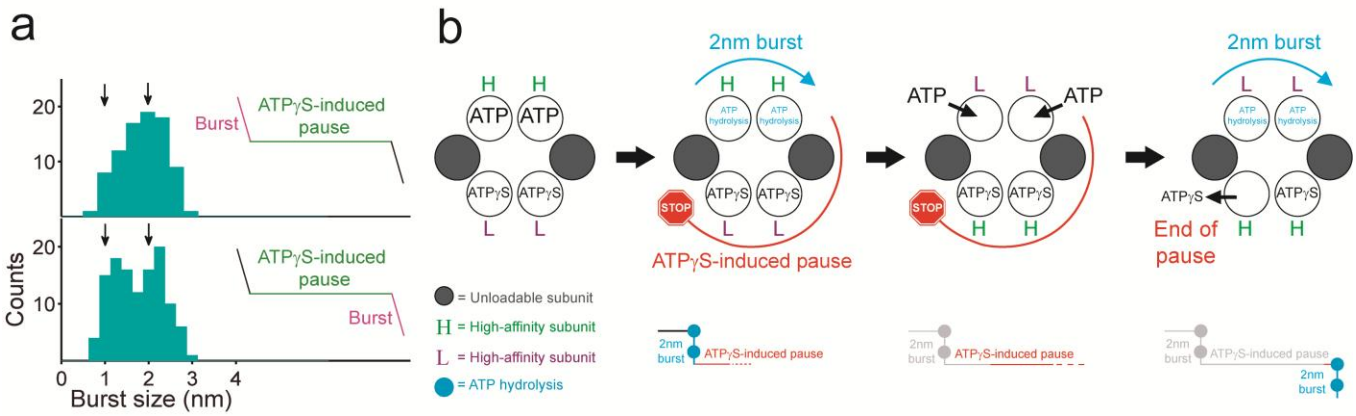

Figure 3.3. **(a)** Size distribution of the bursts that precede (*Top*, *n* = 98 bursts) or follow (*Bottom*, *n* = 118 bursts) an ATPγS-induced pause. (b) ATP-hydrolysis-based Switching Model. For a particular cycle, binding of ATP to the two high-affinity sites and ATPγS to the two low-affinity sites would lead to a 2-nm burst followed by an ATPγS-induced pause. During this pause, the two subunits already pre-bound with ATPγS may switch to become the high-affinity sites, and one or two of the four remaining subunits could bind ATP with low affinity. The onset of the subsequent burst would be determined by the off-rate of ATPγS from the high-affinity sites(Sen et al., 2013), which explains the observed pause duration of more than 1 s, and the burst size would again be at maximum 2 nm contributed from the ATP-hydrolyzing subunits.

It has been proposed that nucleotide binding induces asymmetry in the ClpX hexamer, with two high-affinity, two low-affinity, and two unloadable sites, and that subunits may convert between these states through conformational switching after each ATPase cycle (Hersch et al., 2005; Stinson et al., 2013). This model for the switching of affinity states among subunits could explain how an ATPγS-induced pause can be both preceded and followed by truncated bursts (Fig. 3.3b). Assuming that high-affinity sites hydrolyze first during an ATPase cycle, a 1 or 2-nm burst before an ATPγS-induced pause may originate from one or two ATPs binding and hydrolyzing in high-affinity subunits, while the low-affinity sites are occupied with ATPγS. During the subsequent ATPγS-induced pause, the high-affinity sites would release their ADP, and the ATPγS-bound subunits may switch from the low to the high-affinity state, as they are the first subunits to be occupied with nucleotide in the new ATPase cycle. The empty low-affinity subunits could then fill with one or two ATPs, but would not be able to hydrolyze until at least one of the high-affinity subunits releases its ATPγS (Fig. 3.3b). Based on our previous comparison between the duration of ATPγS-induced pauses and the time constant for ATPγS hydrolysis (Fig. 2.5 and 2.6) (Sen et al., 2013), we can conclude that ATPγS dissociation, not hydrolysis, likely determines the end of the ATPγS-induced pause and the onset of hydrolysis in the ATP-bound subunits to generate the next truncated burst. In case ATPγS initially binds to both high-affinity subunits, ClpX would enter an ATPγS-induced pause right away and continue translocation afterwards with a truncated burst (Fig. 3.3b). However, this scenario is less likely due to the at least two-fold excess of ATP over ATPγS in our experiments.

3.3.2. ADP release and ATP binding occur in the dwell phase

To reveal when ADP is released within the dwell/burst cycle, we lowered the rate of ADP dissociation through the addition of orthovanadate (VO_4^{3-}), a Pi analog whose binding temporally traps ADP in the nucleotide-binding pocket (Baird et al., 1999; Sharma and Davidson, 2000). At saturating [ATP], the addition of VO_4^{3-} significantly reduced the pause-free translocation velocity of ClpXP (Fig. 3.4a) as well as its bulk ATPase rate (Fig.3.4b), but had no effect on the frequency or duration of off-pathway pauses (Fig. 3.4c).

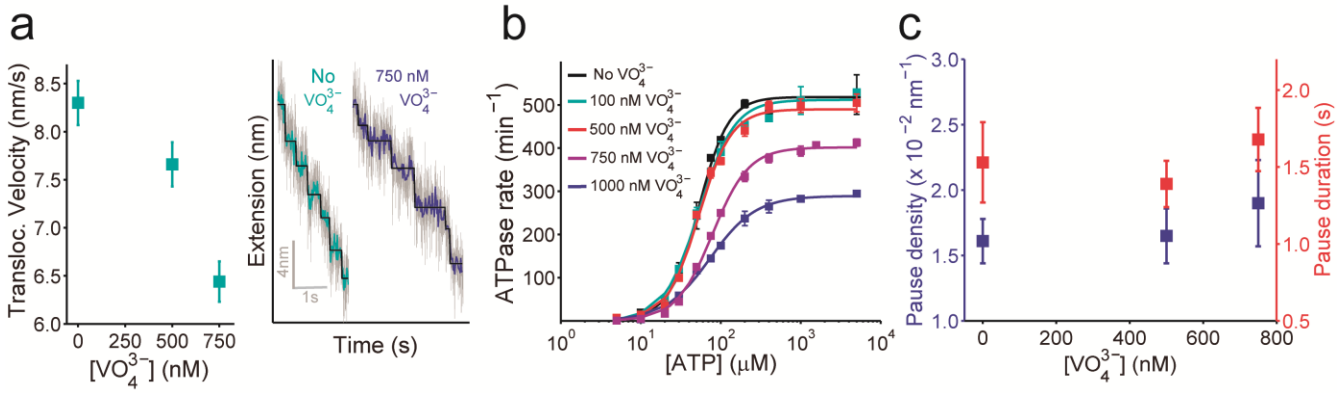

Figure 3.4. (a) Left, dependence of translocation velocity on $[VO_4^{3-}]$ (mean ± SEM) at [ATP] = 5 mM. Right, representative trajectories of ClpXP translocation in the absence and presence of VO_4^{3-}. Raw data were filtered and decimated to 800 Hz (in gray) or 70 Hz (in green and blue). *t* test fits to the data are shown in black. **(b)** ATPase rate by WT ClpXP in the presence of 500 μM titin^{CM}-ssrA at different **$[VO_4^{3-}]$**. The data was fitted to the Michaelis-Menten equation. **(c)** Dependence of the density and duration of pauses on $[VO_4^{3-}]$ (mean ± SEM) at [ATP] = 5 mM.

Given that translocation velocity changes with VO_4^{3-}, we asked whether this change is because VO_4^{3-} lengthens the dwell duration, decreases the burst size, or a combination of both. As shown in Figure 3.5, the burst-size distribution remained unchanged, whereas the mean dwell duration significantly increased with increasing $[VO_4^{3-}]$, indicating that ADP release occurs during the dwell.

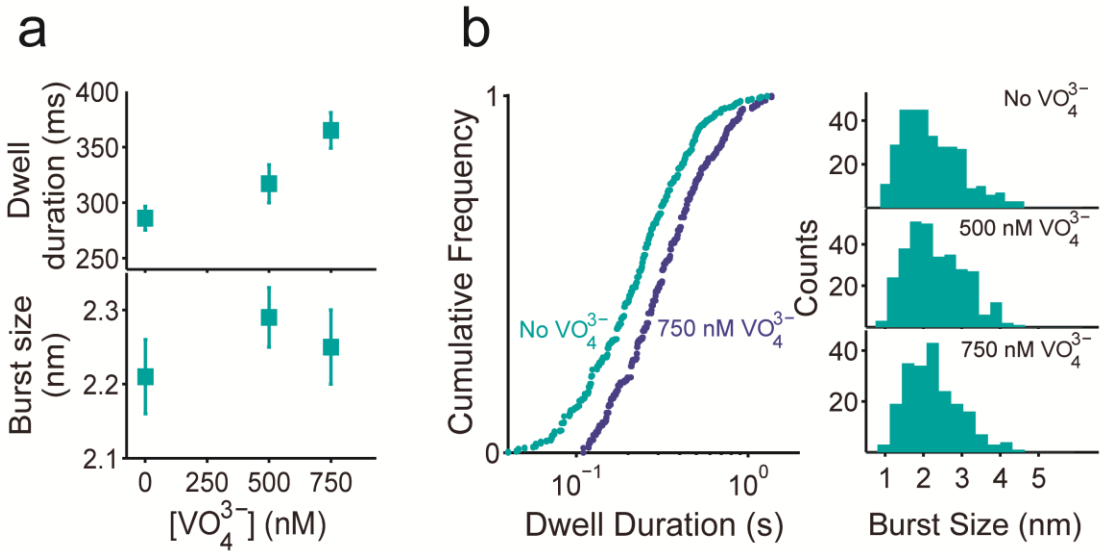

Figure 3.5. (a) Dependence of the dwell duration and burst size on $[VO_4^{3-}]$ (mean ± SEM). The mean dwell duration in the absence and presence of 750 nM VO_4^{3-} was determined to be different with p = 1.04 x 10^{-5} (two-sample Kolmogorov-Smirnov test, null hypothesis: both distributions identical). **(b)** Distribution of bursts sizes (n = 1154 bursts) and dwell durations (*n* = 1060 dwells) at increasing ratios of **[VO_4^{3-}]**.). *n* = 927 dwells and 856 bursts.

On the other hand, ATP binding must occur after the release of ADP, but before ATP hydrolysis (Fig. 2.1). Because ADP is a competitive inhibitor of ClpXP (Fig. 2.4a) (Hersch et al., 2005; Sen et al., 2013), ATP binding can occur as soon as ADP was released from a particular subunit and does not require ADP release from all other subunits in the hexamer. Scenarios where all ADP release and ATP-binding events occur temporally segregated can therefore be ruled out (Fig. 3.6a). Thus, we can conclude that both ADP release and ATP binding happen during the dwell (Fig. 3.7b).

Interestingly, we observed a Hill coefficient for ATP binding and hydrolysis of ~1.6 (Fig. 3.6b and 3.9b), indicating that on average more than one ATPase site in the ClpX hexamer is available for ATP binding. Therefore, albeit interlaced, ADP release and ATP binding are not strictly sequential for successive ClpX subunits (Fig. 3.6a and 3.7b). This scenario is in contrast to the mechanism observed for the F1-ATPase rotary motor (Adachi et al., 2007) or the ϕ29 DNA packaging motor (Chemla et al., 2005; Chistol et al., 2012), which bind ATP around the ring strictly interlaced with ADP release and therefore display a Hill coefficient of 1.

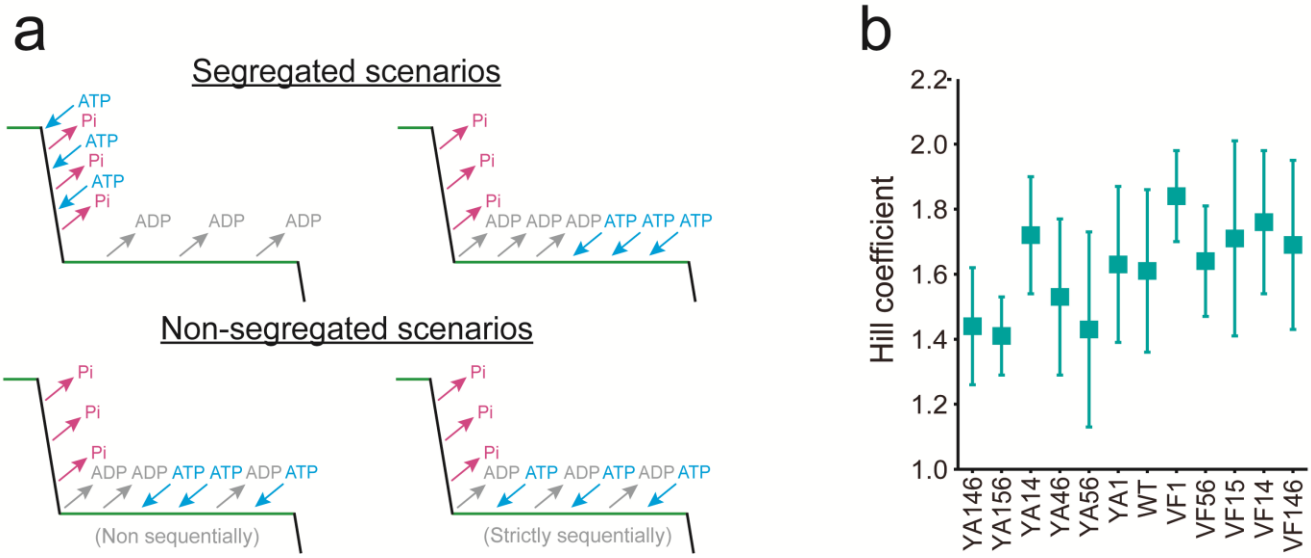

Figure 3.6. (a) Possible scenarios for ATP binding and with respect to ADP release within the dwell/burst cycle of ClpXP. **(b)** Hill coefficient of WT ClpXP and GYVG pore-loop mutants. Hill coefficients were obtained from bulk ATPase measurements in the presence of 1500 μM Ti^{CM}-ssrA substrate. Error bars represent 95 % confidence intervals estimated by fitting the data to the Hill equation.

3.3.3. ADP release is the rate-limiting chemical transition of the dwell

ADP release and ATP binding both occur during the dwell phase (Fig. 3.7b), but which one is the rate-limiting step of this phase? To answer this question, we calculated the value of n_{min} as a lower bound for the number of rate-limiting events during the dwell (Chemla et al., 2005; Moffitt et al., 2009; Schnitzer and Block, 1997). n_{min} is given by the ratio of the squared mean dwell duration over its variance,

$$n_{min} = <\tau>^2/(<\tau^2> - <\tau>^2)$$

For ClpXP we previously reported a value of $n_{min} \sim 2$, indicating that two or more rate-limiting events govern the duration of the dwell, and that those events are likely not associated with ATP binding, since the dwell duration is independent of [ATP] in the range between K_M and saturation (Sen et al., 2013). Since ATP binding and ADP release are the only chemical transitions that occur in the dwell, ADP release is probably the rate-determining step of the dwell. To test this hypothesis we analyzed how n_{min} varies with $[VO_4^{3-}]$. We reasoned that if ADP release is the rate-limiting event of the dwell at $[VO_4^{3-}] = 0$, the value of n_{min} should remain invariant with increasing $[VO_4^{3-}]$, despite the increase in dwell duration. Alternatively, if two events other than ADP release are rate-limiting, then the number of rate-limiting transitions during the dwell should add up as $[VO_4^{3-}]$ increases, leading to a larger value of n_{min}. Despite a ~40% increase in dwell duration, increasing $[VO_4^{3-}]$ did not affect n_{min} (Fig. 3.7a), consistent with ADP release being rate limiting for dwell duration at saturating [ATP].

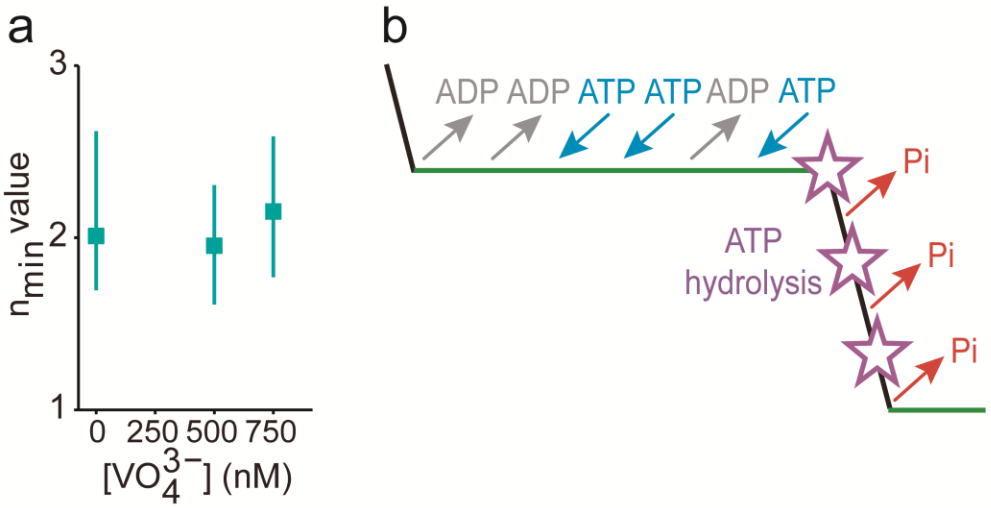

Figure 3.7. (a) Dependence of the n_{min} value on $[VO_4^{3-}]$. Error bars represent 95 % confidence intervals estimated via bootstrapping. **(b)** Possible scenarios for ATP binding and with respect to ADP release within the dwell/burst cycle of ClpXP.

3.3.4. GYVG loops determine the mechanochemical coupling efficiency

After focusing solely on the chemical cycle, we sought to investigate its coupling to the mechanical cycle by perturbing the translocating GYVG loops. These loops are highly-conserved among most prokaryotic and eukaryotic AAA+ protein translocases (Fig. 1.3) and are thought to contact and transmit mechanical force to the substrate (Martin et al., 2008b, 2008c; Siddiqui et al., 2004). By introducing the Y153A or V154F mutation, we decreased or increased the loop size, respectively (Fig. 3.8a), and analyzed the effects on the dwell/burst cycle as well as the role of the GYVG loop in the mechanochemistry of ClpX. The use of single-chain constructs with six covalently linked ClpX subunits (Martin et al., 2005) allowed us to create pseudo-hexamers with different numbers and spatial arrangements of GYVG-mutated subunits (Fig. 3.8a).

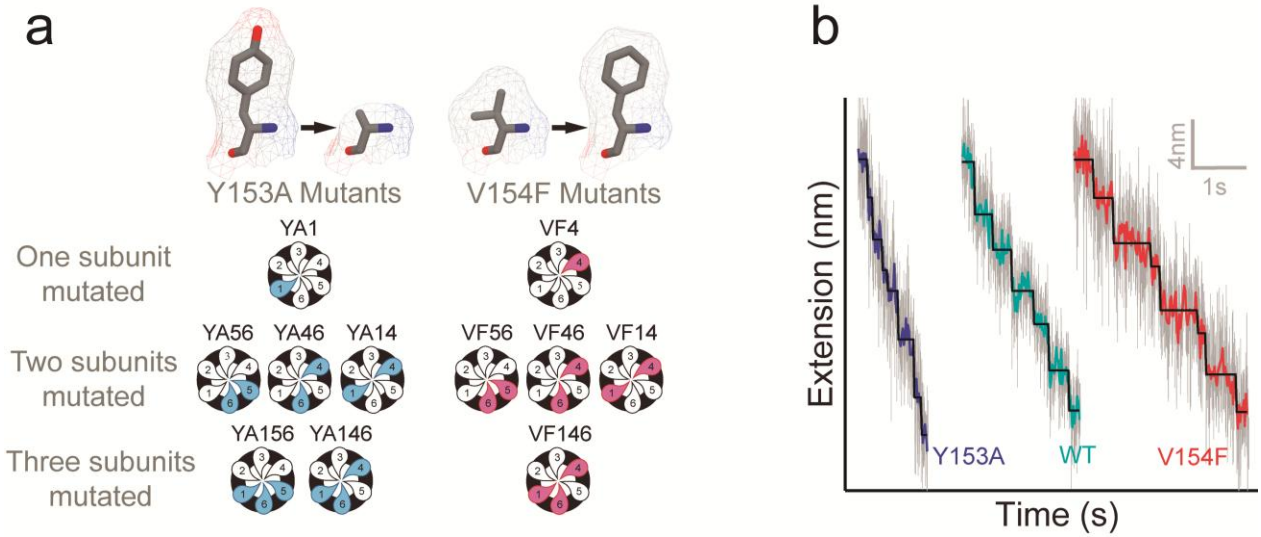

Figure 3.8. (a) The GYVG pore-loop mutations Y153A or V154F were introduced in one, two, or three subunits in different geometries. Numbers behind YA and VF indicate which subunits in the single-chain ClpX hexamer were mutated. **(b)** Representative single-molecule trajectories for translocation by WT ClpXP and GYVG mutants. Raw data were filtered and decimated to 800 Hz (in gray) or 60 Hz (in blue, green, and red). *t* test fits to the data are shown in black.

We first characterized how the increase or decrease of bulkiness inside the ClpX pore affected the translocation velocity at saturating [ATP] (Fig. 3.8b and 3.9a). The pause-free velocity of Y153A mutants increased with the number of mutated subunits, whereas it decreased with increasing number of V154F subunits. Thus, the motor's pause-free velocity is inversely related to the bulkiness of the loops inside the ClpX pore, suggesting that the movement of these loops is affected by their steric hindrance.

Next, we determined the bulk ATPase rate of the GYVG loop mutants as they translocate the permanently unfolded protein substrate Ti^{CM}-ssrA (Fig. 3.9a-b). Importantly, previous studies in bulk (Iosefson et al., 2015a; Martin et al., 2008b) have shown that GYVG loop mutations decrease the affinity of the motor for its protein substrate, which is why we performed our ATPase measurements using 500 μM Ti^{CM}-ssrA to ensure saturation. We observed that, compared to wild type ClpXP (WT), the ATPase rate of Y153A mutants is increased by 100 % - 200 %, a trend that is consistent with a recent independent study of these mutants (Iosefson et al., 2015a). Interestingly, for V154F mutants we observe a modest increase of only ~ 40 %. Thus, GYVG mutations affect both the mechanical and chemical cycles of the motor.

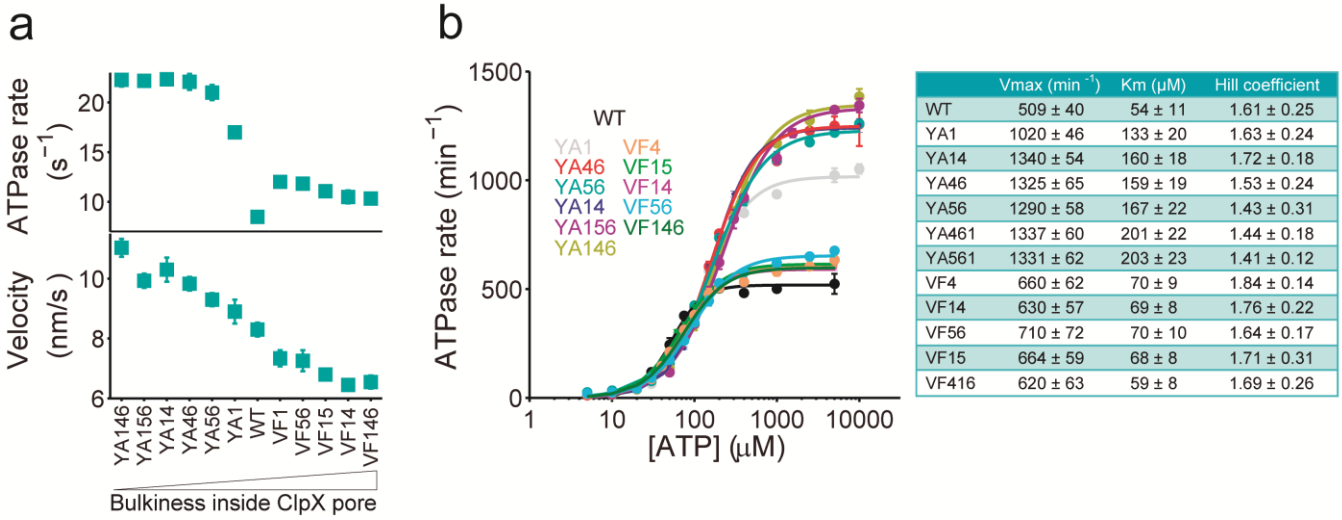

	Vmax (min^{-1})	Km (μM)	Hill coefficient
WT	509 ± 40	54 ± 11	1.61 ± 0.25
YA1	1020 ± 46	133 ± 20	1.63 ± 0.24
YA14	1340 ± 54	160 ± 18	1.72 ± 0.18
YA46	1325 ± 65	159 ± 19	1.53 ± 0.24
YA56	1290 ± 58	167 ± 22	1.43 ± 0.31
YA461	1337 ± 60	201 ± 22	1.44 ± 0.18
YA561	1331 ± 62	203 ± 23	1.41 ± 0.12
VF4	660 ± 62	70 ± 9	1.84 ± 0.14
VF14	630 ± 57	69 ± 8	1.76 ± 0.22
VF56	710 ± 72	70 ± 10	1.64 ± 0.17
VF15	664 ± 59	68 ± 8	1.71 ± 0.31
VF416	620 ± 63	59 ± 8	1.69 ± 0.26

Figure 3.9. (a) *Top:* ATPase rates of WT ClpXP and GYVG mutants during protein translocation, i.e. in the presence of saturating Ti^{CM}-ssrA substrate (500 μM). Rates have an error of approximately ± 5% based on three independent measurements. Numbers indicate mutated subunits in the ClpX hexamer. The X axis presents a series of mutants with the bulkiness inside the ClpX pore increasing from left to right. *Bottom*: Pause-free translocation velocities of GYVG mutants (mean ± SEM) at [ATP] = 5 mM. **(b)** *Left:* ATPse rate by WT ClpXP and GYVG mutants is shown as a function of [ATP] in the presence of 500 μM titin^{CM}-ssrA**.** The data was fitted to the Michaelis-Menten equation. Error bars indicate standard deviation resulting from three independent experiments. *Right*: kinetic parameters of WT ClpXP and GYVG mutants obtained from the fittings in the left panel.

Are all additional ATP-hydrolysis events observed in the ClpX mutants coupled to translocation? Dividing the pause-free velocity (nm/s) by the ATP-turnover value (ATP/s) for each GYVG mutant yields the coupling coefficient (ε), which is a measure for the fraction of ATP-hydrolysis cycles that result in successful substrate translocation (Fig. 3.10a). Consistent with previous reports (Aubin-Tam et al., 2011; Maillard et al., 2011; Martin et al., 2008c), we find for WT that

ε ~ 1 nm/ATP, i.e. every ATP hydrolyzed results in translocation of the substrate by 1 nm. In contrast, we find ε ~ 0.5 for the Y153A mutants, and ε ~ 0.65 for the V154F mutants. A scenario where every ATP hydrolysis results in translocation, but with a reduced step size of 0.5 nm or 0.65 nm, can be ruled out based on our finding that GYVG mutations do not affect the burst size of the motor (Fig. 3.11a-b). Alternatively, an increased ATP consumption could theoretically be caused by defects in initial substrate engagement, but only if the basal ATPase rate—i.e., the rate in the absence of protein substrate—is higher than the ATPase rate during substrate processing. This model can also be dismissed, as the basal ATPase rates of WT and the GYVG mutants are actually 4-6 times lower than the rates during protein translocation (Fig. 3.10b). Interestingly, a recent bulk study (Iosefson et al., 2015a) reported that Y153A mutants have a mechanochemical coupling twice as efficient as WT (ε ~ 2), which is contrary to our results here, and may have arisen from non-saturating substrate concentrations used in those ATPase measurements. Our data suggests that a significant fraction of ATP-hydrolysis events in GYVG mutants actually fail to propel the substrate due to an altered interaction between the loops and the polypeptide, reducing the mechanochemical coupling of the motor.

To evaluate whether GYVG loop mutations affect the grip of the motor, i.e. the strength of contacts with the substrate, we investigated how the translocation velocity of GYVG mutants is affected by increasing external force (F_{ext}) that opposes the force exerted by the motor (F_M) (Fig. 3.10c). At the stall force, F_{ext} equals the maximum force exerted by the motor, and the translocation velocity reaches zero. By fitting the force dependence of the pause-free velocity to a single-barrier Boltzmann equation (Wang et al., 1998), we obtained $F_{1/2}$, the external force at which the translocation velocity drops to half its maximum value (Fig. 3.10c; See Methods).

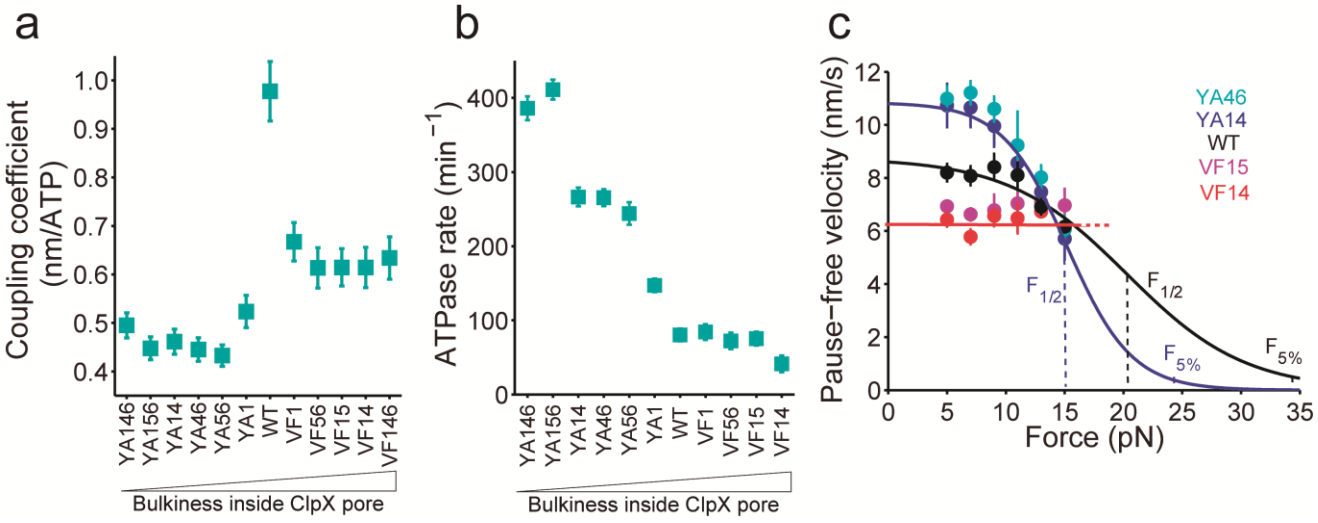

Figure 3.10. (a) Coupling coefficient (ε) between substrate translocation and ATP consumption for WT ClpXP and GYVG mutants (mean ± SEM) at [ATP] = 5 mM. (b) ATPase rate of GYVG mutants in the absence of protein substrate (basal ATPase rate). Rates have an error of approximately ± 5% based on replicate measurements (n = 3). (c) Force-dependence of translocation velocity for WT ClpX and GYVG mutants (mean ± SEM) at [ATP] = 5 mM. The solid line shows a fit to a single-barrier Boltzmann equation (Wang et al., 1998). $F_{1/2}$ refers to the force at which the motor has half its maximum velocity, while $F_{5\%}$ indicates to the force at which the motor reaches 5% of its maximum velocity.

Not knowing the complete force-velocity curve for ClpXP, we cannot simply assume that $F_{1/2}$ equals F_M / 2, but the ratio $F_{1/2}$ / F_M is expected to be identical for different ClpX variants, as F_{ext} has to counterbalance F_M to a similar extent to reach half-maximal translocation velocity for those motors. Thus, we propose that observed differences in $F_{1/2}$ can be related to corresponding changes in F_M, or motor grip, caused by mutations in the GYVG loops. For WT we can extrapolate $F_{1/2}$ = 20.5 ± 1.3 pN, while a Y153A mutation in the 1st and 4th subunits (YA14) showed $F_{1/2}$ = 15.1 ± 1.1 pN, indicating that translocation in Y153A mutants is significantly more sensitive to force compared to WT (Fig. 3.10c). Further extrapolation based on the single-barrier Boltzmann model indicates that WT ClpX would drop to 5 % of its maximum translocation velocity at ~35 pN (Fig. 3.10c), which is in good agreement with previous predictions of its stall force (Aubin-Tam et al., 2011), whereas the YA14 mutant would reach that 5 % velocity already at ~25 pN. In contrast, the variant with V154F mutation in the 1st and 4th subunits (VF14) was insensitive to force up to 13 pN, implying a $F_{1/2}$ and stall force larger than for WT. Thus, Y153A mutations seem to reduce the grip on the substrate—consistent with the results from a recent single-molecule study on Y153A mutants (Iosefson et al., 2015b)—while V154F mutations appear to improve it. Despite this better grip, V154F mutants display a fraction of futile translocation attempts, as indicated by their lower coupling coefficient discussed above (Fig. 3.10a). One possible explanation is that the V154F mutation interferes somewhat with the pore integrity, the arrangement or movement of pore loops, or their interaction with substrate, thus leading to some futile translocation attempts.

In summary, GYVG-loop residues appear to have been selected for optimal coupling between the chemical and mechanical cycles of the motor by providing enough grip on the substrate, without increasing the steric hindrance inside the ClpX pore.

3.3.5. GYVG mutations alter the duration of the dwell

Surprisingly, we found that the burst size remains invariable for all Y153A and V154F mutants compared to WT (Fig. 3.11a-b). This result indicates that the intersubunit coordination of ATP-hydrolysis and Pi-release events during the burst occurs by a GYVG-loop-independent mechanism, which agrees with the proposed model that ATP-hydrolysis-induced conformational changes in one subunit are communicated to neighboring subunits through a topologically constrained set of rigid-body units and hinges that conform the ClpX ring (Fig. 1.1a) (Glynn et al., 2009, 2012; Stinson et al., 2013). Interestingly, ClpX mutants that lack the tyrosine in three of the six GYVG loops (e.g. YA156 and YA146) still produced 4-nm bursts (Fig. 3.11a-b), which is consistent with a recent independent single-molecule study of these mutants (Iosefson et al., 2015b). This behavior can be rationalized if substrates are propelled primarily through contacts with the GYVG loop's backbone, while the tyrosine side chains provide additional contacts and thus a stronger grip on the substrate. Alternatively, these findings would also be consistent with a recently proposed model in which several GYVG loops grip the substrate simultaneously and work synergistically for translocation (Iosefson et al., 2015a, 2015b). ATP-hydrolysis and Pi release in pore-loop defective subunits may thus still drive substrate translocation through coupling with neighboring, intact subunits, albeit at the expense of grip and the maximum force that can be applied for unfolding.

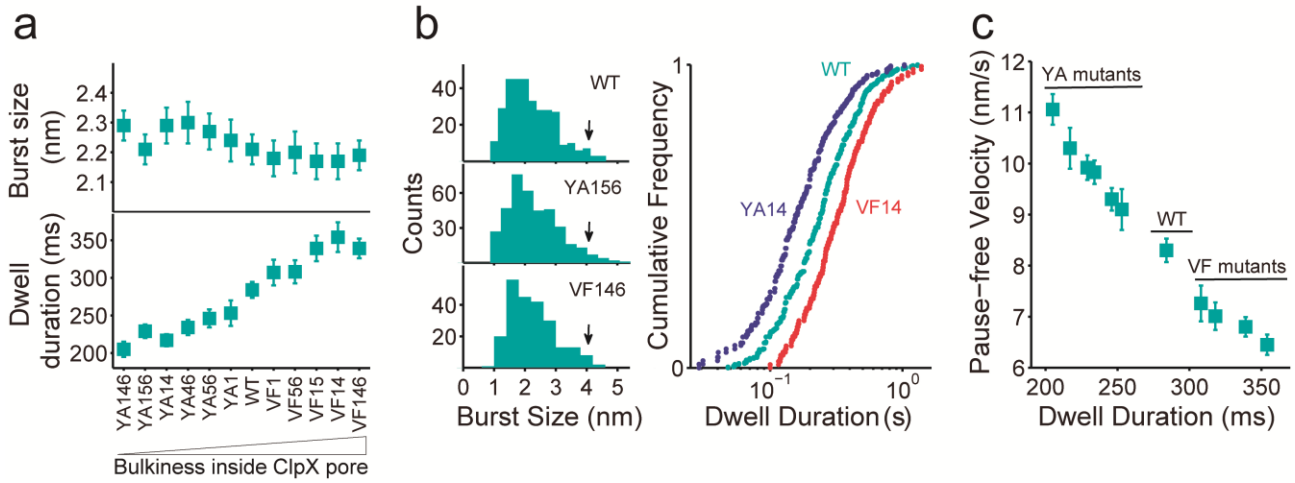

Figure 3.11. (a) Burst size and dwell duration for WT ClpXP and its GYVG mutants (mean ± SEM) at [ATP] = 5 mM. The X axis presents a series of mutants with the bulkiness inside the ClpX pore increasing from left to right. Numbers indicate positions of mutated subunits in the ClpX hexamer. In average, 200 dwells and 150 bursts were analyzed for each GYVG mutant. **(b)** *Left*: Burst-size distribution of GYVG mutants bearing Y153A or V154F mutations in three subunits at [ATP] = 5 mM. The arrows indicate the presence of 4nm bursts. *Right*: Dwell-duration distribution of representative GYVG mutants. **(c)** Correlation of the pause-free velocity (mean ± SEM) of GYVG mutants as a function of their corresponding dwell duration.

In contrast to the unchanged burst-size distribution, the mean dwell duration compared to WT is significantly shorter for Y153A mutants and prolonged for V154F mutants, with the observed changes being proportional to the number of mutant subunits in the ring (Fig. 3.11c). Importantly, these changes in dwell duration solely account for all the measured differences in pause-free velocities of GYVG mutants (Fig. 3.11c).

Our results can be best rationalized if the conformational changes in the GYVG loops during the dwell are coupled to the rate-limiting chemical transition that governs the dwell duration, i.e. the release of ADP, and that GYVG mutations may therefore alter the rate of ADP release. Consistent with this hypothesis, we observed that GYVG mutations affect the ATPase Vmax (Fig. 3.12a)—which depends on all microscopic rate constants except ATP binding (Fig. 2.1) (Chemla et al., 2005; Keller and Bustamante, 2000; Visscher et al., 1999)—but have no effect on Vmax/K_M (Fig. 3.12a)—which is determined only by the microscopic rate constant of initial ATP docking and tight-binding (Fig. 2.1) (Chemla et al., 2005; Keller and Bustamante, 2000; Visscher et al., 1999). Thus, GYVG mutations should affect one or several of the chemical transitions after the irreversible tight-binding of ATP, i.e. ATP hydrolysis, release of Pi, or release of ADP (Fig. 2.1). Out of these transitions only ADP release occurs in the dwell (Fig. 3.7b), and we therefore conclude that GYVG mutations likely affect ADP release from ClpX subunits. Consistent with this conclusion, the mean dwell duration of a variant with two mutated tyrosines (YA14) did not change when [ATP] was reduced to below its K_M (Fig. 3.12b). Limiting [ATP] only decreased the mean burst size and eliminated 4-nm bursts for this mutant (Fig. 3.12b), very similar to the effects observed on WT ClpX (Sen et al., 2013).

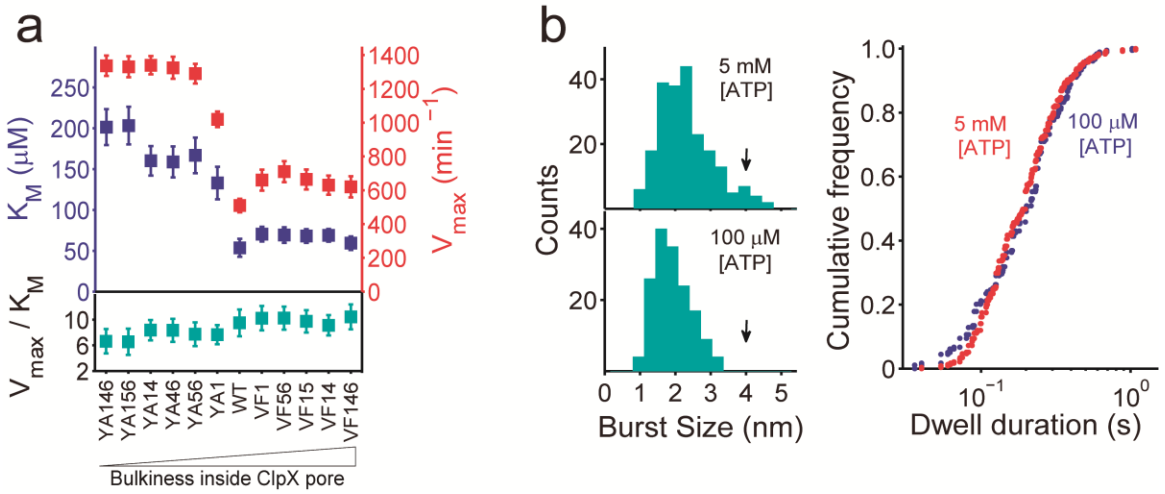

Figure 3.12. (a) Values of Vmax and Vmax/K_M for ATP hydrolysis by WT ClpXP and its GYVG mutants (mean ± SEM). K_M and Vmax values were determined by Michaelis-Menten analyses (*n* = 3 independent experiments). **(b)** Effect of limiting [ATP] on the dwell duration and burst size of the YA14 mutant. The arrows indicate the presence/absence of 4nm bursts. (*n* = 414 dwells and 381 bursts).

Since ADP release occurs after the power stroke and before binding of a new ATP molecule, the GYVG-loop movements linked to this ADP release likely correspond to the loops resetting back into a position that allows them to tightly grip the substrate upon ATP binding and to execute the next power stroke after hydrolysis and Pi release (Fig. 3.13a). Our results thus uncover a previously unknown mechanism for AAA+ motors by which both the chemical and mechanical cycles of the ATPase subunits are set anew through a single coupled conformational change that is affected by the bulkiness of the translocating pore-loop residues. Bulkier pore-loop residues increase the grip on the substrate, at the expense of additional steric hindrance that slows the mechanical and chemical resetting of ClpX and lengthens the dwell time. In contrast, smaller pore-loop residues accelerate the mechanochemical resetting of the motor and thus shorten the dwell, but reduce the grip strength (Fig. 3.13b). Thus, an optimal level of bulkiness inside the crowded ClpX pore—optimal in WT ClpX—ensures an ideal compromise between the grip on the substrate and the pulling rate, leading to maximum *coupling efficiency* (Fig. 3.13b).

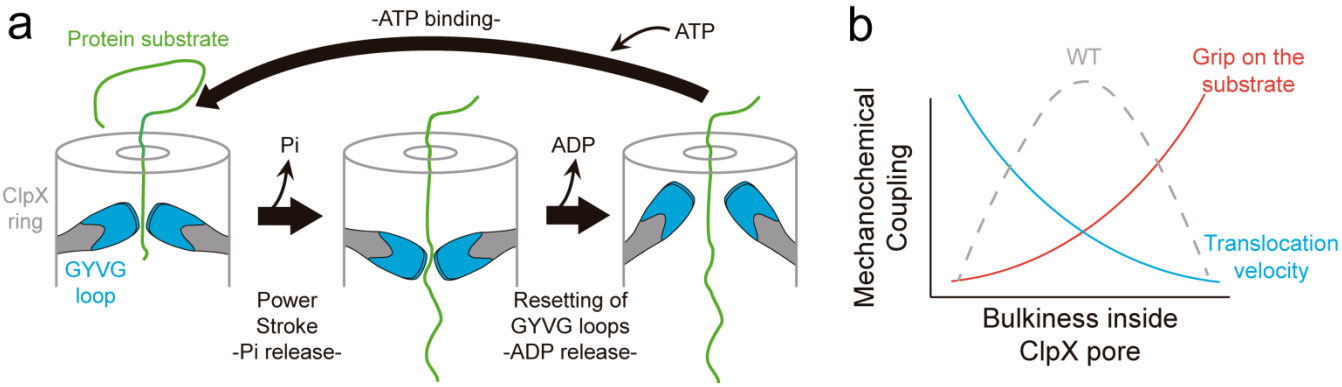

Figure 3.13. (a) Model for the mechanochemical coupling of ClpX, where the GYVG-loop resetting occurs after the power stroke and is coupled to ADP release during the dwell phase. **(b)** Dependence of the mechanochemical coupling on the bulkiness inside the crowded ClpX pore. The coupling efficiency depends on the translocation rate and the grip, i.e. the strength of interactions with the substrate. Based on our results, the mechanochemical coupling of the ClpX motor seems to reach a maximum for the WT GYVG-loop sequence.

3.3.6. Bulkiness of the substrate affects ClpXP translocation

ClpXP is a very promiscuous motor, evidenced by its capacity to successfully translocate not only amino acids with different physicochemical properties, but also synthetic polypeptides containing D-amino acids (Barkow et al., 2009). We asked if all these different amino acids are translocated with the same efficiency by ClpXP. Given the effect of variable pore-loop bulkiness on the operation of the motor described in the previous section, we evaluated if bulkiness of the substrate may also have a similar effect on ClpXP translocation.

To address this question we analyzed the residence time of WT ClpXP in the ybbR-GFP-$(Ti^{CM})_4$-ssrA substrate, i.e. the time that ClpXP resides at a given position of the substrate (Fig. 3.14). Analysis of the ClpXP residence time along the sequence of the four Ti^{CM} is fairly constant, indicating no effect of the Ti^{CM} amino acid sequence on ClpXP translocation (data not shown). Interestingly, ClpXP residence time along the GFP sequence showed that the motor resided consistently more time—observed as translocation pauses—at the region between amino acids 65 and 85 of the GFP sequence (Fig. 3.15a). A closer analysis with bioinformatic tools showed that this region corresponds to the bulkiest part of the GFP protein and it also surrounds the cyclic chromophore of the GFP moiety (Fig. 3.15a). This indicates that bulkiness from the protein substrate—originating either from the linear sequence of the substrate or from the special peptide backbone conformation of the GFP chromophore—induces the motor to enter into a pause, likely due to a steric hindrance effect inside the ClpX pore.

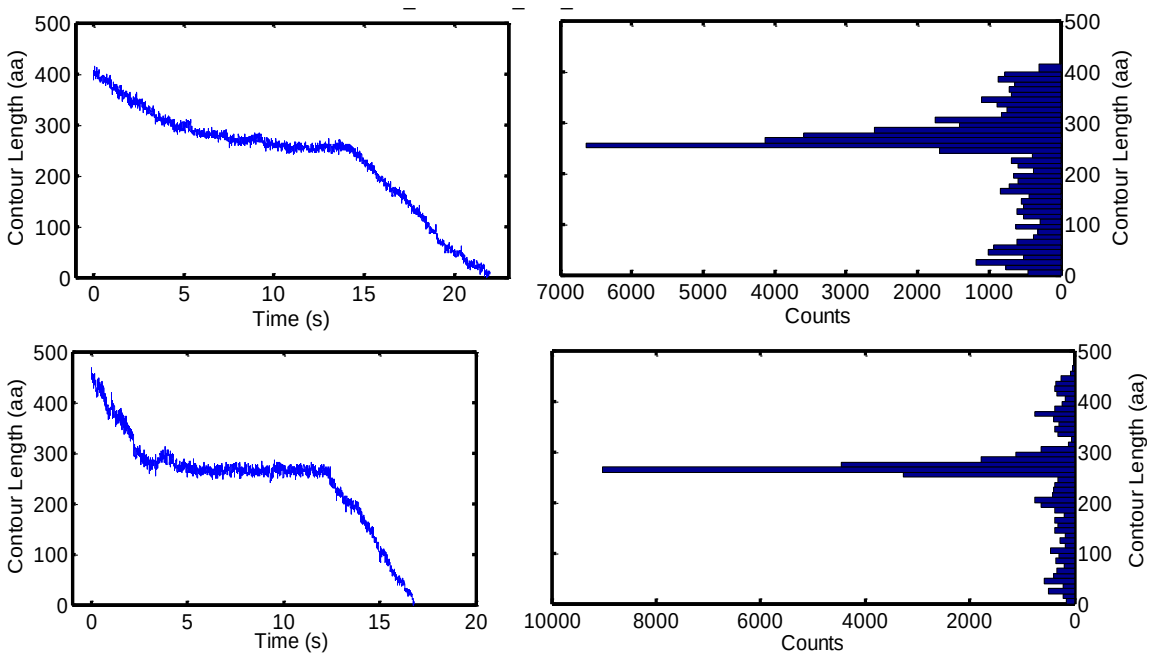

Figure 3.14. *Left panels*, representative trajectories of ClpXP translocation of the four Ti^{CM} moieties of the protein substrate at saturating [ATP]. *Right panels*, residence time—i.e. number of data points per each 10 amino acids bin—of the corresponding trace in the left. Translocation pauses are observed as significant increase in the residence time of the motor at a specific position. Given that the data was acquired at 2000Hz, events with 2000 counts in the residence time plot correspond to events with 1s of duration.

Next, we studied the effect of GYVG mutations on the ClpXP residence time. We observed that GYVG mutations did not increase the mean frequency or duration of pauses during translocation (Fig. 3.15b), except for the region between amino acids 65 and 85 of the GFP sequence, which corresponds to the bulkiest part of the GFP protein and surrounds the cyclic chromophore of GFP (Fig. 3.15a). The duration and frequency of this sequence-induced pause is higher for V154F mutants compared to WT ClpXP, consistent with an additive contribution from the substrate and the GYVG loops to the bulkiness inside the ClpX pore (Fig. 3.15a-c). In contrast, Y153A mutants paused in this specific region as infrequent as in the rest of the GFP (Fig. 3.15a-c), indicating that the bulkiness from the substrate is counterbalanced by the smaller GYVG loops. Together, these results reinforce the idea that bulkiness inside the ClpX pore—originating from the motor loops or the translocating substrate—tunes the movement of the translocating loops.

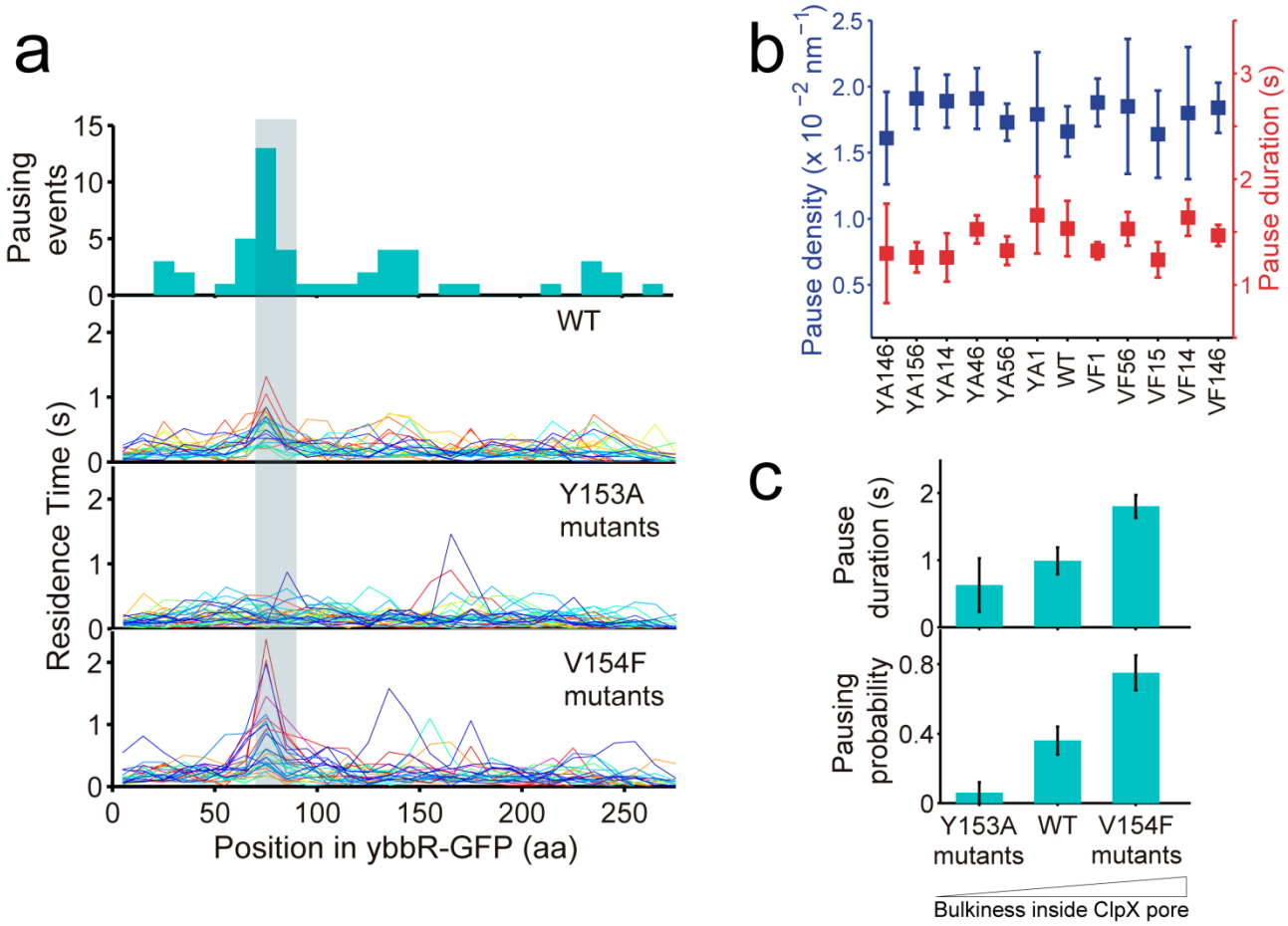

Figure 3.15. (a) *Top:* Pause-frequency distribution of WT ClpXP as it translocates the ybbR-GFP moiety of the GFP-titin substrate. The GFP portion includes an N-terminal Ybbr tag of 18 amino acids, such that the cyclic GFP chromophore is located at position 84 instead of 66. The region surrounding the cyclic GFP chromophore and the bulkiest part of the substrate is underlaid in gray. The resolution of this analysis is 10-15 amino acids. *Bottom:* Residence times along the GFP sequence for WT ClpXP and its pore-loop mutants. Each line represents a single-molecule trace of GFP substrate translocation (n_{WT} = 37 traces; n_{VF} = 28 traces; n_{YA} = 42 traces). Residence times above 0.5 s (which corresponds to the mean residence time plus two SD) are considered pauses. **(b)** Density and duration of translocation pauses in GYVG mutants (mean ± SEM) at [ATP] = 5 mM. Numbers indicate positions of mutated subunits in the ClpX hexamer. **(c)** Effect of GYVG mutations on the duration and frequency of sequence-induced pause. The pausing probability for this specific region was calculated as the number of traces showing a residence time longer than 0.5 s, divided by the total number of traces measured under those conditions: n_{WT} = 37 traces; n_{VF} = 28 traces; n_{YA} = 42 traces. Error bars indicate counting error.

3.3.7. GFP unfolding depends on the power produced by the motor

Protein unfolding represents a higher mechanical barrier for the motor than translocation of an unstructured polypeptide. To test whether the side chains of the GYVG loops have been optimized to enable robust protein unfolding, we analyzed the effects of GYVG mutations on the ability of ClpXP to unfold the GFP moiety of the substrate. For each GYVG mutant we calculated the GFP-unfolding probability as the number of traces displaying a GFP-unfolding event (Fig. 3.16a) divided by the total number of traces. We found that a Y153A or V154F mutation in a single ClpX subunit lowers the GFP-unfolding probability by 50 %, which further decreases with increasing number of mutant subunits in the ring (Fig. 3.16b). The side chains of the GYVG loops are thus critical for the motor's ability to mechanically unfold GFP.

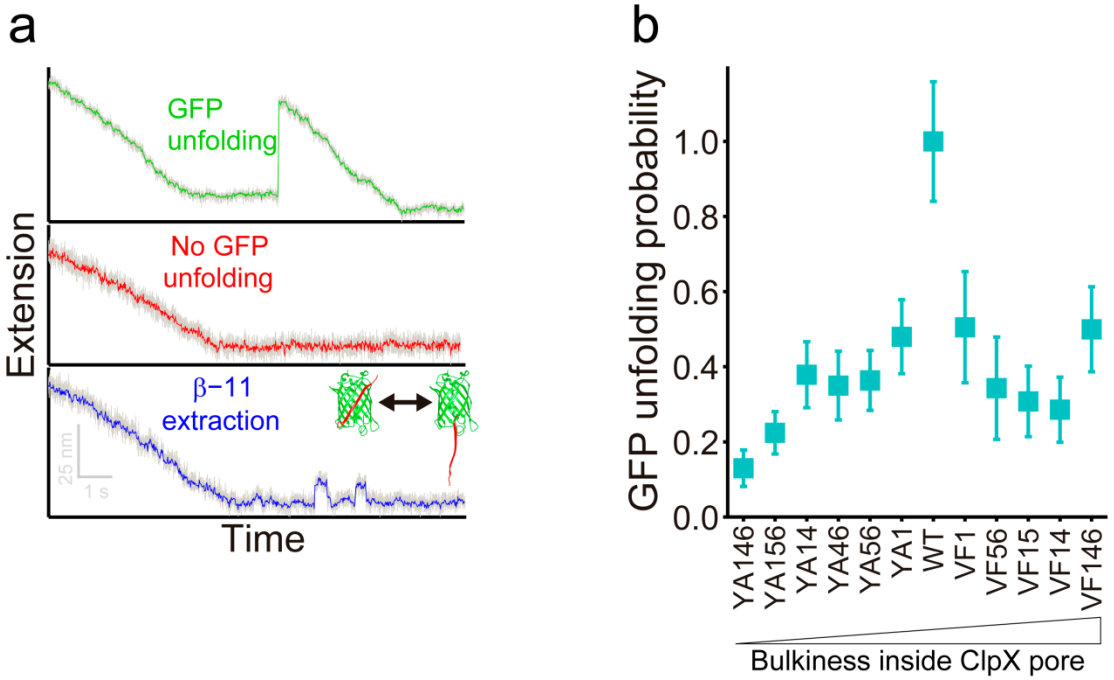

Figure 3.16. (a) Representative single-molecule traces that show successful GFP unfolding (*Top*), no GFP unfolding (*Middle*), and β11-strand extraction/refolding events (*Bottom*). **(b)** GFP unfolding probability for WT ClpXP and its GYVG mutants at [ATP] = 5 mM. Error bars indicate counting error.

We previously proposed that GFP unfolding by WT ClpXP requires the near-simultaneous firing of four subunits (Sen et al., 2013), i.e. 4 nm bursts, which occur only at saturating [ATP] (Fig. 2.7b and 3.12b). Contrary to this model, however, we show here that GYVG mutants are strongly compromised in their ability to unfold GFP, even though they display the same frequency of 4-nm bursts as WT (Fig. 3.11a-b). It was recently proposed that GFP unfolding by ClpXP depends on the coordinated and simultaneous gripping of a high enough number of ClpX subunits (Iosefson et al., 2015a, 2015b). Yet, we found that V154F mutants—which grip the substrate with higher strength than WT (Fig. 3.10c)—are as inefficient in unfolding GFP as the Y153A mutants that display reduced grip strength. Thus, the burst size of the motor or its grip strength independently cannot explain the mechanism of GFP unfolding by ClpXP.

The GFP unfolding probability reaches a maximum at the intermediate GYVG-loop residue size of WT ClpX (Fig. 3.16b). This maximum likely originates from the product of two contributions: one that increases with pore-loop residue size and another one that decreases accordingly. Because the force (F_M) that ClpXP applies to the substrate and its translocation velocity (v) increases and decreases, respectively, with the pore-loop residue size (Fig. 3.9a and 3.10c), their product—i.e. the amount of power (P) generated by the motor—should make a maximum at a certain pore-loop residue size (Fig. 3.17c). We therefore propose that the unfolding ability of ClpXP depends on the motor's generated power (P). Specifically, ClpXP's power output is the product of its force (F_M) applied to a substrate—which equals the external opposing force F_{ext}—and its translocation velocity at that particular force, $v(F_{ext})$. Thus, with $P = F_M \bullet v(F_{ext})$, the power output depends on the external opposing force and approaches zero when F_{ext} is either zero or equals the maximum force of the motor.

For WT ClpXP and its mutants we calculated the power output at $F_{1/2}$, which is close to half the maximum force produced by the motors (Fig. 3.10c). The product of the motor's force and velocity at $F_{1/2}$ is close to the maximum power output. Under these conditions, WT ClpX is able to produce P_{WT} = 90.2 ± 3.1 pN nm s^{-1}, whereas for YA14 this value is only P_{YA14} = 80 ± 2.9 pN nm s^{-1} (See Methods for calculations). The stronger grip of the VF14 mutant made its $F_{1/2}$ experimentally inaccessible (expected to be larger than WT; Fig. 3.10c) and thus prevented us from calculating P_{VF14}.

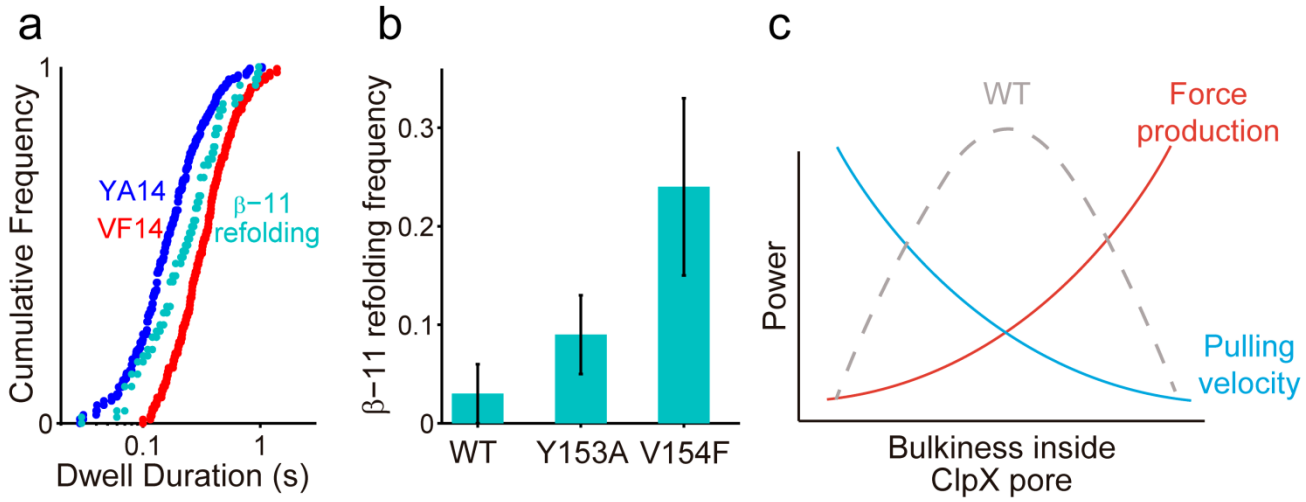

Figure 3.17. (a) Distribution of the β11-strand refolding time (cyan) versus the distribution of the dwell duration for YA14 (blue) and VF14 (red) mutants (n = 58 β11-strand refolding events). **(b)** Frequency of β-11 extraction/refolding events for WT ClpXP and GYVG mutants**,** which was calculated as the ratio of the number of traces displaying these events divided by the total number of traces. Error bars indicate counting error. **(c)** The motor power is a physical parameter that depends on the amount of work produced per unit time. Power was calculated by multiplying $F_{1/2}$ and the corresponding velocity at that force for each ClpX variant. Based on our results, the power produced by the ClpX motor seems to reach a maximum for the WT GYVG-loop sequence, suggesting that evolution has selected the bulkiness of the loop residues to maximize motor power, leading to maximum unfolding capacity.

Our analysis suggests that Y153A mutants fail two to three times more frequently than WT in unfolding GFP, because their weaker grip on the substrate (Fig. 3.10c) reduces the work produced to overcome the mechanical unfolding barrier, even at the maximum burst size of 4 nm. In contrast, V154F mutants grip the substrate with a higher strength (Fig. 3.10c) and produce more work than WT, but still unfold GFP with significantly reduced efficiency (Fig. 3.16b), likely due to their lower pulling frequency. This lower frequency results in reduced motor power and may allow GFP unfolding intermediates to refold in between pulling events. We previously observed that GFP unraveling from the C terminus begins with the extraction of β-strand 11 (β11), which has a strong tendency of refolding within ~ 230 ms (Fig. 2.10b-c) (Sen et al., 2013). To completely unfold GFP, ClpXP must therefore produce enough work to overcome the initial unfolding barrier, but then also translocate β11 faster than its refolding time. V154F mutants may thus fail to unfold GFP because their dwell duration (> 320 ms) is significantly longer than the refolding time of β11 (Fig. 3.17a). Consistent with this hypothesis, we observed β11 extraction and refolding events (Fig. 3.16a) with much higher frequency in traces for V154F mutants than for WT or Y153A mutants (Fig. 3.17b). Thus, an optimal level of bulkiness inside the crowded ClpX pore ensures an ideal compromise between the force delivered to the substrate per translocation event and the pulling velocity, leading to maximum *power production* (Fig. 3.17c).

Based on our results, WT ClpXP seems to have the maximum power value and mechanochemical coupling compared to the other GYVG mutants, which indicates that the bulkiness of the ClpX translocating loops has been selected by evolution in order to maximize these two key features. The results depicted in this dissertation may thus help explain why the sequence in the translocating loops of prokaryotic and eukaryotic AAA+ proteases and other protein translocases—such as the SecA ATPase (Bauer et al., 2014)—is highly conserved (Fig. 1.3).

In summary, our results constitute what is, to our knowledge, the first comprehensive mechanochemical characterization of an AAA+ protein translocase. We provide a detailed picture of how the chemical transitions in the ClpX ATPase cycle are coupled to the dwell and burst phases of the motor, and show that the GYVG pore loops of ClpX play crucial roles in the mechanochemical coupling, power production, and conformational resetting after a power stroke. Given their high homology to ClpX, we expect that related protein translocases—including the eukaryotic 26S proteasome—may use very similar mechanisms for ATP-dependent substrate unfolding and translocation.

3.4. METHODS

3.4.1. Sample Preparation.

Biotinylated ClpX single-chain hexamers, GFP-titin^{CM} I_{27} fusion proteins, and 3 kbp dsDNA handle for protein attached via ybbR tag/Sfp system were prepared as described previously (Sen et al., 2013). Tethers were assembled in a buffer (25 mM HEPES-KCl [pH 7.4], 20 mM $MgCl_2$, 100 mM KCl, and 0.5 mM EDTA) supplemented with [ATP] = 5 mM with ATP regeneration system. Trace amounts of VO_4^{3-}(Sigma) [500 nM and 750 nM] were added to the buffer in presence of 5mM [ATP]. All single-molecule experiments required 500 nM of ClpP for the formation of the ClpXP complex.

3.4.2. Data Collection.

We used a dual-trap optical trapping instrument with a 1064 nm laser in passive mode. The unfolded polypeptide contour length was calculated as previously described (Maillard et al., 2011; Sen et al., 2013). See also methods in Chapter 2.

3.4.3. Data Analysis.

Pause-free velocity was calculated as the end-to-end distance Δx/Δt, after removing pauses longer than 1-1.5s in the Δt component. Steps and dwells were analyzed using pairwise distribution and *t*-test (Moffitt et al., 2009). Data were filtered to 60-100Hz for the *t*-test, and at 15–25 Hz and binned into 0.3 and 0.4 nm for the pairwise distributions. The unfolding events and its related measurements were measured by a previously described method (Maillard et al., 2011).

3.4.4. Fraction of ATPγS-bound Molecules to the Hexamer.

We calculated the fraction of ATPγS molecules bound to the ClpX hexamer as previously reported (Sen et al., 2013). Because ClpX has only four available nucleotide-binding sites at every cycle despite being a hexamer (Glynn et al., 2009; Hersch et al., 2005), we computed the probability of *i* or more ATPγS molecules binding to the motor is given by

$$\sum_i^4 \frac{4!}{i!(4-i)!} p^i q^{4-i} ,$$

where p is the fraction of ATPγS molecules bound to ClpXP at a particular [ATPγS], and $q = 1-p$, which includes both the fraction of empty subunits and bound to a nucleotide other than ATPγS. To calculate p we used the values of the dissociation constants of ATP ($K_d^{(ATP)}$) and ATPγS ($K_d^{(ATP\gamma S)}$) in a buffer containing a specific mixture of [ATP] and [ATPγS]. We used the following equation:

$$p = \frac{[ATP\gamma S]\, K_d^{(ATP)}}{K_d^{(ATP\gamma S)} K_d^{(ATP)} + [ATP\gamma S] K_d^{(ATP)} + [ATP] K_d^{(ATP\gamma S)}}$$

We used the previously reported K_M values of ATP (57 μM) and ATPγS (29 μM) (Fig. 2.5b-c) to establish an upper-bound estimate for the K_d value (Sen et al., 2013).

3.4.5. Measurements of ATPase Rate.

The ATP hydrolysis rate of wild type ClpXP and GYVG mutants was measured using an NADH-coupled ATP-regeneration system as previously described (Kenniston et al., 2003; Sen et al., 2013). Assembled hexamers of ClpX (0.3 μM) were mixed with ClpP (1.5 μM) in a ClpX-100 buffer (25 μM HEPES pH 7.6, 20 mM $MgCl_2$, 100 mM KCl, and 0.5 mM EDTA) containing an NADH-coupled regeneration system (3 U/mL pyruvate kinase, 3 U/mL lactate dehydrogenase, 1

mM NADH, and 7.5 mM phosphoenolpyruvate). The ATP-hydrolysis rate of ClpX was measured both in the presence and absence of 500μM titin^{CM}-ssrA by monitoring the absorbance of NADH (340 nm) at 25º C.

3.4.6. Force dependence of translocation velocity of ClpXP.

By fitting the force dependence of the pause-free velocity to a single-barrier Boltzmann equation (Wang et al., 1998), we obtained $F_{1/2}$, the externally applied opposing force at which the translocation velocity drops to half its maximum value (Fig. 3.10c). We fitted the data to the following equation:

$$v(F) = \frac{v_o(1+A)}{1+Aexp(F\delta/k_BT)}$$

where k_B is the Boltzmann constant, T is the absolute temperature, v_o is the velocity at zero load, δ is the distance to the transition state, and A is a dimensionless constant that determines the ratio of times associated with force dependent versus force-independent reaction steps. Using the data shown in Figure 3.10c, we obtained the following parameters for WT: v_o = 8.7 ± 1.6 nm/s; δ = 0.96 ± 0.4 nm; and A = 0.01 ± 0.1. The small value of A suggests that a force-independent reaction is rate limiting overall for overall ClpXP translocation. Similarly, we obtained the following parameters for YA14: v_o = 10.7 ± 1.4 nm/s; δ = 1.41 ± 0.7 nm; and A = 0.005 ± 0.015.

Extrapolation based on the single-barrier Boltzmann model predicts that translocation for WT would reach 5% of v_o at 32 pN, which could be accounted as the stall force of ClpXP, consistent with the previously reported stall force for ClpXP (Aubin-Tam et al., 2011). Similarly, extrapolation based on the single-barrier Boltzmann model predicts that translocation for YA14 would reach 5% of v_o at 23.5 pN, a value significant smaller compared to WT.

3.4.7. Calculation of Power and Work for WT and mutant ClpX.

The power output (P) of ClpXP working against an opposing force is the product of the force (F_M) it applies to a substrate and translocation velocity ($v = d/t$), where d is the burst size and t is the time needed to complete a dwell/burst cycle, i.e. its dwell duration. Thus, $P = (F_M)(v) = (F_M)(d/t) = W/t$, where W is the work performed by the motor in every cycle. For WT ClpXP and its mutants, we calculated the power output at $F_{1/2}$ (Fig. 3.10c), a condition where the product of the motor's force and velocity at this force is close to the maximum power output of the motor. For WT, we calculated $P_{WT} = F_{1/2} \bullet v(F_{1/2})$ = 20.5 pN • 4.4 nm/s = 90.2 pN nm s^{-1}. For the YA14 mutant, we determined P_{YA14} = 15.1 pN • 5.3 nm/s = 80 pN nm s^{-1}.

The stronger grip of the VF14 mutant (Fig. 3.10c) prevented us from directly determining its $F_{1/2}$, and therefore P_{VF14}. However, based on the similar GFP unfolding probabilities for the V154F and Y153A mutants (Fig. 3.16b), our model suggests that $P_{VF14} \approx P_{YA14}$.

— Chapter 4 —

Concluding Remarks

4.1. BIOLOGICAL IMPLICATIONS OF THE CLPX TRANSLOCATION MECHANISM

This dissertation presents a series of experiments showing in unprecedented detail where and when each chemical transition of the ATP-hydrolysis cycle occurs within the dwell/burst cycle of ClpXP (Fig. 3.7b), and identify the mechanisms that govern each phase of its mechanochemical cycle. Our results show that ClpX translocates substrates using a highly coordinated mechanism in which, regardless of the number of translocating subunits, the average dwell duration is constant and followed by a variable burst size (Fig. 2.7, 2.8 and 3.7b) that reflects the firing of a different number of subunits in rapid succession, where each power stroke occurs upon phosphate release. We found that a process not coupled to ATP binding sets the dwell duration between translocation bursts and that the burst size depends on the number of hydrolyzing ClpX subunits in the hexamer (Fig. 2.7 and 3.12). Although there is a stochastic element during the loading of ATP, we observe a high degree of intersubunit coordination during the rapid burst phase of translocation. Based on bulk biochemical studies, it has been suggested that the ClpXP may operate by a partially probabilistic coordination mechanism, i.e. each subunit operates independently from each other (Glynn et al., 2009; Martin et al., 2005; Stinson et al., 2013). Contrary to this model, our results establish a high degree of coordination between ATP-bound subunits in the ClpX hexamer during the burst phase. These observations present ClpX as machine that employs a novel mechanism of translocation that significantly deviates from canonical motor mechanisms, demonstrating how specialized molecular machines have been optimized to carry out their specific tasks.

The mechanism of a constant cycle time couple to a variable burst size allows flexibility for ClpX to successfully overcome unique chemical and mechanical obstacles during polypeptide translocation. A constant cycle time governed by an internal clock—which corresponds to the conformational resetting of the GYVG loops—provides the motor with a fail-safe mechanism to drive translocation even when some subunits are not loaded with nucleotide. These characteristics may allow the motor to prevent substrate disengagement or prolonged periods of stalling during unfolding attempts when a subset of subunits is unable to maintain grip on the polypeptide.

Because a polypeptide track is aperiodic, ClpX cannot rely on contacting a regularly repeating motif, and its variable burst size (different “gears”) and constant cycle time (constant “rpm”) may have arisen as a flexible mechanism that optimizes its efficiency for robust kinetic trapping of

unfolding intermediates. In contrast, the translocation mechanism of the ϕ29 DNA packaging motor requires that periodic contacts be made by the motor every 10 bp along the helical pitch of double-stranded DNA. In order to achieve a fixed burst size of 10 bp, the motor must wait during the dwell until all subunits are loaded with ATP, which is not the case for ClpXP. This mode of operation may have been optimized to keep the motor in register with the symmetry of its DNA substrate, and provides a fascinating contrast to our results on ClpX. The distinction between these mechanisms offers clear evidence for the evolutionary constraints imposed by the motor's substrates to favor certain mechanisms of operation.

4.2. SIGNIFICANCE FOR OTHER AAA+ MOLECULAR MACHINES

Our results constitute what is, to our knowledge, the first comprehensive mechanochemical characterization of an AAA+ protein translocase. We provide a detailed picture of how the chemical transitions in the ClpX ATPase cycle are coupled to the dwell and burst phases of the motor (Fig. 3.7b), and show that the GYVG pore loops of ClpX play crucial roles in the mechanochemical coupling, power production, and conformational resetting after a power stroke (Fig. 3.13 and 3.17c). Given their high homology to ClpX, we expect that related protein translocases—including the eukaryotic 26S proteasome—may use very similar mechanisms for ATP-dependent substrate unfolding and translocation.

For instance, our power-based unfolding model can explain why ClpA, a *double*-ring AAA+ protease machine, is a better unfoldase than ClpX. A recent single-molecule study (Olivares et al., 2014) showed that ClpAP grips the substrate with a very similar strength as the ClpXP V154F mutants shown here (Fig. 3.10c), suggesting that ClpAP produces more work per translocation burst than WT ClpXP. Because the pulling rate of ClpAP and ClpXP are similar (Olivares et al., 2014), our model predicts that ClpAP generates more *power* than ClpXP, potentially due to additional substrate contacts conferred by the extra AAA+ ring or differences in the pore loops.

Our analysis of motor power reconciles in a single parameter all the different—and sometimes incompatible—models currently available in the literature for the unfolding efficiency of ClpX and related AAA+ protein translocases. This parameter, the product of generated force and translocation velocity, appears to be optimal for the WT GYVG-loop sequence (Fig. 3.17c), thus suggesting that evolution has selected the bulkiness of the pore-loop residues to maximize the power generated by the motor. An optimal level of bulkiness inside the crowded ClpX pore may ensure an ideal balance between the grip of the motor on the substrate and its pulling frequency (Fig. 3.13 and 3.17c). In addition, we show that the translocating GYVG loops are crucial for the coupling efficiency between the chemical and mechanical cycles, which seems to be optimal for WT ClpXP (Fig. 3.10a and 3.13). Conformational resetting of the GYVG loops between consecutive power strokes appears to time both the dwell duration and the release of ADP, which constitutes a novel mechanism of mechanochemical coupling (Fig. 3.13a).

The mechanisms described here thus provide important insights into the operating principles of ATP-dependent proteases and may have critical implications for the understanding of other ring-shaped ATPases of the AAA+ family in general.

4.3. FUTURE DIRECTIONS

4.3.1. ClpXP Operation at Sub-K_M ATP Concentrations

A surprising finding is that, regardless of the number of subunits participating in the translocation cycle, the mean cycle time remains constant for ATP concentrations between ~K_M and saturation (Fig. 2.7c), which is also observed in GYVG mutants (Fig. 3.12b). The mean dwell duration is expected to increase when ATP binding becomes rate limiting, and, to probe this behavior, experiments in the presence of ATP concentrations at or below the K_M for the high affinity subunits (K_M << 35 μM). However, no translocation activity was observed for ATP concentrations below 29 μM in the optical tweezers, although degradation of the Ti^{CM}-ssrA substrate is observed in bulk biochemical assays at this ATP concentration. This suggests that at [ATP] < 29 μM some of the high affinity subunits might be empty, which may compromise not only the initial engagement of the substrate but also the grip of the substrate. To overcome this technical issue, experiments using laminar flow could be used, where ClpXP initially engages its substrate in a buffer containing [ATP] > 29 μM after which the tethered complex is moved to the adjacent buffer containing [ATP] < 29 μM. These experiments could shed light on the operation and coordination of the motor when ATP binding becomes the effective rate-limiting transition.

4.3.2. Spatial and Temporal Order of ClpX Intersubunit Coordination

Although our current model, depicted in Figure 2.8, suggests a spatial and temporal order of ATP-docking events, future single-molecule studies will be required to definitively establish the order of ATP-binding and hydrolysis events around the hexameric ring. Taking advantage of the single-chain ClpX construct, it will be interesting to study the effects on the mechanochemical cycle of the motor of incorporating inactive subunits within the ClpX hexamer in different numbers and different arrangements. Previous bulk studies have tested the effect of inactive subunits on the operation of ClpXP by introducing either of two specific mutations: i) the E185Q mutation (E) in the Walker-B motif, which blocks ATP hydrolysis but allows conformational changes associated to ATP binding, and ii) the R370K mutation (R) in the sensor-2 motif, which also blocks ATP hydrolysis but does not allow the conformational changes associated to ATP binding (Martin et al., 2005). A single molecule study observed that a RWERWE ClpX mutant takes 1-3 nm steps with a predominate peak at 2 nm (Cordova et al., 2014). Further single-molecule studies with these mutants are required to resolve the order of intersubunit coordination. Characterization of each type of mutant separately also will test some of the mechanochemical models proposed in this dissertation.

In addition, it will be important to use a similar strategy to study arginine-finger mutations. Each ClpX subunit contains an arginine finger—highly conserved among ring-shaped AAA+ machines—which contacts in *trans* with the adjacent subunit and therefore plays a role in the intersubunit communication and ATP hydrolysis (Glynn et al., 2009). Single molecule studies using ClpX variants harboring this mutation in a variable number of subunits and with different arrangements will unveil mechanistic insights on how conformational changes in a subunit is propagated to the rest of the ClpX hexamer.

4.3.3. Sequence Dependence

Translocation by ClpXP is a remarkably promiscuous process, demonstrated by the successful degradation of homopolymeric segments of glycine, proline, lysine and even D-aminoacids (Barkow et al., 2009). But, does this promiscuity imply that different substrates are translocated with the same efficiency? The physicochemical properties of a peptide substrate are given by its side chains, which can vary in polarity, hydrophobicity and bulkiness. Consistent with this, bulk studies in ClpXP (Barkow et al., 2009) have shown that the identity of the substrate side chain significantly affects translocation parameters (Vmax, K_M, ATP consumption) and unfolding rate. Then, ClpXP might recognize not only the substrate peptide backbone but also its side chain. In this dissertation we have shown that bulkiness inside the ClpX pore—originating either in the loops or the translocating substrate—affects the translocation and unfolding mechanisms of the motor (Fig. 3.13, 3.15, and 3.16). However, it is not clear the effect of the polarity and hydrophobicity on ClpXP operation. To this end, it will be important to study with optical tweezers the effect on translocation and unfolding of custom-made substrates composed of stretches of hydrophobic, positively and negatively charged residues.

In this dissertation we have also shown that ClpXP tends to pause at a specific region in the GFP substrate, which coincides both with the bulkiest part of the substrate and with the location of the GFP chromophore (Fig. 3.15a). Based on this spatial coincidence, it is not clear if the sequence-induced translocation pause comes from the increased bulkiness of the substrate or the additional bulkiness given by the special cyclic conformation of the GFP chromophore. Single molecule studies with GFP mutants lacking the cyclic conformation of the GFP chromophore will be required to identify the specific source of the observed sequence-induced pauses.

This dissertation has focused on understanding the detailed mechanism of ClpXP-mediated protein degradation. However, future single-molecule studies on related AAA+ proteases are critical to determine whether our current understanding of the ClpX mechanism and the models proposed here can indeed be generalized.

REFERENCES

Adachi, K., Oiwa, K., Nishizaka, T., Furuike, S., Noji, H., Itoh, H., Yoshida, M., and Kinosita, K. (2007). Coupling of Rotation and Catalysis in F1-ATPase Revealed by Single-Molecule Imaging and Manipulation. Cell *130*, 309–321.

Ashkin, A. (1970). Acceleration and trapping of particles using radiation pressure. Phys. Rev. Lett. *24*, 156–159.

Aubin-Tam, M.-E., Olivares, A.O., Sauer, R.T., Baker, T. A, and Lang, M.J. (2011). Single-molecule protein unfolding and translocation by an ATP-fueled proteolytic machine. Cell *145*, 257–267.

Baird, C.L., Harkins, T.T., Morris, S.K., and Lindsley, J.E. (1999). Topoisomerase II drives DNA transport by hydrolyzing one ATP. Proc. Natl. Acad. Sci. U. S. A. *96*, 13685–13690.

Baker, T. A, and Sauer, R.T. (2012). ClpXP, an ATP-powered unfolding and protein-degradation machine. Biochim. Biophys. Acta *1823*, 15–28.

Barkow, S.R., Levchenko, I., Baker, T. A., and Sauer, R.T. (2009). Polypeptide translocation by the AAA+ ClpXP protease machine. Chem. Biol. *16*, 605–612.

Bauer, B.W., Shemesh, T., Chen, Y., and Rapoport, T. A. (2014). A "Push and Slide" Mechanism Allows Sequence-Insensitive Translocation of Secretory Proteins by the SecA ATPase. Cell *157*, 1416–1429.

Burton, R.E., Baker, T. A., and Sauer, R.T. (2003). Energy-dependent degradation: Linkage between ClpX-catalyzed nucleotide hydrolysis and protein-substrate processing. Protein Sci. *12*, 893–902.

Bustamante, C. (2008). In singulo biochemistry: when less is more. Annu. Rev. Biochem. *77*, 45–50.

Bustamante, C., Marko, J.F., Siggia, E.D., and Smith, S. (1994). Entropic elasticity of lambda-phage DNA. Science *265*, 1599–1600.

Cecconi, C., Shank, E. A., Bustamante, C., and Marqusee, S. (2005). Direct observation of the three-state folding of a single protein molecule. Science *309*, 2057–2060.

Chemla, Y.R., Aathavan, K., Michaelis, J., Grimes, S., Jardine, P.J., Anderson, D.L., and Bustamante, C. (2005). Mechanism of force generation of a viral DNA packaging motor. Cell *122*, 683–692.

Chistol, G., Liu, S., Hetherington, C.L., Moffitt, J.R., Grimes, S., Jardine, P.J., and Bustamante, C. (2012). High degree of coordination and division of labor among subunits in a homomeric ring ATPase. Cell *151*, 1017–1028.

Cordova, J.C., Olivares, A.O., Shin, Y., Stinson, B.M., Calmat, S., Schmitz, K.R., Aubin-Tam, M.-E., Baker, T. A., Lang, M.J., and Sauer, R.T. (2014). Stochastic but Highly Coordinated Protein Unfolding and Translocation by the ClpXP Proteolytic Machine. Cell *158*, 647–658.

Dietz, H., and Rief, M. (2004). Exploring the energy landscape of GFP by single-molecule mechanical experiments. Proc. Natl. Acad. Sci. U. S. A. *101*, 16192–16197.

Glynn, S.E., Martin, A., Nager, A.R., Baker, T. A., and Sauer, R.T. (2009). Structures of asymmetric ClpX hexamers reveal nucleotide-dependent motions in a AAA+ protein-unfolding machine. Cell *139*, 744–756.

Glynn, S.E., Nager, A.R., Baker, T. A., and Sauer, R.T. (2012). Dynamic and static components power unfolding in topologically closed rings of a AAA+ proteolytic machine. Nat. Struct. Mol. Biol. *19*, 616–622.

Gottesman, S., Roche, E., Zhou, Y., and Sauer, R.T. (1998). The ClpXP and ClpAP proteases degrade proteins with carboxy-terminal peptide tails added by the SsrA-tagging system. Genes Dev. *12*, 1338–1347.

Hersch, G.L., Burton, R.E., Bolon, D.N., Baker, T. A., and Sauer, R.T. (2005). Asymmetric interactions of ATP with the AAA+ ClpX6 unfoldase: allosteric control of a protein machine. Cell *121*, 1017–1027.

Iosefson, O., Nager, A.R., Baker, T. A., and Sauer, R.T. (2015a). Coordinated gripping of substrate by subunits of a AAA+ proteolytic machine. Nat. Chem. Biol. *11*, 201–206.

Iosefson, O., Olivares, A.O., Baker, T.A., and Sauer, R.T. (2015b). Dissection of Axial-Pore Loop Function during Unfolding and Translocation by a AAA+ Proteolytic Machine. Cell Rep. 1–10.

Joshi, S. A., Hersch, G.L., Baker, T. A., and Sauer, R.T. (2004). Communication between ClpX and ClpP during substrate processing and degradation. Nat. Struct. Mol. Biol. *11*, 404–411.

Kalafut, B., and Visscher, K. (2008). An objective, model-independent method for detection of non-uniform steps in noisy signals. Comput. Phys. Commun. *179*, 716–723.

Keller, D., and Bustamante, C. (2000). The mechanochemistry of molecular motors. Biophys. J. *78*, 541–556.

Kenniston, J. A., Baker, T. A., Fernandez, J.M., and Sauer, R.T. (2003). Linkage between ATP consumption and mechanical unfolding during the protein processing reactions of an AAA+ degradation machine. Cell *114*, 511–520.

Kim, Y.I., Burton, R.E., Burton, B.M., Sauer, R.T., and Baker, T. A. (2000). Dynamics of substrate denaturation and translocation by the ClpXP degradation machine. Mol. Cell *5*, 639–648.

Lyubimov, A.Y., Strycharska, M., and Berger, J.M. (2011). The nuts and bolts of ring-translocase structure and mechanism. Curr. Opin. Struct. Biol. *21*, 240–248.

Maillard, R. A., Chistol, G., Sen, M., Righini, M., Tan, J., Kaiser, C.M., Hodges, C., Martin, A., and Bustamante, C. (2011). ClpX(P) generates mechanical force to unfold and translocate its protein substrates. Cell *145*, 459–469.

Martin, A., Baker, T. A., and Sauer, R.T. (2005). Rebuilt AAA + motors reveal operating principles for ATP-fuelled machines. Nature *437*, 1115–1120.

Martin, A., Baker, T. A., and Sauer, R.T. (2008a). Diverse pore loops of the AAA+ ClpX machine mediate unassisted and adaptor-dependent recognition of ssrA-tagged substrates. Mol. Cell *29*, 441–450.

Martin, A., Baker, T. A., and Sauer, R.T. (2008b). Pore loops of the AAA+ ClpX machine grip substrates to drive translocation and unfolding. Nat. Struct. Mol. Biol. *15*, 1147–1151.

Martin, A., Baker, T. A., and Sauer, R.T. (2008c). Protein unfolding by a AAA+ protease is dependent on ATP-hydrolysis rates and substrate energy landscapes. Nat. Struct. Mol. Biol. *15*, 139–145.

Moffitt, J.R., Chemla, Y.R., Izhaky, D., and Bustamante, C. (2006). Differential detection of dual traps improves the spatial resolution of optical tweezers. Proc. Natl. Acad. Sci. U. S. A. *103*, 9006–9011.

Moffitt, J.R., Chemla, Y.R., Smith, S.B., and Bustamante, C. (2008). Recent advances in optical tweezers. Annu. Rev. Biochem. *77*, 205–228.

Moffitt, J.R., Chemla, Y.R., Aathavan, K., Grimes, S., Jardine, P.J., Anderson, D.L., and Bustamante, C. (2009). Intersubunit coordination in a homomeric ring ATPase. Nature *457*, 446–450.

Moore, S.D., and Sauer, R.T. (2005). Ribosome rescue: tmRNA tagging activity and capacity in Escherichia coli. Mol. Microbiol. *58*, 456–466.

Mueller-Cajar, O., Stotz, M., Wendler, P., Hartl, F.U., Bracher, A., and Hayer-Hartl, M. (2011). Structure and function of the AAA+ protein CbbX, a red-type Rubisco activase. Nature *479*, 194–199.

Olivares, A.O., Nager, A.R., Iosefson, O., Sauer, R.T., and Baker, T. A. (2014). Mechanochemical basis of protein degradation by a double-ring AAA+ machine. Nat. Struct. Mol. Biol. 1–6.

Oster, G., and Wang, H. (2000). Why Is the Mechanical Efficiency of F 1 -ATPase So High ? J. Bioenerg. Biomembr. *32*, 459–469.

Schnitzer, M.J., and Block, S.M. (1995). Statistical kinetics of processive enzymes. Cold Spring Harb. Symp. Quant. Biol. *60*, 793–802.

Schnitzer, M.J., and Block, S.M. (1997). Kinesin hydrolyses one ATP per 8-nm step. Nature *388*, 386–390.

Sen, M., Maillard, R. A., Nyquist, K., Rodriguez-Aliaga, P., Pressé, S., Martin, A., and Bustamante, C. (2013). The ClpXP protease unfolds substrates using a constant rate of pulling but different gears. Cell *155*, 636–646.

Sharma, S., and Davidson, A. L. (2000). Vanadate-induced trapping of nucleotides by purified

maltose transport complex requires ATP hydrolysis. J. Bacteriol. *182*, 6570–6576.

Siddiqui, S.M., Sauer, R.T., and Baker, T. A. (2004). Role of the processing pore of the ClpX AAA+ ATPase in the recognition and engagement of specific protein substrates. Genes Dev. *18*, 369–374.

Stinson, B.M., Nager, A.R., Glynn, S.E., Schmitz, K.R., Baker, T. A., and Sauer, R.T. (2013). Nucleotide Binding and Conformational Switching in the Hexameric Ring of a AAA+ Machine. Cell *153*, 628–639.

Visscher, K., Schnitzer, M.J., and Block, S.M. (1999). Single kinesin molecules studied with a molecular force clamp. Nature *400*, 184–189.

Wang, M.D., Schnitzer, M.J., Yin, H., Landick, R., Gelles, J., and Block, S.M. (1998). Force and velocity measured for single molecules of RNA polymerase. Science *282*, 902–907.